

XRD of gallium nitride and related compounds: strain, composition and layer thickness

PANalytical

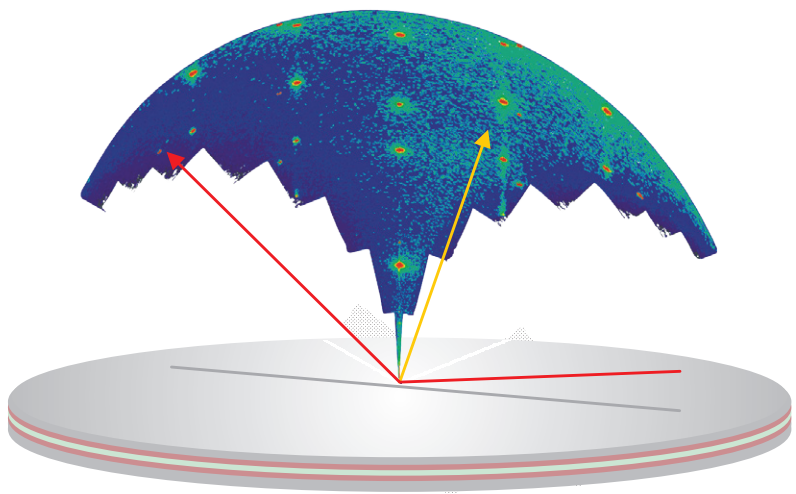


Table of contents

1.	GaN device technology and structural metrology	9
1.1	Brief overview of GaN device technology	10
1.1.1	Device manufacture	10
1.1.2	Substrates	11
1.1.3	Thin film growth	12
1.1.4	Buffer layers	13
1.1.5	Active region	13
1.1.6	Photonic structures	15
1.1.7	Device processing	15
1.2	Structural metrology	16
1.2.1	Layer strain and composition	17
1.2.2	Layer thickness	17
1.2.3	Crystallographic orientation and layer quality	18
1.2.4	Device fingerprinting	18
1.2.5	Crystallographic defects and layer quality	18
1.2.6	Challenges for structural metrology	18
2.	Crystallography and crystal structures of GaN and related compounds	21
2.1	Crystal structure and orientation	21
2.1.1	General concepts	21
2.1.1.1	The unit cell	22
2.1.1.2	Directions in crystals	23
2.1.1.3	Lattice planes	23
2.1.1.4	Plane spacings d_{hkl}	24
2.1.1.5	Angles between planes	25
2.1.1.6	Stereographic projection	25
2.1.1.7	Reciprocal lattice	26
2.1.1.8	Atomic positions	28
2.1.1.9	Polarity in GaN crystals	30
2.1.2	Orientations in substrate wafers and epitaxial layers	31
2.1.2.1	Planes and orientations of substrate wafers	31
2.1.2.2	Crystallographic flats and offcut	33
2.1.2.3	Azimuths on wafers	34
2.1.2.4	Planes and orientations in GaN epitaxial layers	35
2.2	Elasticity theory and distortion coefficients	36
2.2.1	Layer orientation	37
2.2.2	Stresses in the film	37
2.2.3	Strains in the film	38
2.2.4	Fundamental elasticity equations for single crystals	39
2.2.4.1	General form	39
2.2.4.2	Stiffness constants for cubic crystals	41
2.2.4.3	Stiffness constants for hexagonal crystals	41

2.2.4.4	Stiffness constants for an isotropic material	42
2.2.5	Simplifying for biaxial strain in thin layers	42
2.2.5.1	Cubic (001) orientation	43
2.2.5.2	Cubic (111) orientation	43
2.2.5.3	Hexagonal (0001) orientation	44
2.2.6	Fundamental elasticity equations for general isotropic layers (engineering)	44
2.2.7	Simplifying for biaxial strain in isotropic thin layers	45
2.2.8	The distortion coefficient, D	46
2.2.9	Strain equations for low symmetry orientations	46
2.2.9.1	Simplified strain equation for (01-10) oriented GaN	47
2.2.9.2	Simplified strain equation for (2-1-10) oriented GaN	48
2.2.10	Error and assumptions	49
2.2.10.1	High strains	49
2.2.10.2	Imperfect material	50
2.2.10.3	Textured layers	50
2.2.10.4	Ultra thin layers	50
2.2.11	Principles for measurement of strains in thin films	51
2.2.11.1	Choice of (hkil) planes for (0001) oriented hexagonal GaN layers	53
2.2.12	Calculation of composition of thin films using Vegard's law	54
2.2.12.1	Worked solution for the calculation of composition of hexagonal (0001) oriented $\text{In}_x\text{Ga}_{(1-x)}\text{N}$	55
2.2.13	Definition of mismatch in thin films	57
2.2.14	Calculation of relaxation in epitaxial thin films	59
2.3	Crystal truncation and crystallographic defects	61
2.3.1	Thin layers: crystal truncation	61
2.3.2	Dislocations	62
2.3.3	Mosaic blocks	63
2.3.4	Point defects	64
2.3.5	Stacking faults	64
2.3.6	Domains	65
2.3.7	Twins	65
2.3.8	Phases	66
2.3.9	Precipitates	67
2.3.10	Quantum dots	67
2.3.11	Pores and voids	67
3.	Principles of measurement	69
3.1	Bragg's law and measurement of Bragg peaks	69
3.1.1	Measurement in a diffractometer	69
3.1.2	Bragg's law depicted in real space	70
3.1.3	Bragg's law depicted in reciprocal space	71
3.1.4	Alignment of azimuth into the diffraction plane	73
3.1.4.1	Major azimuths in (0001) oriented GaN layers	73
3.1.5	Accessible reflections	74
3.1.6	Scanning	76
3.1.6.1	Scan units	77

3.1.6.2	2Theta/omega scan	78
3.1.6.3	2Theta/omega vs omega map	79
3.1.6.4	Omega rocking curve	80
3.1.7	Experimental procedure	81
3.1.7.1	Equipment	82
3.1.7.2	Placing the 2 θ axis on an absolute scale	82
3.1.7.3	Placing ω on an absolute scale	83
3.1.7.4	Setting the ϕ and ψ positions for a reflection	83
3.1.7.5	Performing a rocking curve	84
3.1.7.6	Performing a TA scan	84
3.2	Calculating <i>d</i> -spacings, layer thicknesses and multi-layer repeat periods	85
3.2.1	<i>d</i> -spacings from reciprocal space maps	85
3.2.1.1	Calculation of <i>d</i> -spacings with reference to 000	85
3.2.1.2	Calculation of <i>d</i> -spacings from two measurements to account for offcut	87
3.2.2	<i>d</i> -spacings from rocking curves	88
3.2.2.1	Obtaining a <i>d</i> -spacing from a symmetrical rocking curve where there is no layer tilt	90
3.2.2.2	Obtaining a <i>d</i> -spacing from two symmetrical rocking curves where there is layer tilt	91
3.2.2.3	Obtaining a <i>d</i> -spacing from two asymmetrical rocking curves where there is layer tilt	92
3.2.3	Using fringes to calculate superlattice periods and layer thicknesses	94
3.2.4	Refractive index correction	98
4.	Solutions for strain composition and thickness via simulation and fitting	101
4.1	Introduction	101
4.2	Theoretical simulation of diffraction	101
4.3	Simulation and fitting software	102
4.3.1	Data collection	103
4.3.2	Sample file	104
4.3.3	Fitting	105
4.4	Imperfections	106
4.4.1	Peak broadening from defects	106
4.4.2	Anomalous peak intensities	106
4.4.3	Summary	107
5.	Studies of defects	109
5.1	Introduction	109
5.2	Characterization of dislocations and mosaic blocks	109
5.3	Broadening of reciprocal lattice spots	110
5.4	FWHM as a measure of crystalline quality	112
5.5	Measurement strategies	112
5.5.1	Accessible reflections	112
5.5.2	Coplanar symmetric reflections	113

5.5.3	Coplanar asymmetric reflections	114
5.5.4	In-plane reflections	115
5.5.5	Non-coplanar reflections	116
5.5.6	Summary	117

PANalytical

PANalytical



PANalytical



PANalytical



PANalytical

Preface

At the time of writing, gallium nitride, GaN, and related compounds are emerging as major players in the business of electronics. This book provides an introduction to the X-ray diffraction analysis of key structural parameters in epitaxial GaN layers. Fundamental crystallographic concepts are introduced and related to the specific requirements of the technological structures created for optoelectronic and electronic devices employing GaN and related compounds.

The book is written for those who wish to gain a deeper appreciation of the principles behind XRD applications in the ever advancing field of compound semiconductor devices. It is also written for those who are engaged in the measurement of epitaxial layers who are looking for a background explanation of the concepts employed in proprietary analysis software such as X'Pert Epitaxy, and those looking for a pathway through the analysis process so that they can design their own calculations. Whilst the solutions and the examples presented here are focused on GaN technology, the principles are generally transferable to solutions for other compound semiconductor systems.

The solutions discussed in this booklet apply to results from high resolution rocking curves and reciprocal space maps. These methods are not the only methods used to investigate advanced materials although they are the most common applications in GaN device technology. Other X-ray diffraction methods, often used in a research environment, include reflectometry, in-plane scattering, SAXS and GISAXS. New methods are emerging to assist rapid measurement and automation. The details of the experimental methods will be considered in a separate publication. All of the measurements referred to in the booklet can be carried out on PANalytical X'Pert MRD and X'Pert MRD XL equipment.

This booklet describes the precise and quantitative measurements that can be made on epitaxial device structures. A number of alternative methods can also be employed to measure the relative quality of defective epitaxial layers. Such approaches include peak shape and width measurements and via this route an exploration of mosaic block sizes, crystallographic tilts and rotations and estimations of defect densities and textural spread. The principles involved in qualitative analyses are also introduced.

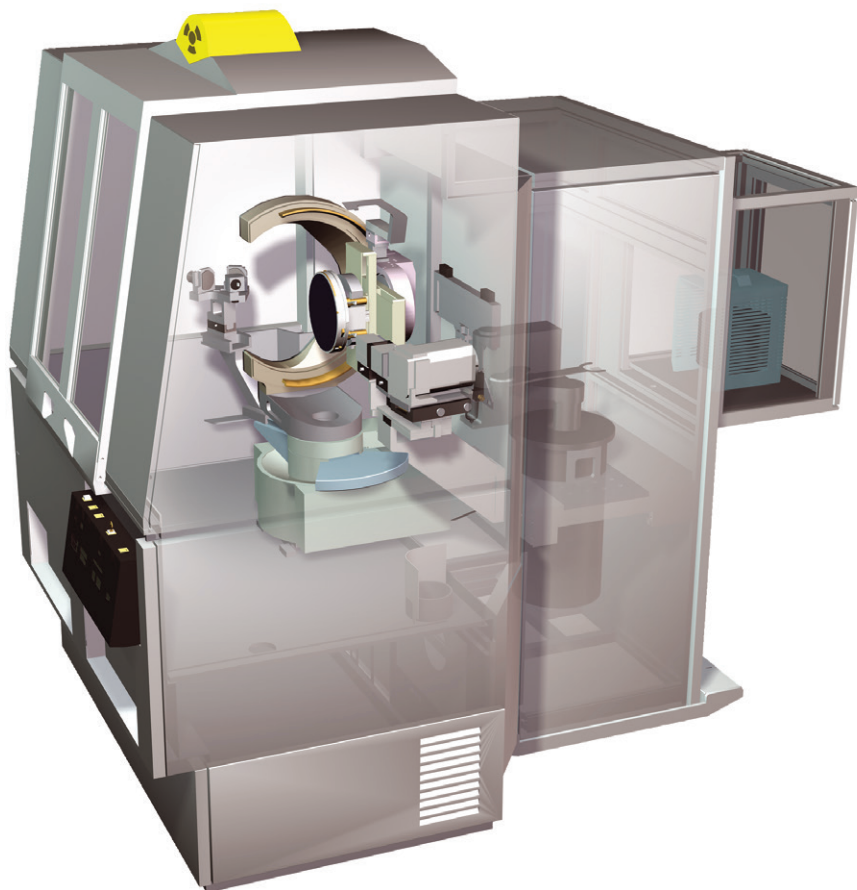
Chapter 1 introduces, very briefly, concepts in GaN device technology that are relevant to XRD metrology.

Chapter 2 provides the background to expressions of crystal structure, crystal dimensions and crystal orientation, and procedures for calculating strain, composition and layer thickness in epitaxial thin films.

Chapter 3 introduces the principles of experiments used to obtain diffraction peak positions and the application of Bragg's law to obtain crystallographic d -spacings.

Chapter 4 introduces the methods of diffraction pattern simulation and fitting as an alternative route to obtaining epitaxial layer thicknesses, compositions and strains.

Chapter 5 describes in principle how measurements of peak widths can be used to give some guide to mosaic block sizes and tilts and hence dislocation densities in GaN buffer layers.



1. GaN device technology and structural metrology

Section 1.1 provides a very brief overview of device technology employing epitaxial GaN and related compounds.

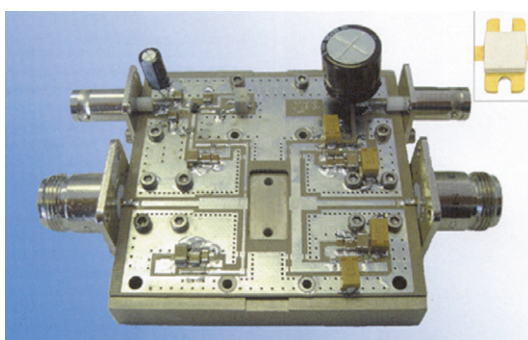
Section 1.2 outlines the areas in structural metrology in which XRD methods have a key part to play and also briefly discusses future requirements and challenges affecting structural metrology.



Osram Opto semiconductors uses silicone encapsulants in its Golden Dragon LEDs. Shown here is the new warm-white version.



Sony is using its hugely successful Playstation games platform to help launch the Blu-ray Disc data storage format that uses GaN-based blue laser technology.



The Korean company RFHIC says that early next year it will start to deploy power amplifier products that feature 50 W GaN-on-silicon transistors developed by Nitronex (inset)

Figure 1: Some examples of current exploitation of GaN-based devices in the market (images copyright: Compound Semiconductor Magazine)

1.1 Brief overview of GaN device technology

GaN and related compounds are direct band gap semiconductors, which makes them suitable materials for optoelectronics. They have wider electronic band gaps than other III-V compounds, such as GaAs, AlAs, InAs and InP. In optoelectronics this wider band gap results in light emission or light detection at higher energies and thus smaller wavelengths, namely the green, blue and UV part of the spectrum.

Advances in the production of GaN-based light emitting diodes (LEDs) have been rapid. There is currently a push towards high brightness LEDs to compete with traditional incandescent light bulbs and fluorescent strip lights. LEDs for illumination are expected to have a high impact on the home consumer market by 2010.

White light is a combination of colors. Because LEDs generally emit a single characteristic wavelength, white light can be obtained via a number of routes. For example, by using combinations of different colored LEDs in a single housing or by using high energy blue or UV LEDs with methods to down-convert some of the wavelengths into lower energy reds and greens through the use of chemical phosphors or photonic materials.

Blue lasers based on GaN technology are expected to form an integral part of the new 'Blu-ray' electronics for high density DVD applications.

GaN based semiconductors have also found applications in wide-band gap electronic devices. High power GaN-based microwave and high bandwidth transmitters and receivers are to be used, for example, in radar and in wireless communications.

1.1.1 Device manufacture

There are many steps in the process of device manufacture starting with the raw materials and ending with a functional electronic device. GaN and related nitrides, (e.g. InGaN, AlGaN) belong to a class of semiconductors formed from group III and group V elements in the periodic table. GaN-based devices are fabricated in a manner very similar to other III-V semiconductor devices.

Most commonly, very thin (< 1 micron) high quality single crystal semiconductor multi-layers, that comprise the active device, are grown by thin-film deposition methods on appropriate substrates. Substrates are usually in the form of wafers with diameters ranging from 1 – 30 cm and thicknesses of the order 0.5 mm. The substrate provides mechanical stability for the device and in some cases also plays an integral part in the device electronics.

III	IV	V
	4 C Carbon	7 N Nitrogen
13 Al Aluminum	14 Si Silicon	15 P Phosphorous
31 Ga Gallium	32 Ge Germanium	33 As Arsenic
49 In Indium		

Figure 2: A section of the periodic table showing the elements commonly used in compound semiconductors

X-Ray diffraction is one of the analytical tools used in foundries where semiconductor thin films are grown. It is used to characterise the crystal orientation and quality of the substrate crystals and to measure the structural properties of the GaN alloy layers. Because XRD is a non-destructive technique, XRD data often accompanies a batch of 'epi-wafers' as they are transferred from the foundry to the device processing plant.

1.1.2 Substrates

The substrate is usually a single crystal wafer. GaN and related devices would ideally be grown on GaN substrates. However, these are difficult and expensive to produce. Large scale growth is currently more likely to occur, for example, on SiC and sapphire substrates. There is a technology push towards growth on larger and cheaper wafers using materials such as silicon.

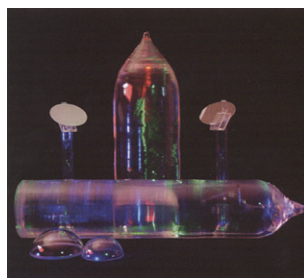
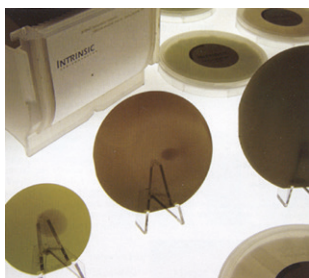


Figure 3: Some examples of SiC (top left) and sapphire (top right) crystals and wafers that serve as device substrates (images copyright: Compound Semiconductor Magazine)

Substrate manufacture and subsequent thin film growth can often be separate business units.

For substrate manufacture, large, highly perfect single crystal ingots are pulled or cast from a melt. Thin (<1 mm) wafers are sawn from the ingots. The wafers are mechanically and chemically polished to remove the surface layer of crystal that has been damaged in the cutting process. They are finally etched to remove any damage from the mechanical and chemical polishing. They are cleaned and packaged and are then shipped to thin film deposition foundries.

PANalytical PANalytical

1.1.3 Thin film growth

Thin film growth of the active device structure of compound semiconductors is called 'epitaxial growth'. The substrate acts as an atomic template for monolayer by monolayer growth of single crystal 'epi-layers'. Growth is performed typically by HVPE (Hydride Vapor Phase Epitaxy), MOCVD (Metal-Organic Chemical Vapor Deposition), MBE (Molecular Beam Epitaxy) or CVD (Chemical Vapor Deposition). The main characteristic of compound semiconductor thin films used in optoelectronic devices is that they are usually single crystals with very low defect densities.

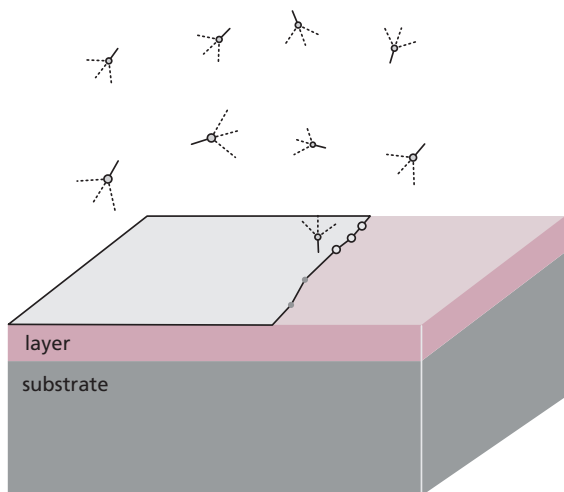


Figure 4: In epitaxial growth atom groups are deposited typically in monolayer by monolayer step-flow growth.

Single crystal epitaxial semiconductor thin films may not be the only materials types in the device architecture. Polycrystalline and amorphous solid or porous thin films of insulating and conducting materials may also be incorporated for example to provide insulating regions for device isolation, dielectric regions for capacitance, or conducting regions for electrical contacts.

PANalytical

PANalytical

1.1.4 Buffer layers

The first layer grown on the substrate is called a ‘buffer layer’ and, in the case where the substrate material is different from the active region, this buffer layer acts as the true atomic template for the multi-layer device structure. The buffer layer may have a thickness of several microns.



PANalytical

Figure 5: A buffer layer of typically a few microns thick is grown on the substrate. The buffer layer surface provides the atomic template for the subsequent multi-layer device structure.

In the case of GaN alloy layers on sapphire, SiC, or Si there is a large lattice parameter mismatch between the crystal unit cell of the GaN alloy and the substrate crystal. When a buffer layer of GaN is grown onto the substrate it acts as a ‘virtual substrate’ because it provides a growth surface which has the GaN unit cell parameters. GaN buffer layers grown on sapphire or SiC substrates are also called ‘relaxed layers’ because they are not strained in order to fit to the substrate unit cell, but have ‘relaxed’ back to the natural bulk GaN lattice parameters regardless of the substrate that they are on. In order for this to happen there have to be crystallographic defects at the interface between the substrate and the buffer layer. Some of these defects propagate through the buffer layer as it grows. Unless steps are taken to reduce these defects at the top surface of the buffer layer, they will also propagate into the active device region. Crystallographic defects deleteriously affect the lifetime and performance of a device and so steps are taken to try to reduce the defect densities at the surface of the buffer layer.

Defect reducing strategies may include the incorporation of thin strained layers within the buffer layer, or even multiple strained layers (known as strained layer superlattices, SLS). These are not part of the active device, but by virtue of their strain-fields, act as a mechanical barrier to the propagation of dislocations.

1.1.5 Active region

When alloying GaN with AlN or InN the resulting compound exhibits optoelectronic properties with values between those of the binary components. In simplistic terms, alloying GaN with AlN, to make the compound $\text{Al}_x\text{Ga}_{(1-x)}\text{N}$, moves the band gap towards the higher energy and for optoelectronics that means moving from the blue wavelengths (GaN) towards UV wavelengths (AlN). Alloying GaN with InN, to make the compound $\text{In}_x\text{Ga}_{(1-x)}\text{N}$, moves from the blue wavelengths (GaN) towards the longer green wavelengths (InN).

PANalytical

PANalytical

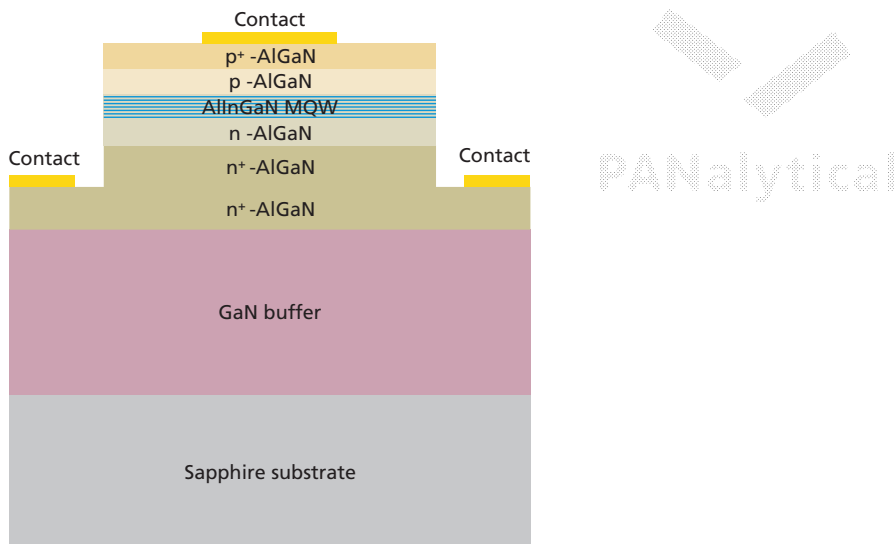


Figure 6: The active region of the device is grown on top of the buffer layer. It needs to be defect free and the layer composition and thickness parameters need to be precisely controlled.

The actual optoelectronic properties of a device are also determined by other factors such as crystallographic strain in individual alloy layers. Highly strained layers may be achieved through alloying. The basic unit cell of the alloy layer is strained to fit the substrate upon which it is grown, this can create subtle and interesting changes to the electronic band structure of the material. Highly strained layers are necessarily thin in order to prevent crystallographic defects being introduced into the layers via relaxation. Relaxation occurs when the strained layer exceeds a critical thickness, where this thickness is a function of the magnitude of the mismatch between the alloy unit cell and the atomic template upon which it is growing.

The band structure and electronic behavior is also affected by the thinness of alloy layers. Very thin layers behave as quantum wells (QW) and have special properties as a result.

To increase the total output from quantum wells and thin strained layers they are often incorporated in a multi-quantum well (MQW) or multi-layer (ML) stack.

Layers of discrete islands or quantum dots (QD) can also be produced in certain growth conditions.

The crystallographic orientation of the layers also determines how the strains and the thinness of the layers will affect the band structure. GaN is a polar along the [0001] direction and this also means that piezoelectric fields can be a contributing factor in the electronic behavior of the device.

1.1.6 Photonic structures

The multi-layer structure may also include multi-layer stacks that comprise approximately 50-100 repeat periods of alloy layers where the alloy compositions are chosen so that their refractive indexes are appropriate to create reflecting interfaces. These multi-layer stacks are called Bragg Stacks or Distributed Bragg Reflectors (DBRs) or multi-layer mirrors. Their purpose is to reflect some of the light that is emitted from the active region of the device. In the case of lasers they contribute to the formation of a resonant wave in the optical cavity of the device.

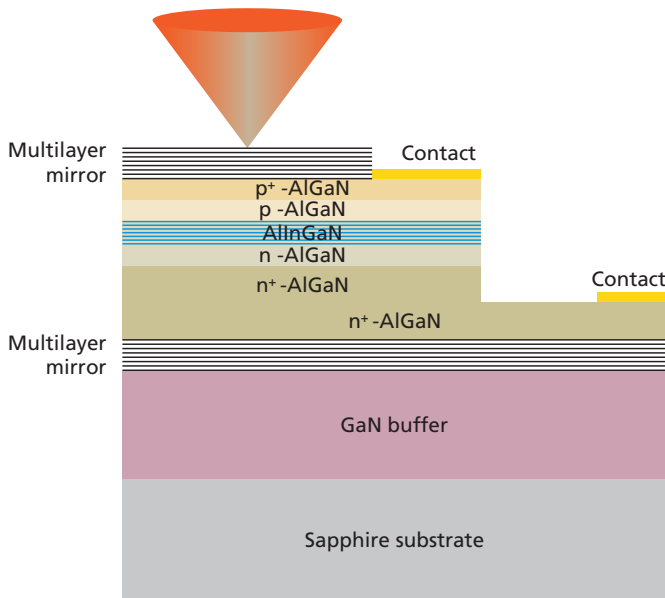


Figure 7: In addition to the active region there may be photonic regions such as illustrated here where multi-layers behave as light directing mirrors.

1.1.7 Device processing

Up until this point the wafers and epitaxial layers are grown epitaxially and the grower is generally aiming to achieve low defect densities, and homogeneity and uniformity of the film parameters over the entire wafer surface. X-ray diffraction methods that measure the compositions and thicknesses, strains and quality of epitaxial layers measure an average of these properties over the illuminated area of the wafer.

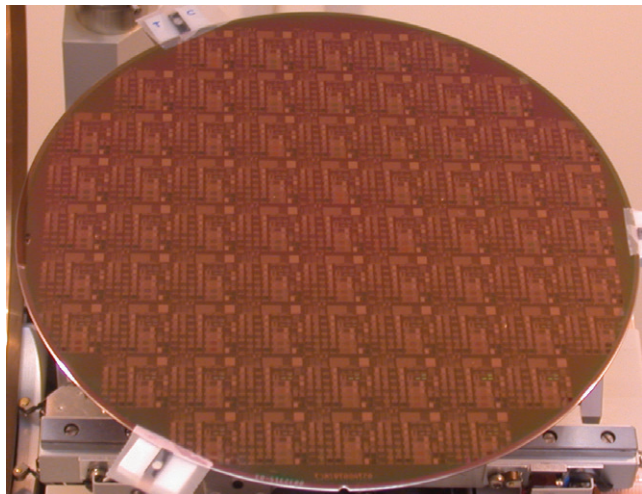


Figure 8: Photograph of a partially processed silicon device wafer showing the laterally repeated pattern of copper interconnects

The dimensions of the illuminated area can range from a few tens of microns to several millimetres depending upon the instrumentation used. Often different areas on the same wafer are measured and the results are used to create a map of structural properties across the wafer.

There are many processing steps after epitaxial growth. The subsequent steps include patterning in which the area of the wafer is divided into discrete regions. The architecture of the device then evolves in 3 dimensions. (Methods to achieve this may involve photolithography and subsequent evaporation of dielectric, conducting or phosphorescent layers). Eventually devices will be cleaved from the wafer and packaged as discrete units.

1.2 Structural metrology

The layer structure of an epitaxial device has characteristic parameters such as crystallographic orientation and strain, layer composition, layer thickness and the quality of the interface between layers. These parameters all contribute to both the absolute position and the fine-scale features of a Bragg diffraction pattern.

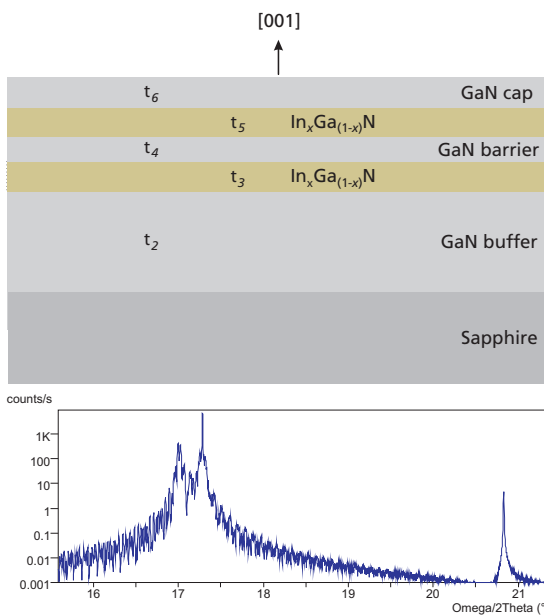


Figure 9: The diffraction pattern from a layer structure contains information about the strain, composition, thicknesses, crystalline orientation, layer quality and structural order and is like a ‘fingerprint’ of the whole device.

1.2.1 Layer strain and composition

Epitaxial strain plays a big part in the device architecture. Because alloy layers will have different lattice parameters from the GaN, an alloy epitaxial layer will be biaxially strained in the interface plane. This strain can modify the band structure of the material and can be a key feature of the device. However, the strain can lead to structural instabilities in the multi-layer stack and needs to be controlled within certain limiting tolerances. This has implications for the alloy compositions that can be used in device designs. XRD can be used to measure lattice strain and alloy composition in these layers to tens of ppm precision.

1.2.2 Layer thickness

Devices are grown with thin layers (typically tens of nanometers). The thinness of the alloy layers directly affects the optoelectronic properties of the device and is a key design parameter. Also the strain energy in a layer increases with thickness and so there are limits on the thicknesses of layers that can be grown before misfit dislocations are produced and the crystal lattice ‘relaxes’ towards its bulk unstrained value. XRD can be used to measure strained-layer thicknesses to less than monolayer precision.

1.2.3 Crystallographic orientation and layer quality

Buffer layers that are used to provide the device template, regardless of which substrate is used, also need to be characterised for their suitability prior to costly device growth and processing. XRD can be used to measure the extent of crystal relaxation, crystallographic orientation, strain, tilt and crystalline quality.

PANalytical

PANalytical

1.2.4 Device fingerprinting

There are many different possibilities and combinations for device architecture. Each device engineer develops their own unique device structure with its own device characteristics. These engineering strategies result in a number of key structural parameters that need to be verified in the epitaxial multi-layer before it is sent for processing. Each multi-layer provides a unique 'fingerprint' in the fine structure of its X-Ray diffraction profile. Solving the fingerprint by simulating the diffraction pattern verifies that the architecture has been faithfully reproduced, namely that the layers are in the correct order and that the contributing layer parameters such as thickness, composition and strain are correct. These parameters require measurement in order that the device properties can be predicted and understood (research and development) and better controlled (production). For this kind of characterisation XRD can be used to simulate the diffraction patterns to measured patterns and fit the layer parameters until an ideal match is obtained.

1.2.5 Crystallographic defects and layer quality

Despite successful device engineering, the capacity of GaN to emit light whilst containing an appreciable number of crystallographic defects still remains an unsolved mystery to device and materials physicists. The characterisation and control of defects will continue to be a scientific challenge to the GaN research community. XRD has a part to play in this, in its capacity to investigate crystalline quality non-destructively by consideration of the shapes and widths of diffracting peaks.

1.2.6 Challenges for structural metrology

For GaN epitaxial thin films the most common crystallographic phases are a stable hexagonal (wurtzite) phase and a metastable cubic (zinc blende) phase. There is mounting evidence that crystallographic defects such as mixed crystallographic phases, stacking faults and reverse polarity domains are prevalent in GaN thin films.

GaN crystals are polar in their nature. When grown on the hexagonal basal plane, as is common for growth on SiC and sapphire or the cubic [111] plane on Si substrates, the resulting material has a natural polarity perpendicular to the interface strongly influencing the electronic behavior. Irrespective of whether the polarity is useful or not, it needs to be characterised and controlled. The issue of how to measure the net polarity, how to grow crystals with a predictable polarity and how polarity is distributed in domains is a hot topic for device engineers and

metrologists alike. Control of polarity, from the point of view of device design, is an important issue and so growth on different orientations of substrates, for example on different facets of sapphire is a common research theme.

There are seemingly endless possibilities for design and production of devices with an ever increasing variation of optical and electronic characteristics. Success of a device design depends on how well components can be alloyed and grown. The chemistry of alloying and growth remains a challenging area and the XRD methods remain a robust laboratory tool for crystal growers to calibrate and appraise the outcome of their work.



PANalytical



PANalytical



PANalytical

2. Crystallography and crystal structures of GaN and related compounds

Section 2.1 introduces general concepts of crystal structure and orientation with emphasis on how they are used to describe the crystals of GaN and their orientations when they are grown as epitaxial layers on substrate wafers.

In Section 2.2 the basic concepts of biaxial elasticity as they refer to these layers are introduced. The growth of mismatched layers causes long-range strains in the unit cells of the epitaxial layers. Characterising these strains is important for the prediction of electronic properties. Stoichiometric GaN, AlN and InN are binary compounds with characteristic unit cell dimensions. By mixing quantities of these compounds solid solution ternary phases are formed, where the unit cell dimensions of the alloys scale in proportion to the quantities of each alloy in the mixture. The size of the unit cell of a layer also gives a measure of the composition of a ternary phase, but care has to be taken to treat separately the effects of mismatch strain from compositional lattice expansion.

In Section 2.3 are introduced the properties of the crystal that disrupt the long-range order namely the truncation of the crystal (meaning the dimensions and shape of the crystal including layer thickness) and the presence of crystallographic defects within the crystal. The ideal X-Ray diffraction pattern is modified by the presence of crystallographic defects that change the observed intensities and pattern shapes (tending to weaken and broaden them). Slight crystallographic distortions in the vicinity of defects also add 'diffuse' scatter in the diffraction pattern.

2.1 Crystal structure and orientation

2.1.1 General concepts

Crystals are understood as having three-dimensional lattices, in which the atoms of the crystal are arranged in a regular and periodic array.

There are different ways of expressing this periodicity. There are many different types of crystal structure. The crystallography of GaN and related compounds as used in epitaxial devices requires knowledge and understanding of both cubic and hexagonal systems¹.

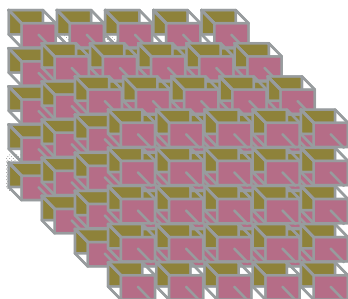


Figure 10: A crystal is described as a three dimensional regular lattice.

2.1.1.1 The unit cell

The unit cell is defined as the smallest block of the crystal which when repeated along its three major axes (the unit cell vectors a , b and c) builds the full crystal. The unit cell vectors are related to each other by their angles α , β and γ . Where α is the angle between the vectors b and c , β is the angle between vectors a and c and γ is the angle between vectors a and b .

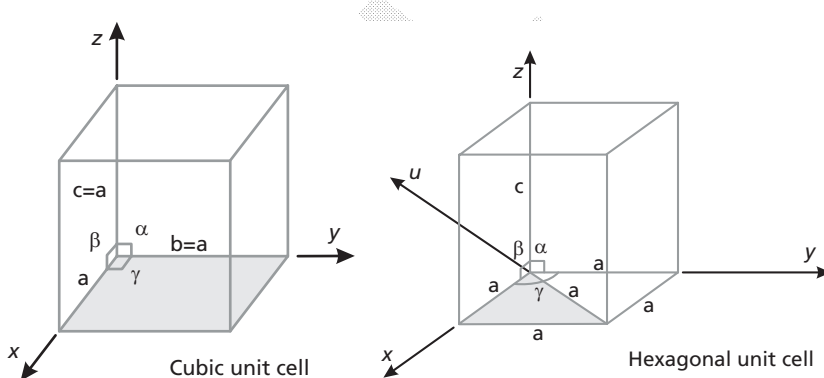


Figure 11: Diagrams of the cubic and hexagonal unit cells

The cubic unit cell is characterised by having lattice parameters $a = b = c$ and unit cell angles $\alpha = \beta = \gamma = 90^\circ$.

The hexagonal unit cell is characterised by having lattice parameters $a = b \neq c$ and unit cell angles $\alpha = \beta = 90^\circ$, $\gamma = 120^\circ$.

The lattice parameters of the individual phases of most semiconductors are known to high precision (~1 ppm) and can be obtained from reference sources. Alternatively, lattice parameters can be determined to 1 ppm using high-resolution XRD². However when looking for agreement between the values of reference standards and those of lab samples it is important to be aware that departures

from the standard values will exist due to growth variations which incorporate impurities and lattice strains. Some reference unit cell dimensions for GaN and related compounds are listed in the table below³.

	a (Å)	c (Å)
Hexagonal GaN	3.1893	5.1851
Cubic GaN	4.4904	a
Hexagonal AlN	3.1130	4.9816
Hexagonal InN	3.538	5.7020
Sapphire	4.7564	12.989
SiC-4H	3.0730	10.0530
SiC-6H	3.0806	15.1173
Si	5.43105	a

2.1.1.2 Directions in crystals

There is also the concept of directions in crystals. Direction vectors are defined with respect to the unit cell axes and dimensions. Note the use of parentheses: $[uvw]$ is used to specify a unique direction; $\langle uvw \rangle$ is used to specify the set of directions that share the same properties.

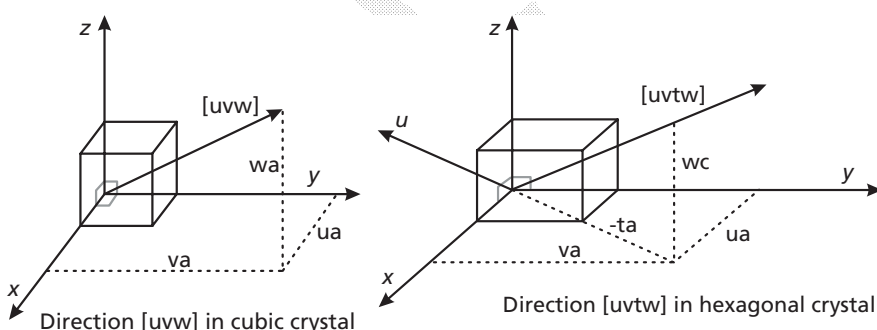


Figure 12: Directions in crystals with respect to the unit cell

As for the planes, there are three Miller indices, $\langle uvw \rangle$, to describe directions in cubic crystals and four Miller-Bravais indices, $\langle uvtw \rangle$, to describe directions in hexagonal crystals, where $t = -(u+v)$.

2.1.1.3 Lattice planes

The lattice planes in the crystal are visualised as a stack of parallel planes, where each plane contains a sheet of lattice points. All of the planes are identical and the crystal is created by repeating the sheet of lattice points at a regular interval. The planes are described by Miller indices (hkl), that are related to the unit cell axes and unit cell dimensions of the crystal. This concept is used a lot in X-ray diffraction.

because of Bragg's law which relates the angle of diffraction (θ) to the repeat spacing of the crystallographic planes $d_{(hkl)}$. Note the use of parentheses: (hkl) is used to specify a unique plane; $\{hkl\}$ is used to specify the set of planes that share the same atomic arrangements and have the same spacings, but are at different orientations with respect to the crystallographic axes.

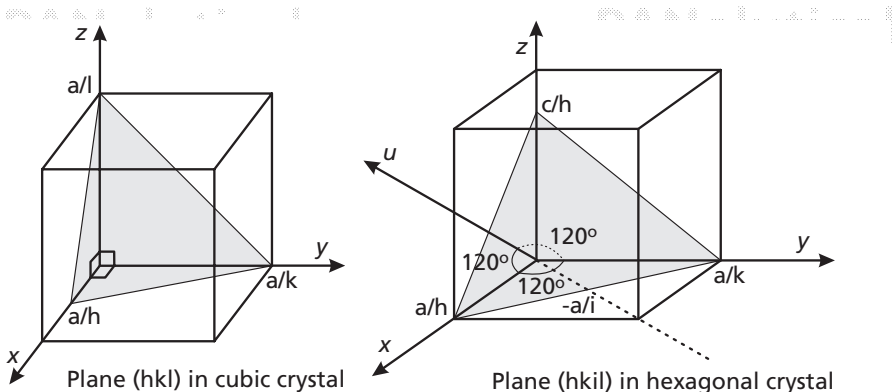


Figure 13: Diagrams showing how lattice planes are indexed with respect to the unit cell

There are three Miller indices, $\{hkl\}$, to describe planes in cubic crystals and four Miller indices, $\{hkil\}$, to describe planes in hexagonal crystals where $i = -(h+k)$. Using three Miller indices for hexagonal systems is possible and often used, but it does not adequately describe the six-fold symmetry of the hexagonal lattice, for example the planes $(-1-120)$ and (-2110) belong to the same set, but in three Miller indices they would be written $(-1-10)$ and (-210) respectively and could mistakenly be thought of as belonging to different sets.

2.1.1.4 Plane spacings d_{hkl}

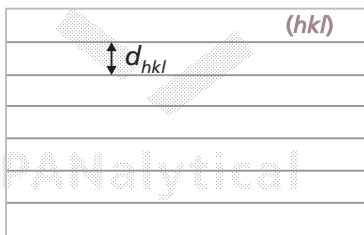
The absolute spacings of crystallographic planes can be calculated from their Miller indices and their unit cell dimensions according to the following equations:

Cubic plane spacing:

$$d = \sqrt{\frac{a^2}{h^2 + k^2 + l^2}} \quad (1)$$

Hexagonal plane spacing:

$$d = \sqrt{\frac{1}{(h^2 + k^2 + hk)\frac{4}{3}a^2 + \frac{l^2}{c^2}}} \quad (2)$$



PANalytical

Figure 14: Plane spacing is the perpendicular separation of neighboring planes.

2.1.1.5 Angles between planes

The angle, ϕ , between two planes (hkl) and $(h'k'l')$ can be calculated according to the equations:

$$\text{For cubic interplanar angles: } \cos \phi = \frac{hh' + kk' + ll'}{\sqrt{h^2 + k^2 + l^2} \sqrt{h'^2 + k'^2 + l'^2}} \quad (3)$$

Hexagonal interplanar angles:

$$\cos \phi = d_{hkl} d_{h'k'l'} \left\{ \left[hh' + kk' + \frac{1}{2}(hk' + kh') \right] \frac{4}{3a^2} + \frac{ll'}{c^2} \right\} \quad (4)$$

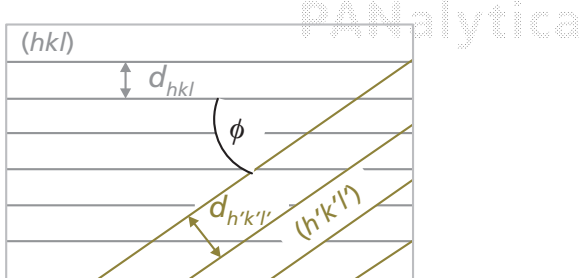


Figure 15: Diagram illustrating the angle ϕ between planes

2.1.1.6 Stereographic projection

A stereographic projection depicts the angles between plane normals and can be useful as a 2-D representation of planes and their orientation relationship to each other. A plane can often be represented by the direction normal to it. In a stereographic projection it is imagined that the crystal is placed at the center of a sphere. The point where a plane normal intersects the northern hemisphere of the sphere is connected by a straight line to the south pole of the sphere. The positions

where the lines intersect the equatorial plane are represented as dots on a two-dimensional image. They are labelled with the hkl indices of the plane.

When a new type of substrate wafer is obtained and new types of epitaxial layers are grown, stereographic projections are often used to gain familiarity with the orientations of the major crystallographic planes with respect to the wafer.

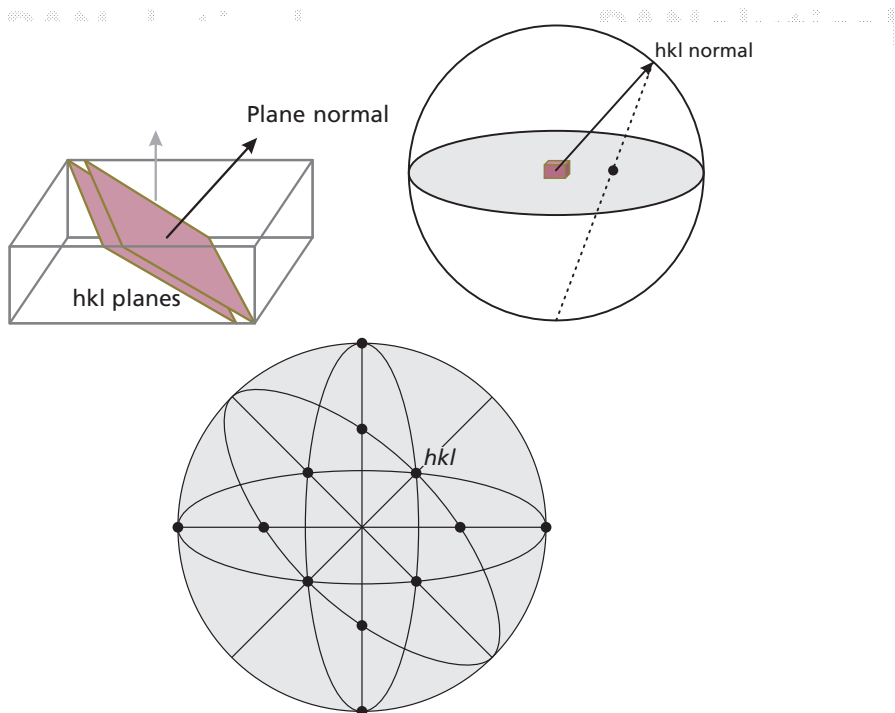


Figure 16: Diagrams showing the construction of a stereographic projection. Top left: The plane orientation; Top right: The construction; Bottom: The projection

2.1.1.7 Reciprocal lattice

The reciprocal lattice is a particularly useful method for illustrating a crystal structure. It combines the information regarding both plane spacings and interplanar angles in a single construction. It has a sound mathematical basis and corresponds effectively to the Fourier transform of the real space structure of the crystal. In the reciprocal lattice, the crystal and its orientation are represented in 3 dimensions by a lattice of 'reciprocal lattice points' (RLPs) where each point represents a set of parallel crystal planes (hkl). The points are generated from the reciprocal lattice origin (000) where the vector, $d^*(hkl)$, from the origin to the RLP has the direction of the plane normal and length given by the reciprocal of the plane spacing.

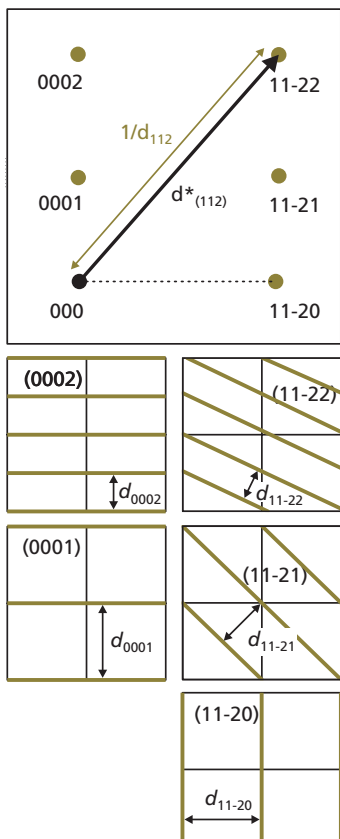


Figure 17: A 2-dimensional reciprocal lattice (top) is constructed by considering the spacings and orientations of each set in a group of low index planes, where all of the planes lie perpendicular to the image.

The axes for a reciprocal lattice construction also represent the real space orientation of the crystal. For example, for epitaxial layers the reciprocal lattice is usually constructed with the z axis normal to the surface symmetric planes and the x and y axes approximately parallel to the interface. The reciprocal lattice directly relates to the crystal and if a crystal's orientation is rotated the reciprocal lattice rotates by the same amount.

For epitaxial layers it is common to show 2-D cross sections of the reciprocal lattice of the layers and substrates relating to a specific azimuth on the wafer surface.

Because of its direct depiction of d -spacing and crystallographic orientation, the reciprocal lattice construction is used frequently in XRD analysis as will be illustrated in Chapter 3.

2.1.1.8 Atomic positions

Within the unit cell the atom species of the crystal take up coordinate positions, where the coordinates are fractions of the unit cell vectors. Whilst the unit cell type defines the symmetry of the crystal, i.e. cubic or hexagonal, the atomic positions within the unit cell (i.e. the atoms that are associated with a lattice point and how they are arranged) define the crystal class that a material belongs to: GaN, InN, AlN, 4H-SiC and 6H-SiC commonly have the hexagonal 'wurtzite' structure [space group notations C46v or P63mc].

Sapphire is one of the aluminium oxide phases, $\alpha\text{-Al}_2\text{O}_3$ and has the hexagonal 'corundum' structure [D63d or R-3c].

Si and 3C-SiC have the cubic diamond structure [T2d or F-43m].

GaN also has a metastable cubic phase, zinc blende (also known as sphalerite) [T2d or F-43m]. This phase is also common to the other III-V compound semiconductors such as GaAs, InP and AlAs.

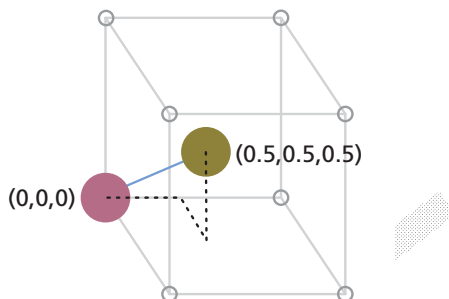
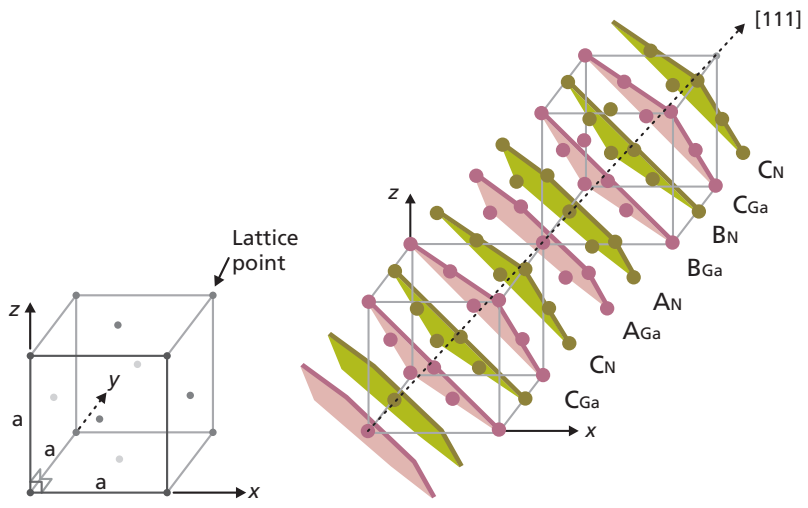


Figure 18: In a crystal a group of atoms are associated with each lattice point. Their coordinates relative to every reciprocal lattice point are usually given in fractions of a unit cell dimension.

Cubic GaN, whilst being metastable with respect to hexagonal GaN, is very easily formed during growth. The lattice unit cell is face-centered cubic (fcc), there are 4 lattice points per unit cell. This is illustrated in Figure 19. The actual arrangement of atoms in cubic GaN is shown in Figure 19. It is commonly known as the zinc blende structure in which two atoms are associated with each lattice point of the face-centred cubic unit cell. The positions of the atoms are given by coordinates with respect to a lattice point. This group of two is repeated for every lattice point and in this way the entire crystal is constructed. The figure only shows the atoms associated with one lattice point, for clarity. Figure 19 shows the effect of this group of atoms being repeated for every lattice point. The {111} close packed lattice planes are illustrated. The ABCABC... characteristic stacking sequence is also illustrated.



GaN, AlN, InN (zinc blende)

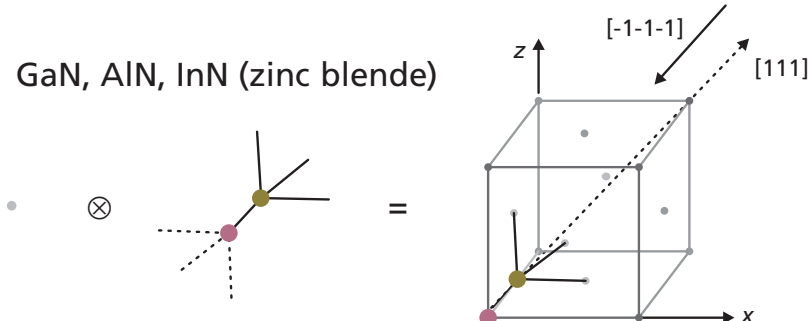


Figure 19: Diagrams of cubic GaN. The fcc unit cell (top left). Several unit cells filled with atoms showing $A_{Ga}A_NB_NB_GaC_N$ stacking sequence (top right). Two atoms are associated with each lattice point in the fcc unit cell (bottom). The red sticks illustrate their tetragonal chemical bonding arrangement (note that this is very similar to that in hexagonal GaN. The sense of bonding is opposite (hence polar) for the directions [111] and [-1-1-1]. The coordinate set for both atoms with respect to each lattice point (expressed as fractions of the (a,a,a) cell parameters) are as follows: Group III atom (Ga, In, Al) (0,0,0), Group V atom (N) (0.25, 0.25, 0.25)

Figure 20 illustrates the hexagonal wurzite structure. Associated with every lattice point is the same arrangement of atoms. For the wurzite structure four atoms are associated with each lattice point. The positions of the atoms are given by coordinates with respect to the lattice point. This group of four is repeated for every lattice point and in this way the entire crystal is constructed. The figure only shows the atoms associated with one lattice point, for clarity. Figure 20 shows the effect of this group of atoms being repeated for every lattice point. The {0001} close packed lattice planes are illustrated. The ABAB... characteristic stacking sequence is also illustrated.

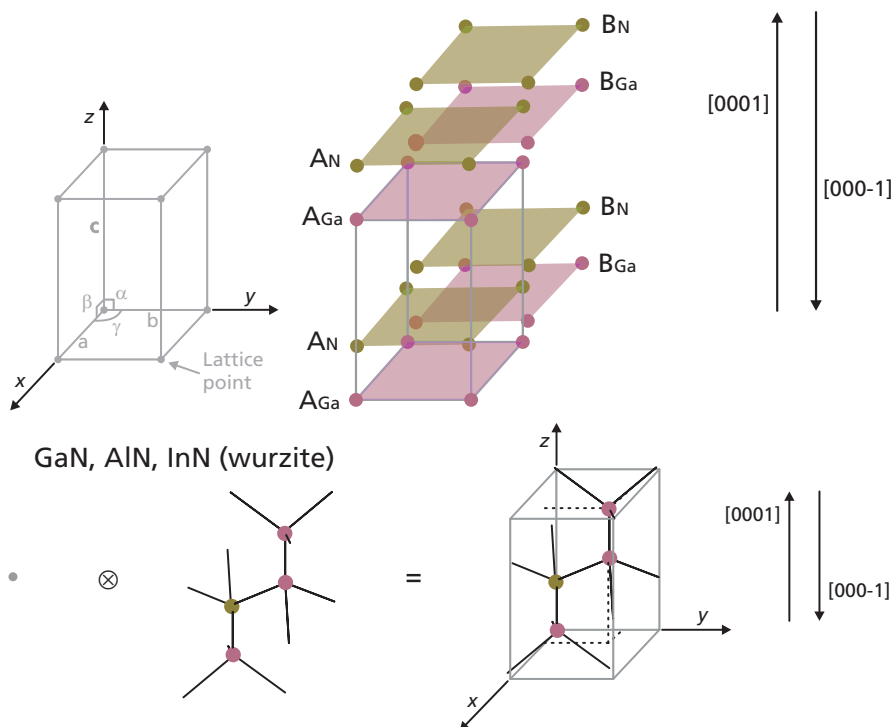


Figure 20: Diagrams of hexagonal GaN. The Hexagonal unit cell (top left). Unit cell filled with atoms showing $A_{Ga}A_NB_{Ga}B_NA_{Ga}A_NB_{Ga}B_N$ stacking and illustrating polarity (top right). Four atoms are associated with each lattice point in the hexagonal unit cell (bottom). The sticks illustrate their tetragonal chemical bonding arrangement. The sense of bonding is opposite (hence polar) for the directions [0001] and [000-1]. The coordinate set for all four atoms with respect to each lattice point are as follows: Group III atom (Ga, In, or Al) (0,0,0) and (1/3, 2/3, 1/2) Group V atom (N) (0,0,0.37308) and (1/3, 2/3, 0.89231) There is some uncertainty in the precise value of the z coordinate of the N atom position.

2.1.1.9 Polarity in GaN crystals

The direction of maximum polarity which is also the direction normal to the close packed planes is $\langle 111 \rangle$ for the cubic crystal and $\langle 0001 \rangle$ for the hexagonal crystal. In this direction the two crystals appear very similar, the main difference being the stacking sequence of the close packed crystallographic planes. These are the (0001) planes with ABABAB... stacking sequence for hexagonal GaN and the (111) planes with ABCABCABC... stacking sequence in cubic GaN.

Stacking faults are easily created in GaN buffer layers leading to mixtures of both cubic and hexagonal domains and also reverse polarity domains. The control of these domains, their relative concentrations and sizes is the subject of much ongoing research.

There are efforts to grow cubic GaN on, for example, (001) oriented Si substrates. Growth of (001) cubic GaN potentially overcomes some of the polarity-enhanced effects observed in (111) cubic GaN or (0001) hexagonal GaN. Also Si substrates are a lot cheaper than the sapphire and SiC alternatives.

2.1.2 Orientations in substrate wafers and epitaxial layers

2.1.2.1 Planes and orientations of substrate wafers

For substrates, a seed crystal is used as the starting point for ‘pulling’ an ingot from the melt and this determines the major crystallographic directions in the single crystal ingot. The size of the ingot that can be grown depends upon the chemical, mechanical and thermal properties of the ingot chemistry. The exact crystallographic directions of the substrate wafer are determined by the way in which it is cut from the ingot. Many wafers are cut perpendicular to the major axis of the ingot and so the surface normal is defined by this major axis. Because the ingots are often cylindrical in shape the substrate wafer is circular. But substrate wafers can have other shapes, e.g. elliptical or rectangular shapes depending upon the angle at which the wafer is cut from the ingot.

Hexagonal sapphire wafers can have the following surface orientations:

C-plane = parallel to the {0001} plane

also known as the *basal* or *close-packed* plane of the hexagonal unit cell

A-plane = parallel to the {2-1-10} plane

M-plane = parallel to the {1-100} plane

also known as the ‘prism’ plane of the hexagonal unit cell

R-plane = parallel to the {1-102} directions

also an interesting orientation as it can be used as a substrate in Si device technology, so there is also the opportunity for GaN/Si hybrid devices.

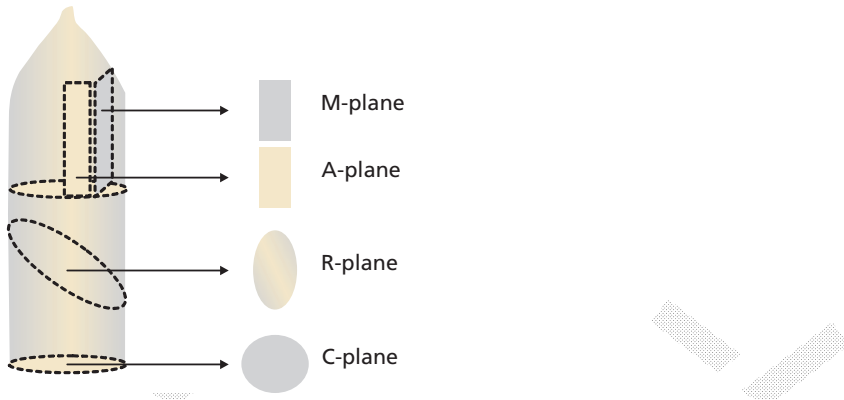


Figure 21: Diagram illustrating how wafers are cut from a sapphire ingot

Figure 22 shows a schematic stereographic projection of the plane normals for a sapphire (0001) substrate illustrating the sets of planes that are commonly used for XRD. Also shown on the stereographic projection are the traces of the other possible planes used as wafer surface orientations.

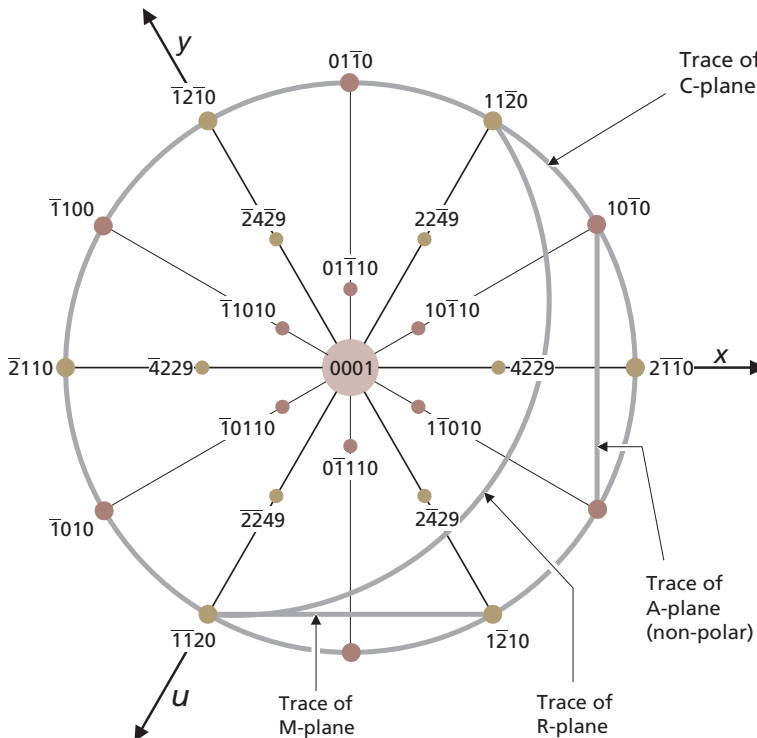


Figure 22: Schematic stereographic projection (i.e. not to scale) of sapphire with the [0001] direction normal to the image, showing the normals to the useful planes for XRD analysis (spots) and traces of common wafer planes (solid grey lines).

SiC is also used as a substrate. SiC has several hexagonal forms of which SiC-4H and SiC-6H are the most popular. Whilst the C-plane is the most common substrate orientation, growth can be performed on wafers with other low index orientations as for sapphire.

Si (111) wafers can be used, in particular, for AlN devices. There is increasing interest in growth of AlGaN and even InGaN devices on AlN buffer layers on Si. If the number of defects arising from the different thermal expansion coefficients of the layer and substrate materials can be sufficiently reduced the use of such a cheap substrate becomes advantageous. See Figure 23 for a schematic stereographic projection of plane normals for a Si (111) substrate.

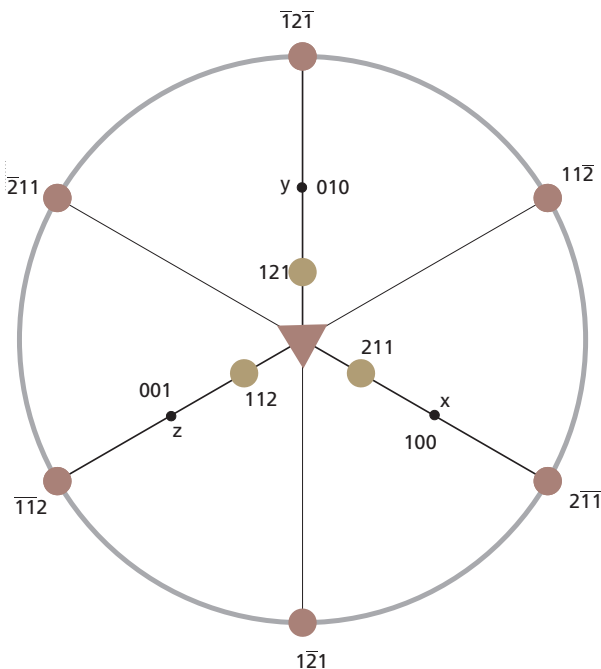


Figure 23: Schematic stereographic projection (i.e. not to scale) of cubic silicon with the (111) plane parallel to the image, showing the normals to the useful planes for XRD analysis (spots).

2.1.2.2 Crystallographic flats and offcut

The substrate may have a crystallographic flat that indicates where one of the major directions can be found. The orientation of the flat is provided, together with the tolerance on the known orientation of the wafer surface, by the substrate manufacturer to the epitaxial grower. For example a substrate specification might include the following:

Crystal:	LED grade sapphire
Sapphire purity:	>99.99%
Orientation:	(0001) c axis, $\pm 0.2^\circ$
Diameter:	50.8 ± 0.25 mm
Thickness:	0.332 or 0.432 ± 0.025 mm
Primary flat:	(11-20) a axis $\pm 0.3^\circ$
Flat length:	16.0 ± 1.5 mm

The offcut is a measure of angular difference between the closest major crystallographic plane and the true wafer surface. Typically the offcut can be controlled to within a quarter of a degree. The offcut is easily measurable in an XRD experiment. In the example above the intended offcut is 0° , but the actual offcut measured may

be anything up to 0.2° . When there is an intended offcut the sense of the offcut, is also indicated, usually by an angle of rotation away from the primary flat.

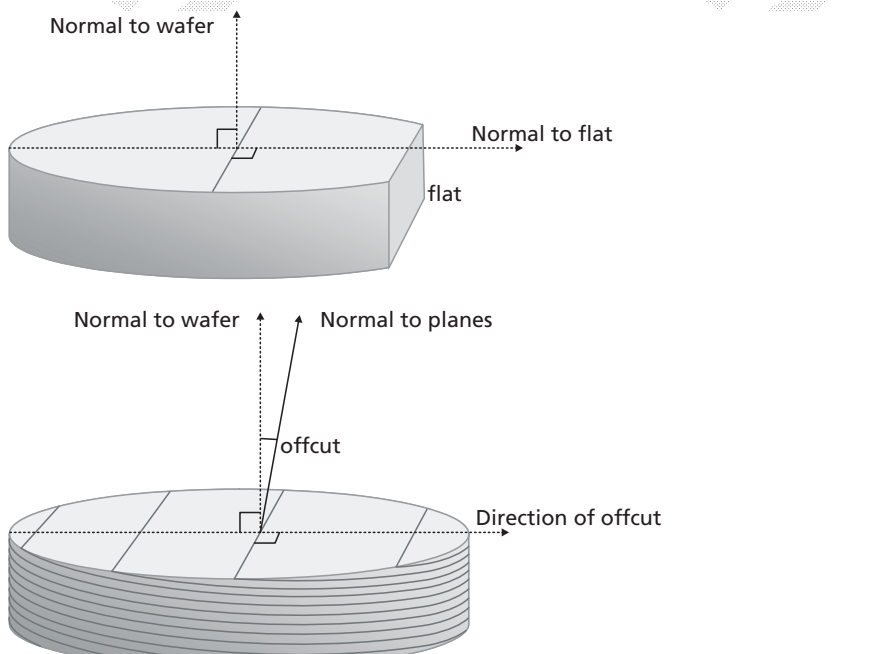


Figure 24: Diagram of a wafer (exaggerated thickness) showing the flat, the normal to the flat and normal to the wafer (top) and the direction of offcut and the angle of offcut of the surface with respect to the near-surface planes (bottom).

2.1.2.3 Azimuths on wafers

In this context, the term 'azimuth' refers to the trace of the diffraction plane across the wafer. The surface of the wafer is usually parallel to the sample stage. Different 'azimuths' are investigated by rotation of the wafer about its sample normal which also coincides with the phi axis, as illustrated in Figure 25.

Finding the correct azimuth position in order to do a measurement is an important part of the alignment process and requires that the major crystallographic directions in the sample are either previously known (for example by the positioning of 'flats' on the wafer by the substrate manufacturer) or are ascertained from a series of phi scans on the diffractometer.

The crystal symmetry determines how many unique azimuths can be investigated by diffraction. For example in a $[0001]$ oriented GaN wafer similar azimuths are each repeated with sixfold symmetry around the $\langle 0001 \rangle$ direction. There are two major azimuth types, containing the plane normals to the $\{11\bar{2}0\}$ and $\{10\bar{1}0\}$ planes

respectively, and one minor azimuth type containing the plane normals to the {12-30} planes. These are illustrated in Figure 26.

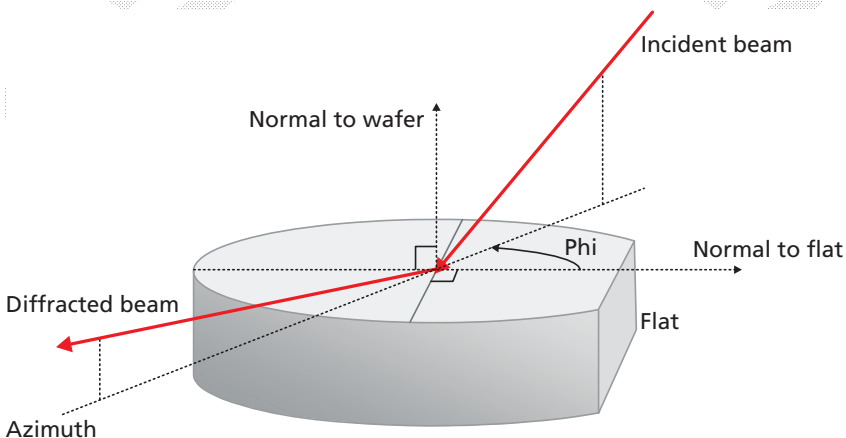


Figure 25: Diagram of a wafer (exaggerated thickness) showing the azimuth as the trace that the incident and diffracted beam makes on the wafer surface, measured as angle phi.

2.1.2.4 Planes and orientations in GaN epitaxial layers

When GaN grows on any substrate its orientation is determined by the orientation of the substrate. Good quality epitaxial GaN tends to grow with a reproducible orientation relationship to the substrate. When GaN grows on C-plane sapphire it grows with surface normal parallel to the <0001> direction. Within the interface plane the GaN <1-100> direction is parallel to the sapphire <2-1-10> direction. The in-plane *d*-spacing mismatch between the GaN and the sapphire substrate is too great for growth of a coherently strained interface and GaN is generally grown as a relaxed buffer layer or a 'virtual substrate' on the sapphire platform. Strained epitaxial layers of InGaN and AlGaN are then grown coherently on the GaN buffer layers.

Figure 26 shows a schematic representation of the plane normals for a GaN layer illustrating the sets of planes that are commonly measured using XRD. The wafer has a sixfold symmetry, there are 6 azimuths along which we can expect to measure diffraction from the same types of planes.

GaN is most commonly an hexagonal crystal with the wurtzite crystal structure. It is a polar crystal with the polar axis parallel to the <0001> direction. This polarity can have an effect on the properties of devices. Attempts are made to avoid this by growing more exotic epitaxial orientations for example:

{11-22} plane grown on M-plane sapphire produces semi-polar films

{11-20} A-plane GaN grown on R-plane sapphire has no polarity normal to the surface.

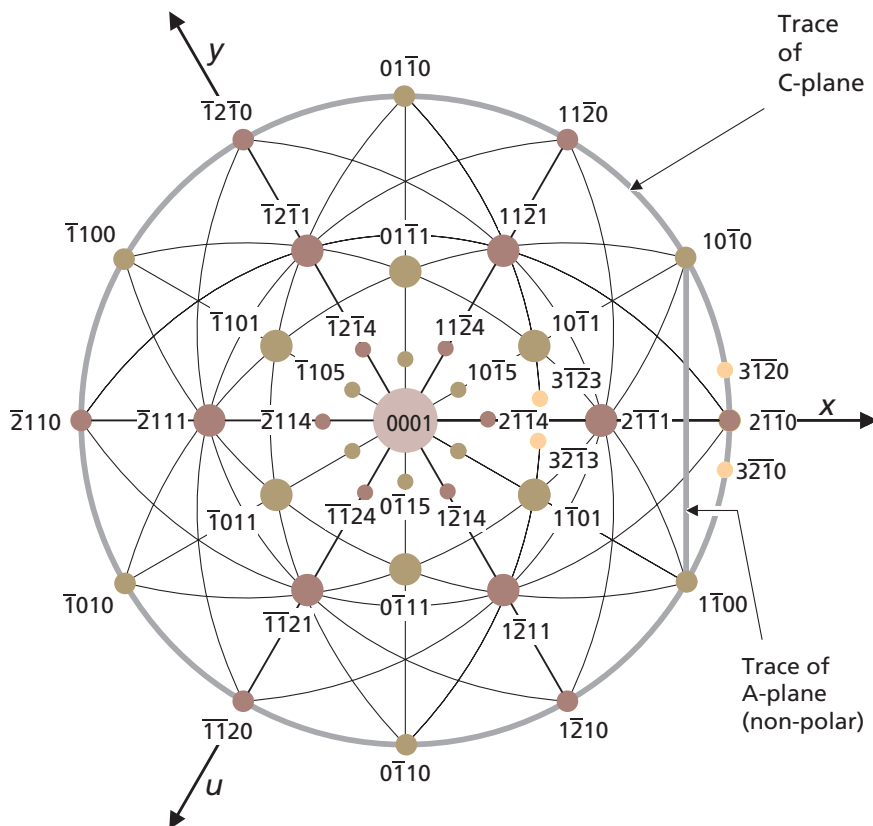


Figure 26: Schematic stereographic projection (i.e. not to scale) of hexagonal GaN with the [0001] direction normal to the image, showing the normals to the useful planes for XRD analysis (spots) and traces of common growth surfaces (solid grey lines)

GaN can also grow in the cubic form. When grown on {0001} oriented sapphire wafers the cubic {111} plane is parallel to the surface. The stereographic projection of the GaN layer is similar to that for the Si{111} oriented substrate (see Figure 23).

2.2 Elasticity theory and distortion coefficients

The unit cell of an epitaxial layer may be distorted to fit the atomic template of the surface layer upon which it is grown. The basic principle of X-ray methods for measuring strain and composition of alloy layers is to measure a d -spacing within the layer and relate it to the value it is known to have in the bulk or 'relaxed' state. To do this requires an understanding of the lattice distortions that accompany epitaxial layer growth. For well behaved materials the distortions are assumed to be biaxial, regular and homogeneous throughout a layer. If this is the case

then simplifying assumptions can be made about the strain state of the material removing the need to make too many measurements and calculations.

2.2.1 Layer orientation

In the analysis of epitaxial thin films the layers are described here as having a small dimension in the z direction and a practically infinite dimension along both x and y. The film may have an epitaxial relationship with the substrate, in which case measurements of the substrate structure may be used in the subsequent analysis of the film. The film may have no epitaxial relationship with the substrate, the role of the substrate being simply to support the film, in which case the film will be analysed independently of the substrate.

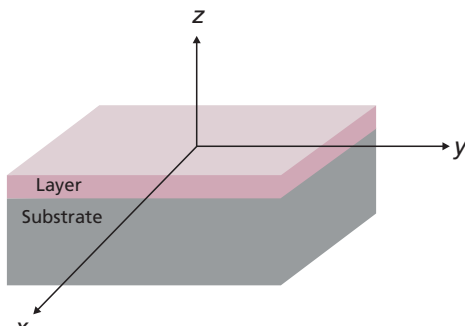


Figure 27: For analysis of epitaxial layers the axes x, y and z must be defined with respect to the sample. z is usually normal to the layer-substrate interface. x and y are parallel to the interface. Where possible, x, y and z are parallel to major crystallographic axes.

For the analysis the x, y, and z axes must be defined. Since the sample surface is used for alignment of the diffractometer it is most convenient to define z as the surface normal. x and y are therefore in the plane of the surface. Various convenient simplifying assumptions are commonly used:
If the film has uniform thickness then the x-y plane also corresponds to the interface plane.
If the film has uniform thickness and the surface corresponds to a crystallographic plane then x, y and z can correspond to important crystallographic directions in the layer

2.2.2 Stresses in the film

Due to some registry with the substrate, the films are subjected to biaxial stresses, σ_x and σ_y (this is sometimes termed 'interface stress' or 'misfit stress'). The most common simplifying assumption then made is that the interface is perfectly flat over a long range (i.e. no curvature) in which case the axial stress $\sigma_z = 0$, and the shear stresses, $\tau_{xy} = \tau_{yx} = \tau_{xz} = \tau_{zx} = \tau_{yz} = \tau_{zy} = 0$.

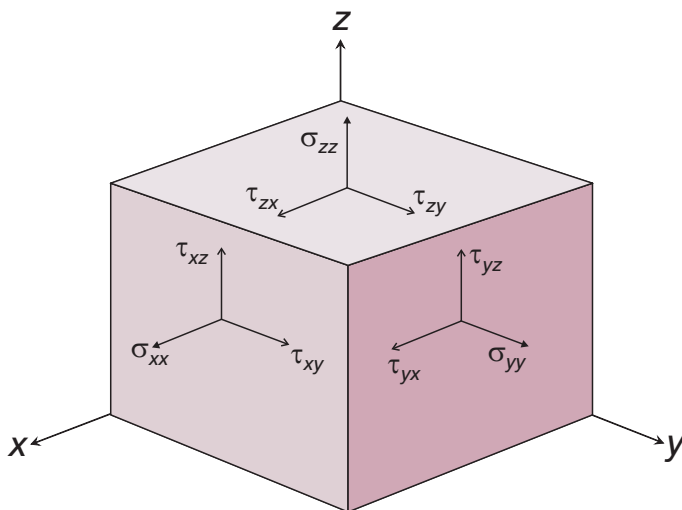


Figure 28: Stresses in the film are defined with respect to the x, y and z axes.

2.2.3 Strains in the film

In epitaxial layers the misfit stresses produce biaxial elastic strains in the unit cell, where the in-plane unit cell dimensions of the layer are forced to register with the unit cell of the substrate. There are three descriptions that are commonly used to describe the strain state of the layer:

Unstrained or ‘fully relaxed’: In this state the principal strains in the film are zero. Whilst the layer unit cell may retain an orientation relationship with the substrate the dimensions, d_x , d_y and d_z of the layer unit cell maintain their bulk or ‘relaxed’ values, d_{xr} , d_{yr} and d_{zr} .

Fully strained or ‘coherently epitaxial’: In this state the layer is in total registry with the substrate across the layer/substrate interface. The layer suffers strain parallel to the interface. The in-plane unit cell dimensions, d_x and d_y , of the layer are the same as those of the substrate, d_x^s and d_y^s . There is no stress perpendicular to the interface, but the unit cell is distorted in that direction due to the Poisson effect and so the out of plane dimension, d_z is different from the layer relaxed value, d_{zr} .

Residually strained also known as ‘partially coherent’ or ‘partially relaxed’: In this state the layer is between being fully strained and unstrained. The d_x , d_y and d_z dimensions of the layer unit cell are equal to neither the substrate dimensions nor the bulk values for the layer.

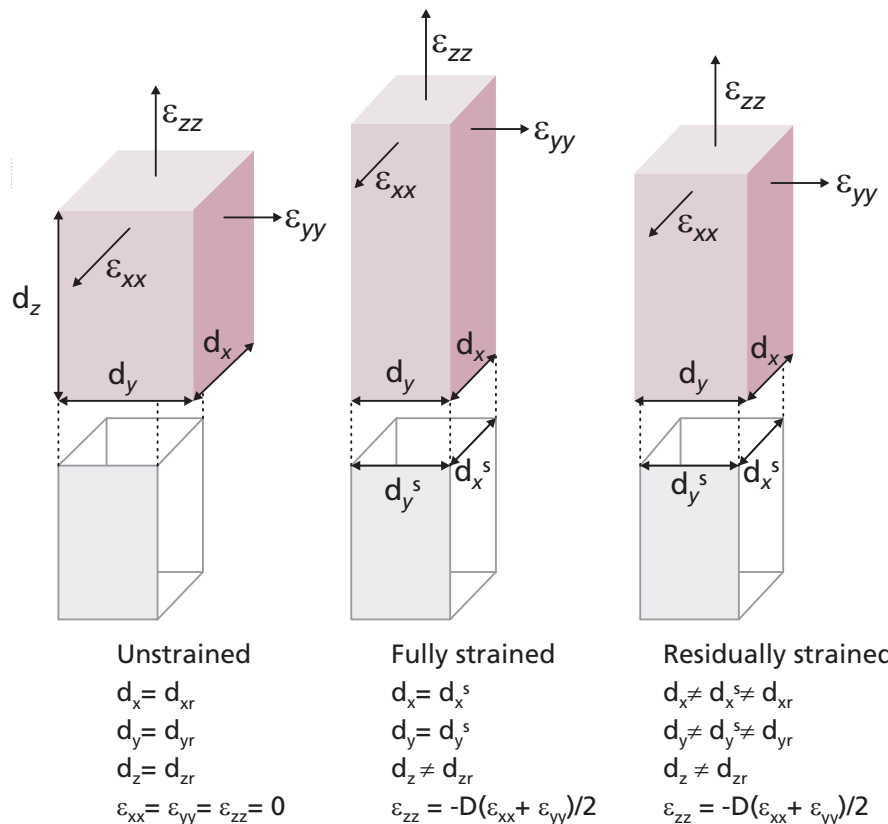


Figure 29: Strains in the film are defined with respect to the principal stresses and suitable d -spacings are chosen for measurement. By considering the bulk unit cells of the alloy layers and the unit cells of the substrates, the layers are defined as unstrained, fully strained or residually strained.

2.2.4 Fundamental elasticity equations for single crystals

2.2.4.1 General form

The most general forms for the elasticity relations are^{4,5}:

$$\sigma = c_{ijkl} e_{kl} \quad \text{and} \quad e_{ij} = S_{ijkl} \sigma_{kl} \quad (1)$$

The constants c_{ijkl} and S_{ijkl} are called the stiffness constants and compliances respectively. All stress-strain calculations can be carried out using equations (1), however, the stress and strain (second rank) tensors have each 9 components and the stiffness and compliance (forth rank) tensors have 81 components which

together create lengthy calculations. The stress and strain tensors are symmetric ($\sigma_{ij} = \sigma_{ji}$, etc.) and the calculation can be simplified by taking account of the symmetry using the Voigt⁶ notation which reduces the number of independent strain and stress components to 6 and the number of independent compliances and stiffness components to 36 as follows:

PANalytical

$$\begin{bmatrix} \sigma_x & \tau_{xy} & \tau_{xz} \\ \tau_{yx} & \sigma_y & \tau_{yz} \\ \tau_{zx} & \tau_{zy} & \sigma_z \end{bmatrix} \rightarrow \begin{bmatrix} \sigma_{xx} & \sigma_{xy} & \sigma_{xz} \\ \sigma_{xy} & \sigma_{yy} & \sigma_{yz} \\ \sigma_{xz} & \sigma_{yz} & \sigma_{zz} \end{bmatrix} \rightarrow \begin{bmatrix} \sigma_{xx} \\ \sigma_{yy} \\ \sigma_{zz} \\ \sigma_{yz} \\ \sigma_{zx} \\ \sigma_{xy} \end{bmatrix} \equiv \begin{bmatrix} \sigma_1 \\ \sigma_2 \\ \sigma_3 \\ \sigma_4 \\ \sigma_5 \\ \sigma_6 \end{bmatrix} \quad (2)$$

and

$$\begin{bmatrix} e_x & e_{xy} & e_{xz} \\ e_{yx} & e_y & e_{yz} \\ e_{zx} & e_{zy} & e_z \end{bmatrix} \rightarrow \begin{bmatrix} e_{xx} & 2e_{xy} & 2e_{xz} \\ 2e_{xy} & e_{yy} & 2e_{yz} \\ 2e_{xz} & 2e_{yz} & e_{zz} \end{bmatrix} \rightarrow \begin{bmatrix} e_{xx} \\ e_{yy} \\ e_{zz} \\ 2e_{yz} \\ 2e_{zx} \\ 2e_{xy} \end{bmatrix} \equiv \begin{bmatrix} \varepsilon_1 \\ \varepsilon_2 \\ \varepsilon_3 \\ \varepsilon_4 \\ \varepsilon_5 \\ \varepsilon_6 \end{bmatrix} \quad (3)$$

Note that the strain and stress tensors have become matrices. The factors of 2 appear in the strain matrices because the equation in (1) has reduced to $\sigma_j = c_{jk}\varepsilon_k$. (In the full tensor notation for example, σ_{11} would include two equivalent components, $c_{1121}e_{21}$ and $c_{1112}e_{12}$, which have now to be accounted for in one component). The stiffness constants can be written in the form of matrices with 36 numbers comprising 21 independent terms. The general elasticity equation becomes:

$$\begin{bmatrix} \sigma_1 \\ \sigma_2 \\ \sigma_3 \\ \sigma_4 \\ \sigma_5 \\ \sigma_6 \end{bmatrix} = \begin{bmatrix} C_{11} & C_{12} & C_{13} & C_{14} & C_{15} & C_{16} \\ C_{12} & C_{22} & C_{23} & C_{24} & C_{25} & C_{26} \\ C_{13} & C_{23} & C_{33} & C_{34} & C_{35} & C_{36} \\ C_{14} & C_{24} & C_{34} & C_{44} & C_{45} & C_{46} \\ C_{15} & C_{25} & C_{35} & C_{45} & C_{55} & C_{56} \\ C_{16} & C_{26} & C_{36} & C_{46} & C_{56} & C_{66} \end{bmatrix} \begin{bmatrix} \varepsilon_1 \\ \varepsilon_2 \\ \varepsilon_3 \\ \varepsilon_4 \\ \varepsilon_5 \\ \varepsilon_6 \end{bmatrix} \quad (4)$$

In the following text the equivalences, $\sigma_1 = \sigma_{xx}$, $\sigma_2 = \sigma_{yy}$, $\sigma_3 = \sigma_{zz}$, $\varepsilon_1 = \varepsilon_{xx}$, $\varepsilon_2 = \varepsilon_{yy}$ and $\varepsilon_3 = \varepsilon_{zz}$ are observed.

The equation in terms of compliances can be derived in a similar manner (see also ⁷).

By considering the symmetry elements in crystal structures, it becomes apparent that some values for c_{ij} (and s_{ij}) must be zero and others must be equivalent. The forms of the (s_{ij}) and (c_{ij}) matrices for the different crystal classes are given in Ref 5. The c_{ij} matrices for cubic and hexagonal are given below.

2.2.4.2 Stiffness constants for cubic crystals

By convention, the primary axes correspond to major symmetry axes. For example for the cubic system, c_{11} is parallel to [100] $\equiv x$, c_{22} is parallel to [010] $\equiv y$ and c_{33} is parallel to [001] $\equiv z$.

$$c_{ij}(\text{cubic}) = \begin{pmatrix} c_{11} & c_{12} & c_{12} & 0 & 0 & 0 \\ c_{12} & c_{11} & c_{12} & 0 & 0 & 0 \\ c_{12} & c_{12} & c_{11} & 0 & 0 & 0 \\ 0 & 0 & 0 & c_{44} & 0 & 0 \\ 0 & 0 & 0 & 0 & c_{44} & 0 \\ 0 & 0 & 0 & 0 & 0 & c_{44} \end{pmatrix} \quad (5)$$

2.2.4.3 Stiffness constants for hexagonal crystals

For hexagonal systems the major crystal axes do not correspond to the Cartesian axes, x , y , z . By convention⁸, the definition of the axes has been fixed such that c_{33} is parallel to the major hexad axis [0001] $\equiv z$. The sense of c_{11} is parallel to [2-1-10] $\equiv x$. Therefore the sense of c_{22} is parallel to [01-10] $\equiv y$.

$$c_{ij}(\text{hexagonal}) = \begin{pmatrix} c_{11} & c_{12} & c_{13} & 0 & 0 & 0 \\ c_{12} & c_{11} & c_{13} & 0 & 0 & 0 \\ c_{13} & c_{13} & c_{33} & 0 & 0 & 0 \\ 0 & 0 & 0 & c_{44} & 0 & 0 \\ 0 & 0 & 0 & 0 & c_{44} & 0 \\ 0 & 0 & 0 & 0 & 0 & \frac{1}{2}(c_{11} - c_{12}) \end{pmatrix} \quad (6)$$

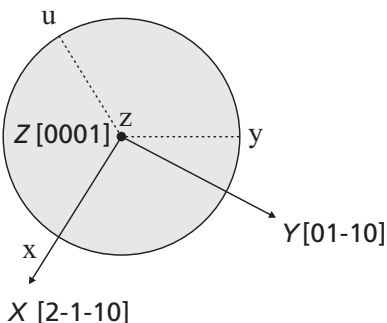


Figure 30: Orthogonal cartesian axes X , Y and Z compared to the crystallographic axes for the hexagonal structure: x , y , u and z

2.2.4.4 Stiffness constants for an isotropic material

The form of the matrix for a completely isotropic material is obtained from the cubic matrix by requiring that the components should be unaltered by rotations of 45° about the reference axes⁵.

$$isotropic = \begin{pmatrix} C_{11} & C_{12} & C_{12} & 0 & 0 & 0 \\ C_{12} & C_{11} & C_{12} & 0 & 0 & 0 \\ C_{12} & C_{12} & C_{11} & 0 & 0 & 0 \\ 0 & 0 & 0 & \frac{1}{2}(C_{11} - C_{12}) & 0 & 0 \\ 0 & 0 & 0 & 0 & \frac{1}{2}(C_{11} - C_{12}) & 0 \\ 0 & 0 & 0 & 0 & 0 & \frac{1}{2}(C_{11} - C_{12}) \end{pmatrix} \quad (7)$$

2.2.5 Simplifying for biaxial strain in thin layers

In general for a layer $\sigma_{zz} = 0$, and the shear stresses, τ_{xy} , τ_{xz} and $\tau_{yz} = 0$, also the shear strains ε_{zy} , ε_{zx} and ε_{xy} can be assumed to be zero, so the general form of the stress-strain relationship in equation (4) is simplified to:

$$\begin{pmatrix} \sigma_{xx} \\ \sigma_{yy} \\ 0 \\ 0 \\ 0 \\ 0 \end{pmatrix} = \begin{pmatrix} C_{11} & C_{12} & C_{13} & C_{14} & C_{15} & C_{16} \\ C_{12} & C_{22} & C_{23} & C_{24} & C_{25} & C_{26} \\ C_{13} & C_{23} & C_{33} & C_{34} & C_{35} & C_{36} \\ C_{14} & C_{24} & C_{34} & C_{44} & C_{45} & C_{46} \\ C_{15} & C_{25} & C_{35} & C_{45} & C_{55} & C_{56} \\ C_{16} & C_{26} & C_{36} & C_{46} & C_{56} & C_{66} \end{pmatrix} \begin{pmatrix} \varepsilon_{xx} \\ \varepsilon_{yy} \\ \varepsilon_{zz} \\ 0 \\ 0 \\ 0 \end{pmatrix} \quad (8)$$



Because it is assumed that $\sigma_{zz}=0$ the third equation in the matrix can be used to solve for the strain relationship namely:

$$0 = C_{13}\varepsilon_{xx} + C_{23}\varepsilon_{yy} + C_{33}\varepsilon_{zz} \quad (9)$$

thus

$$\varepsilon_{zz} = -\frac{(C_{13}\varepsilon_{xx} + C_{23}\varepsilon_{yy})}{C_{33}} \quad (10)$$

2.2.5.1 Cubic (001) orientation

For the cubic₀₀₁ system, for an (001) oriented thin film, $c_{13} = c_{23} = c_{12}$ also $c_{33} = c_{11}$ and so equation (9) is simplified to:

$$0 = C_{12}\varepsilon_{xx} + C_{12}\varepsilon_{yy} + C_{11}\varepsilon_{zz} \quad (11)$$

Thus

$$\varepsilon_{zz} = -\frac{2C_{12}}{C_{11}}(\varepsilon_{ave}) \quad (12)$$

where

$$\varepsilon_{ave} = \frac{(\varepsilon_{xx} + \varepsilon_{yy})}{2} \quad (13)$$

2.2.5.2 Cubic (111) orientation

For other cubic orientations i.e. to transform to other axes, the most rigorous method is to go back to the tensor notation in equation (1) and perform the appropriate rotations. Some solutions have been provided for other orientations^{9,10} notably for the orientation [111] = z in the cubic system where:

$$cubic_{111} = \begin{pmatrix} c_{11} & c_{12} & c_{12} & 0 & 0 & 0 \\ c_{12} & c_{11} & c_{12} & 0 & 0 & 0 \\ c_{12} & c_{12} & c_{11} & 0 & 0 & 0 \\ 0 & 0 & 0 & c_{44} & 0 & 0 \\ 0 & 0 & 0 & 0 & c_{44} & 0 \\ 0 & 0 & 0 & 0 & 0 & c_{44} \end{pmatrix} + C \begin{pmatrix} \frac{1}{2} & -\frac{1}{6} & -\frac{1}{3} & 0 & \frac{1}{3\sqrt{2}} & 0 \\ -\frac{1}{6} & \frac{1}{2} & -\frac{1}{3} & 0 & -\frac{1}{3\sqrt{2}} & 0 \\ -\frac{1}{3} & -\frac{1}{3} & \frac{2}{3} & 0 & 0 & 0 \\ 0 & 0 & 0 & -\frac{1}{3} & 0 & -\frac{1}{3\sqrt{2}} \\ \frac{1}{3\sqrt{2}} & -\frac{1}{3\sqrt{2}} & 0 & 0 & -\frac{1}{3} & 0 \\ 0 & 0 & 0 & -\frac{1}{3\sqrt{2}} & 0 & -\frac{1}{6} \end{pmatrix} \quad (14)$$

Where the anisotropy factor, $C = (2c_{44} - c_{11} + c_{12})$.

Considering the simplification for biaxial strains, as in equation (9) leads to the relation:

$$\varepsilon_{zz} = -\left(\frac{2c_{12} - \frac{2C}{3}}{c_{11} + \frac{2C}{3}}\right)(\varepsilon_{ave}) \quad (15)$$

Which, when substituting for C gives:

$$\varepsilon_{zz} = -\left(\frac{2c_{11} + 4c_{12} - 4c_{44}}{c_{11} + 2c_{12} + 4c_{44}}\right)(\varepsilon_{ave}) \quad (16)$$

2.2.5.3 Hexagonal (0001) orientation

Similarly for the hexagonal₀₀₀₁ system, for an (0001) oriented thin film, $c_{13} = c_{23}$ and so equation (9) is simplified to:

$$0 = C_{13}\varepsilon_{xx} + C_{13}\varepsilon_{yy} + C_{33}\varepsilon_{zz} \quad (17)$$

Thus

$$\varepsilon_{zz} = -\frac{2C_{13}}{C_{33}}(\varepsilon_{ave}) \quad (18)$$

where

$$\varepsilon_{ave} = \frac{(\varepsilon_{xx} + \varepsilon_{yy})}{2} \quad (19)$$

2.2.6 Fundamental elasticity equations for general isotropic layers (engineering)

The engineering isotropic approximations for a material are the simplest elasticity equations, and are used for a more empirical approach assuming that a material's stiffness can be measured experimentally and without reference to its microstructure. They are often used for uniformly random polycrystalline materials. The assumption that the material's response to applied stress is the same for all directions gives the result that the principal strains are in the same directions as the principal stresses and hence the elasticity stress and strain tensors can be simplified considerably. Some single crystal layers have to be treated as isotropic engineering components when their crystalline c_{ij} stiffness tensor is not known. The general

stress-strain equations for isotropic materials are given in various forms (see basic texts on elasticity^{11,12}). The stress tensor is given in terms of the strain tensor by:

$$\sigma_{ik} = \frac{E}{1+\nu} \left(\varepsilon_{ik} + \frac{\nu}{1-2\nu} \varepsilon_{ii} \delta_{ik} \right) \quad (20)$$

PANalytical

PANalytical

Where E is Young's modulus and ν is Poisson's ratio¹³, for the layer material. This expands to give 6 independent equations:

$$\sigma_{xx} = \frac{E}{(1+\nu)(1-2\nu)} [(1-\nu)\varepsilon_{xx} + \nu(\varepsilon_{yy} + \varepsilon_{zz})] \quad (21)$$

$$\sigma_{yy} = \frac{E}{(1+\nu)(1-2\nu)} [(1-\nu)\varepsilon_{yy} + \nu(\varepsilon_{xx} + \varepsilon_{zz})] \quad (22)$$

$$\sigma_{zz} = \frac{E}{(1+\nu)(1-2\nu)} [(1-\nu)\varepsilon_{zz} + \nu(\varepsilon_{xx} + \varepsilon_{yy})] \quad (23)$$

$$\tau_{xy} = \frac{E}{1+\nu} \varepsilon_{xy}, \quad \tau_{xz} = \frac{E}{1+\nu} \varepsilon_{xz}, \quad \tau_{xz} = \frac{E}{1+\nu} \varepsilon_{xz} \quad (24)$$

The remaining three equations are equivalent to (24) because $\tau_{xy} = \sigma_{xy} = \sigma_{yx}$, $\tau_{xz} = \sigma_{xz} = \sigma_{zx}$, $\tau_{yz} = \sigma_{yz} = \sigma_{zy}$.

2.2.7 Simplifying for biaxial strain in isotropic thin layers

For the case of $\sigma_{zz} = 0$, equation (23) can be used to obtain the following strain relation:

$$\varepsilon_{zz} = -\frac{\nu}{(1-\nu)} (\varepsilon_{xx} + \varepsilon_{yy}) \quad (25)$$

or

$$\varepsilon_{zz} = -\frac{2\nu}{(1-\nu)} (\varepsilon_{ave}) \quad (26)$$

The term $-2\nu/(1-\nu)$ is sometimes referred to as a 'biaxial Poisson ratio'.

PANalytical

PANalytical

2.2.8 The distortion coefficient, D

A general 'distortion coefficient' for thin films, D, is given by:

$$D = -\frac{\varepsilon_{zz}}{\varepsilon_{ave}} \quad (27)$$

Some expressions for D are presented in the table below.

Table 1. Equations for the distortion coefficient, D, for biaxial stress in the x-y plane (isotropic materials and selected crystal structures and crystal orientations)

Crystal system and layer orientation	Cubic 001	Cubic 111	Hexagonal 0001	Isotropic (crystal)	Isotropic (engineering)
D	$\frac{2c_{12}}{c_{11}}$	$\frac{2c_{11} + 4c_{12} - 4c_{44}}{c_{11} + 2c_{12} + 4c_{44}}$	$\frac{2c_{13}}{c_{33}}$	$\frac{2c_{12}}{c_{11}}$	$\frac{2\nu}{(1-\nu)}$

For isotropic (engineering) materials a Poisson ratio, ν , needs to be obtained. For single crystals, both the matrix of the stiffness constants, c_{ijl} , and film orientation, hkl , must be known. Numerical values are obtained from databases compiling the known experimental and theoretical results for each crystal. Values for GaN and related compounds are being refined continually. Some examples of well used values are presented in the table below. Sometimes, for ease of use, the engineering equations for isotropic thin films are used for semiconductor single crystal thin films, for this reason a value for the Poisson ratio is often stated although usually it has been derived from the single crystal stiffness constants.

Table 2. Some values for the distortion coefficients for GaN and related compounds¹⁴

Material	ν (0001) ¹⁵	c_{11} (GPa)	c_{12} (GPa)	c_{13} (GPa)	c_{33} (GPa)	c_{44} (GPa)
GaN (hexagonal)	0.203	390	145	106	398	105
AlN (hexagonal)	0.225	345	125	120	395	118
InN (hexagonal)	0.291	190	104	121	182	10
GaN (cubic)	-	293	159	-	-	155
AlN (cubic)	-	304	160	-	-	193
InN (cubic)	-	187	125	-	-	86

It is possible that the uncertainties involved in the experiment and analysis may outweigh the necessity to calculate D precisely and that a value in the range 0.5 to 1 will suffice.

2.2.9 Strain equations for low symmetry orientations

Solutions for D for the crystal systems in the high symmetry (001), (0001) and (111) orientations are possible because $\varepsilon_{xx} = \varepsilon_{yy}$. The elasticity equations for any general crystallographic orientation can be obtained but may be mathematically quite complicated. Below are presented two of the more accessible strain relations based on considerations of equivalent directions. The following two simplified

solutions can be made because for the orientations stated the principal axes used for defining stiffness in the crystal are still coincident with the orthogonal x, y, z axes used as the major strain axes. Other orientations require more general applications of the elasticity equations and are not presented here.

2.2.9.1 Simplified strain equation for (01-10) oriented GaN

In this orientation the x direction is equivalent to [0001], y direction is equivalent to [2-1-10] and z direction is equivalent to [01-10].

Start from equation (8) that is assuming that there is no stress perpendicular to the film and no shear strains within the film:

$$\begin{pmatrix} \sigma_{xx} \\ \sigma_{yy} \\ 0 \\ 0 \\ 0 \\ 0 \end{pmatrix} = C_{ij} \begin{pmatrix} \varepsilon_{xx} \\ \varepsilon_{yy} \\ \varepsilon_{zz} \\ 0 \\ 0 \\ 0 \end{pmatrix} \quad (28)$$

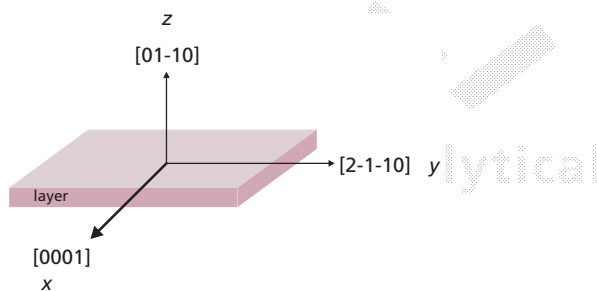


Figure 31: Orthogonal cartesian axes x , y and z defined for (01-10) oriented GaN layers

But this time introduce a general stiffness matrix with axes defined relative to the layer orientation:

$$C'_{ij} = \begin{pmatrix} C'_{11} & C'_{12} & C'_{13} & C'_{14} & C'_{15} & C'_{16} \\ C'_{12} & C'_{22} & C'_{23} & C'_{24} & C'_{25} & C'_{26} \\ C'_{13} & C'_{23} & C'_{33} & C'_{34} & C'_{35} & C'_{36} \\ C'_{14} & C'_{24} & C'_{34} & C'_{44} & C'_{45} & C'_{46} \\ C'_{15} & C'_{25} & C'_{35} & C'_{45} & C'_{55} & C'_{56} \\ C'_{16} & C'_{26} & C'_{36} & C'_{46} & C'_{56} & C'_{66} \end{pmatrix} \quad (29)$$

As before, the third equation in the matrix is used:

$$0 = C'_{13} \varepsilon_{xx} + C'_{23} \varepsilon_{yy} + C'_{33} \varepsilon_{xx} \quad (30)$$

Which re-arranges to give:




$$\varepsilon_{zz} = -\frac{1}{C'_{33}} (C'_{13} \varepsilon_{xx} + C'_{23} \varepsilon_{yy}) \quad (31)$$

However, in this matrix:

- C'_{11} is the stiffness constant along [0001] which is the same as the old C_{33}
- C'_{22} is the stiffness constant along [2-1-10] which is the same as the old C_{11}
- C'_{33} is the stiffness constant along [01-10] which is the same as the old C_{22} and for the hexagonal system this is equivalent to C_{11}
- C'_{13} is the stiffness value relating to [0001] and [01-10] and is the same as the old C_{23} which is the same as the old C_{13} by symmetry of the hexagonal crystal
- C'_{23} is the stiffness value relating to [2-1-10] and [01-10] and is the same as the old C_{12}

So in terms of the conventional axes and the conventional C_{ij} values:



$$\varepsilon_{zz} = -\frac{1}{C_{11}} (C_{13} \varepsilon_{xx} + C_{12} \varepsilon_{yy}) \quad (32)$$

The equation cannot be simplified further into one single distortion coefficient, D.

2.2.9.2 Simplified strain equation for (2-1-10) oriented GaN

This orientation is grown often on R-plane sapphire. In this orientation the x direction is equivalent to [0001], y direction is equivalent to [0-110] and z direction is equivalent to [2-1-10].

As before, the third equation in the matrix is used:

$$0 = C'_{13} \varepsilon_{xx} + C'_{23} \varepsilon_{yy} + C'_{33} \varepsilon_{xx} \quad (33)$$

Which re-arranges to give:




$$\varepsilon_{zz} = -\frac{1}{C'_{33}} (C'_{13} \varepsilon_{xx} + C'_{23} \varepsilon_{yy}) \quad (34)$$

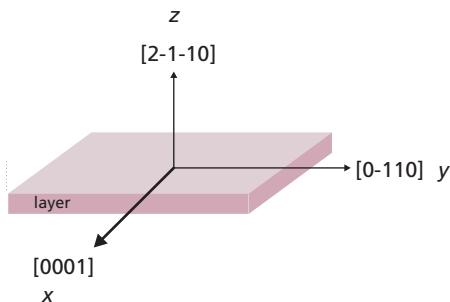


Figure 32: Orthogonal cartesian axes x , y and z defined for (2-1-10) oriented GaN layers

However, in this matrix:

C'_{11} is the stiffness constant along [0001] which is the same as the old C_{33}

C'_{22} is the stiffness constant along [01-10] which is the same as the old C_{22}

C'_{33} is the stiffness constant along [2-1-10] which is the same as the old C_{11}

C'_{13} is the stiffness value relating to $[0001]^*[2-1-10]$ and is the same as the old C_{13}

C'_{23} is the stiffness value relating to $[1-100]^*[2-1-10]$ and is the same as the old C_{12}

So in terms of the conventional axes and the conventional C_{ij} values:

$$\varepsilon_{zz} = -\frac{1}{C_{11}}(C_{13}\varepsilon_{xx} + C_{12}\varepsilon_{yy}) \quad (35)$$



2.2.10 Error and assumptions

2.2.10.1 High strains

The elasticity relations used here all assume Hooke's law i.e. that the materials are strained in the linear regime. There may be some errors associated with this assumption. It is known, that for some materials, the linear elastic limit may be exceeded before the elastic limit (limit of reversible strain) is reached. In which case, for high stresses and strains, analysis based on linear elastic theory may be insufficient. Semiconductor strained layers frequently exhibit strains up to as much as 0.02, which are in excess of elastic strains usually observed in bulk materials.



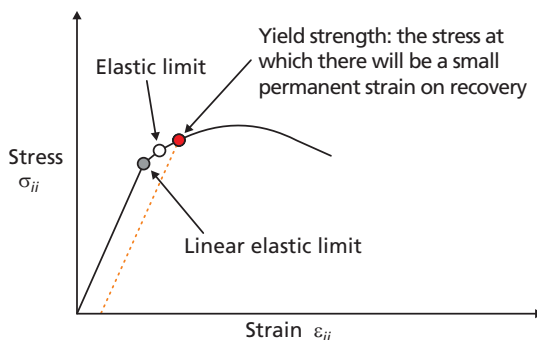


Figure 33: Illustration of typical stress strain curve showing linear elastic limit, elastic limit and beyond.

2.2.10.2 Imperfect material

Having obtained an expression for D it is necessary to obtain numerical values for the stiffness constants, c_{ij} , for the material of interest. These values are listed in databases and may have been obtained through experiment or theory. In either case there will always be a question over the validity of these values for the material being examined. For example, if the material is single crystal and of a poor quality, the concentration of point and line defects and impurities may be sufficient to change the numerical values of the stiffness constants (this may explain, for example, the wide range in c_{ij} values reported for GaN). It may be necessary to link the precision of the result to a measure of crystal quality, such as the Bragg peak FWHM. This will be, not only for the purpose of defining an error on the peak position, but also as an indicator of a 'confidence' value that can be associated with database values such as c_{ij} .

2.2.10.3 Textured layers

Some elasticity values may be required for strongly textured thin films. It will be necessary to define an appropriate distortion coefficient in each case. The material single crystal values may go some way towards providing an appropriate value for D , however it should be understood that without a more detailed understanding of the layer microstructure, the outcome of the analysis can only be approximate.

2.2.10.4 Ultra thin layers

Some thin films are extremely thin with thicknesses anything from a few unit cells down to one monolayer. There is a question over whether it is appropriate to use bulk parameters, such as stiffness constants, for very thin layers. It has been suggested that lattice constants can change by as much as 5% and elastic constants by more

than 50% in going from the bulk crystal to the monolayer¹⁶. Care must be taken in assigning high precision to calculations of composition etc. to such thin layers.

2.2.11 Principles for measurement of strains in thin films

The state of strain of the layer can be deduced by comparing the measured dimensions of the layer unit cell with database values for the bulk or relaxed unit cell. If the measured dimensions are denoted d_x , d_y , and d_z and the database values for the bulk are, d_{xr} , d_{yr} and d_{zr} , the strains are given by:

'perpendicular' strain

$$\varepsilon_{zz} = \frac{d_z - d_{zr}}{d_{zr}} \quad (36)$$

and 'parallel' or 'in-plane' strains are each

$$\varepsilon_{xx} = \frac{d_x - d_{xr}}{d_{xr}} \quad (37)$$

and

$$\varepsilon_{yy} = \frac{d_y - d_{yr}}{d_{yr}} \quad (38)$$

The task of the XRD experiment is to measure those crystal dimensions, d_x , d_y and d_z as precisely as possible.

The measurement of d_x , d_y and d_z , depends upon it being possible to find suitable planes for measurement. A plane is suitable for measurement of strain along a principal strain axis, if it is parallel to at least one of the other two principal strain axes. Figure 34 illustrates this for measurement of the spacing d_x that is parallel to ε_{xx} . If the plane is parallel to both of the other principal strain axes, ε_{yy} and ε_{zz} then the d -spacing measured is already in the sense of the principal strain axis. If the plane is parallel to only one of the other principal axes then the correct d_x value is the projection of the d -spacing onto that axis, namely:

$$d_x = \frac{d_{hkl}}{\sin \alpha} \quad (39)$$

Where

α is the inclination of the hkl plane with respect to ε_{xx} .

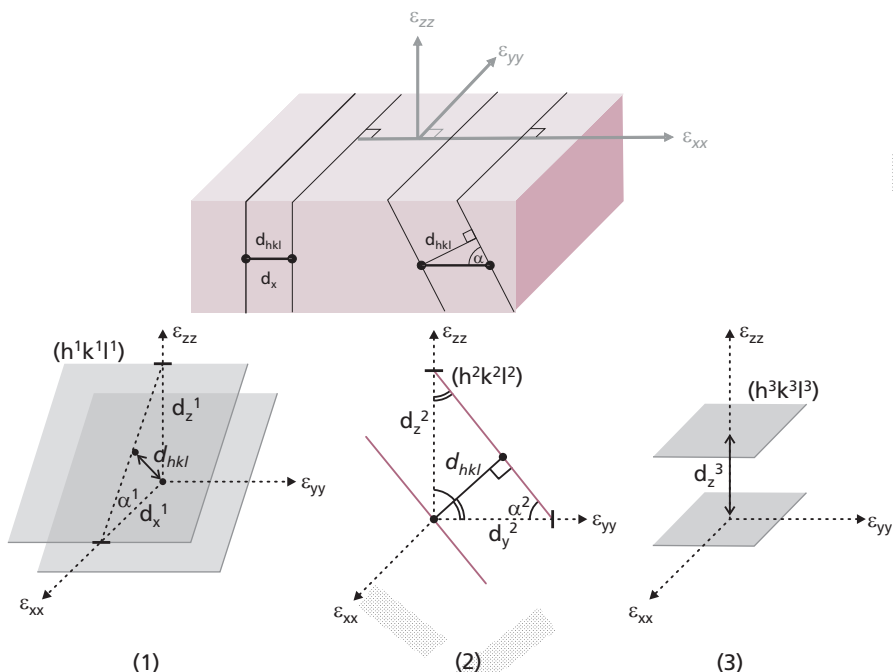


Figure 34: A plane spacing is suitable for measurement if the planes are parallel to at least one principal direction (top). For planes that are inclined with respect to principal directions the angle of inclination must be known and the plane spacings in the principal directions are calculated using trigonometry.

Figure 34 illustrates various possibilities for obtaining values d_x , d_y , and d_z . For planes that are parallel to only one principal axis there is the possibility of obtaining a second d -spacing value from the same measurements. For example, in both of the cases (1) and (2) a value for d_z can also be obtained using the equation:

$$d_z^1 = \frac{d_{h^1k^1l^1}}{\cos \alpha_1} \quad \text{for (1)} \quad (40)$$

$$d_z^2 = \frac{d_{h^2k^2l^2}}{\cos \alpha_2} \quad \text{for (2)} \quad (41)$$

A more direct measure of d_z is shown in Figure 34 (3).

Note that in each case the values d_x^n , d_y^n and d_z^n must remain referenced to their $(h^n k^n l^n)$ origins so that the corresponding database values for d_{x^n} , d_{y^n} and d_{z^n} can be found.

In some circumstances where it is considered through symmetry that $\varepsilon_{xx} = \varepsilon_{yy}$, it is common practice to perform calculations using ε_{ave} strain data from a single d_x measurement, rather than combining data from measurements of d -spacings along orthogonal ε_{xx} and ε_{yy} axes. This can considerably speed up measurement times.

In Chapter 3 some practical steps towards precise measurements of d -spacings and their angles of inclination, will be described.

2.2.11.1 Choice of (hkl) planes for (0001) oriented hexagonal GaN layers

As an example Figure 31 illustrates that in order to measure the appropriate d -spacings for strain calculations in (0001) oriented hexagonal GaN layers planes have to be found whose normals are along the azimuths containing [2-1-10] for ε_{xx} and [01-10] for ε_{yy} . Typical choices for appropriate planes in XRD reflection geometry are the (2-1-14) planes and (01-15) planes respectively. Values for d_z can also be obtained from these planes or alternatively from a surface symmetric reflection such as from (0002) as shown in Figure 35. Higher order reflections e.g. (0004) and (20-24) may be less intense but can provide improved strain resolution.

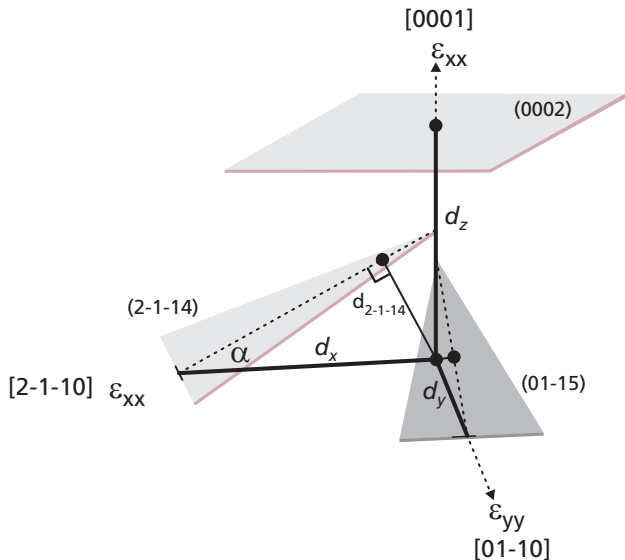


Figure 35: Typically in (0001) oriented GaN, plane spacings for (2-1-14), (01-15) and (0002) are used to measure ε_{xx} , ε_{yy} and ε_{zz} respectively.

2.2.12 Calculation of composition of thin films using Vegard's law

Strained epitaxial layers with different compositions are grown by alloying two binary compounds. The compounds that can be alloyed to form a homogeneous layer are those that form continuous solid solutions that are stable against dissociation into heterogeneous phases. The relative proportions of alloys that can be mixed depend on the solubility of one binary in the other. For example in an alloy such as $\text{In}_x\text{Ga}_{(1-x)}\text{N}$, all of the N sites in the crystal lattice are occupied by nitrogen atoms. A fraction, X, of the Ga sites are occupied by indium atoms and the remaining $(1-X)$ Ga sites are occupied by gallium atoms. The bulk unit cell of InN is larger than that of GaN. When In atoms are randomly distributed it is expected that the $\text{In}_x\text{Ga}_{(1-x)}\text{N}$ unit cell will have a size that is somewhere between the values of the two binaries. In fact Vegard's law, which is used here, assumes that the unit cell dimensions scale in proportion to the fraction of sites that are occupied by the alloying binary¹⁷. This means that for an alloy $\text{In}_x\text{Ga}_{(1-x)}\text{N}$ a d-spacing in the bulk crystal, d_r is given by:

$$d_r^X = X(d_r^{\text{InN}} - d_r^{\text{GaN}}) + d_r^{\text{GaN}} \quad (42)$$

This relation is more often expressed in terms of unit cell lattice parameters, a and c:

$$a^X = X(a^{\text{InN}} - a^{\text{GaN}}) + a^{\text{GaN}} \quad (43)$$

And

$$c^X = X(c^{\text{InN}} - c^{\text{GaN}}) + c^{\text{GaN}} \quad (44)$$

In a more general form, for an alloy $A_xB_{(1-x)}C$ made from components AC and BC:

$$d_r^X = X(d_r^{\text{AC}} - d_r^{\text{BC}}) + d_r^{\text{BC}} \quad \text{and so on.} \quad (45)$$

If the composition of a layer, X, is unknown, then the expressions for ε_{xx} , ε_{yy} and ε_{zz} shown in the previous section, 2.2.9 can not be solved individually, because the bulk values d_r^X etc. are not known.

To solve for X, the strain equations are combined with Vegard's law and rearranged. There are many routes through to a final solution. The complexity of the mathematics can become high and obviously depends upon the crystal structure of the layer and its orientation. Analytical software tools can be created to calculate the composition for specific combinations of layer type and measurement. As a worked example a solution for hexagonal (0001) oriented InGaN is shown below.

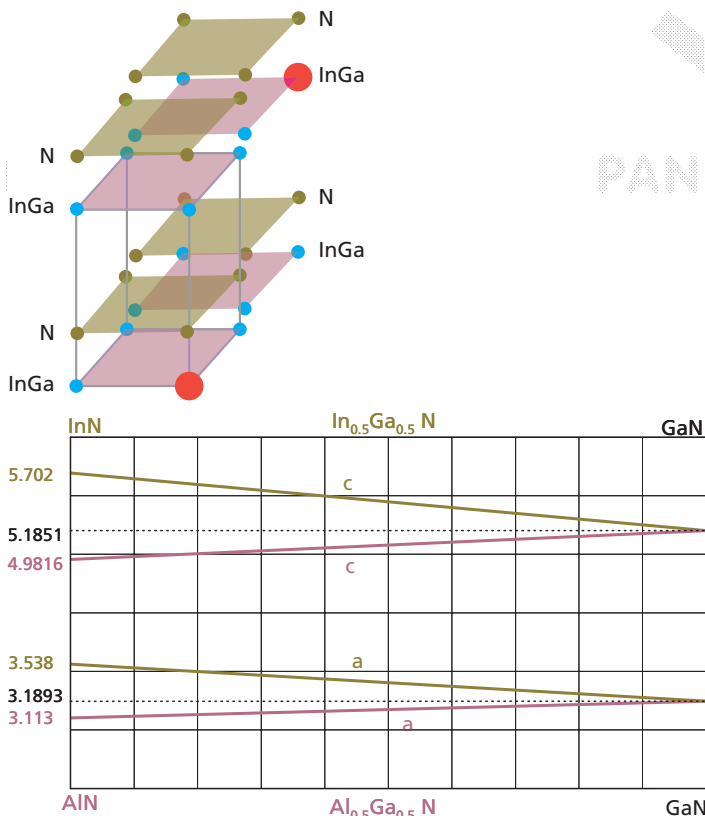


Figure 36: In a solid solution the solute atoms are randomly sited in Ga positions (top) and have the overall effect of expanding or contracting the lattice parameter in proportion to their concentration (bottom).

2.2.12.1 Worked solution for the calculation of composition of hexagonal (0001) oriented $\text{In}_x\text{Ga}_{(1-x)}\text{N}$

The simplified equation for biaxial strain in (0001) oriented hexagonal layers (17) is:

$$0 = C_{13}\varepsilon_{xx} + C_{13}\varepsilon_{yy} + C_{33}\varepsilon_{zz} \quad (46)$$

For hexagonal symmetry it is reasonable to assume for a flat layer that $\varepsilon_{xx} = \varepsilon_{yy}$
hence:

$$\varepsilon_{zz} = -2 \frac{C_{13}}{C_{33}} \varepsilon_{xx} = -D\varepsilon_{xx} \quad (47)$$

Substituting the strain equations (36) and (37) from above gives:

$$\frac{d_z - d_{zr}}{d_{zr}} = -D \left(\frac{d_x - d_{xr}}{d_{xr}} \right) \quad (48)$$

d_z and d_x are measured values, but d_{zr} and d_{xr} are unknown because the composition is unknown. Therefore substituting the appropriate expressions for compositions d_{zr} and d_{xr} namely:

$$d_{xr} = d_{xr}^X = X(d_{xr}^{InN} - d_{xr}^{GaN}) + d_{xr}^{GaN} \quad (49)$$

and

$$d_{zr} = d_{zr}^X = X(d_{zr}^{InN} - d_{zr}^{GaN}) + d_{zr}^{GaN} \quad (50)$$

gives

$$\frac{d_z - (X(d_{zr}^{InN} - d_{zr}^{GaN}) + d_{zr}^{GaN})}{(X(d_{zr}^{InN} - d_{zr}^{GaN}) + d_{zr}^{GaN})} = -D \frac{(d_x - (X(d_{xr}^{InN} - d_{xr}^{GaN}) + d_{xr}^{GaN}))}{(X(d_{xr}^{InN} - d_{xr}^{GaN}) + d_{xr}^{GaN})} \quad (51)$$

To solve for X requires rearrangement. When rearranged this equation forms a quadratic equation of the type:

$$aX^2 + bX + c = 0 \quad (52)$$

Where:

$$a = (1 + D)(d_{xr}^{GaN}(d_{zr}^{InN} - d_{zr}^{GaN}) - d_{xr}^{InN}(d_{zr}^{InN} - d_{zr}^{GaN})) \quad (53)$$

$$b = d_z(d_{xr}^{InN} - d_{xr}^{GaN}) + Dd_x(d_{zr}^{InN} - d_{zr}^{GaN}) - (1 + D)(d_{xr}^{InN}d_{zr}^{GaN} + d_{zr}^{InN}d_{xr}^{GaN} - 2d_{xr}^{GaN}d_{zr}^{GaN}) \quad (54)$$

And

$$c = d_zd_{xr}^{GaN} + Dd_xd_{zr}^{GaN} - (1 + D)d_{xr}^{GaN}d_{zr}^{GaN} \quad (55)$$

The solution for X is the positive root obtained from:

$$X = \frac{-b \pm \sqrt{b^2 - 4ac}}{2a} \quad (56)$$

The distortion coefficient D has different values for different binary compounds as shown in Table 2 in section 2.2.6. It is widely assumed, for solid solution alloys of binary compounds, that the distortion coefficient also follows Vegard's law. Namely:

$$D^X = X(D^{AC} - D^{BC}) + D^{BC}$$

PANalytical (57)

The stiffness constants c_{ij} can be similarly interpolated.

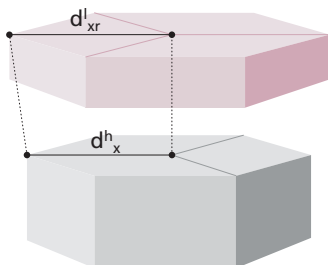
In order to solve for X above it is common practice to start with an approximate value for D to obtain a first approximation for X. The solution is then re-calculated with a value for D that has been determined from Vegard's law using the first approximation for X. The process continues for successive iterations, the final iteration being that for which no significant change in the value of X is observed.

2.2.13 Definition of mismatch in thin films

Mismatch is a general term most commonly used in the description of the relationship between two crystals across an interface. In epitaxial thin films, the mismatch refers to the relative differences between comparable lattice dimensions in the bulk relaxed layer, l , and in its host, h . The host provides the atomic template that the layer is strained to correspond to at the interface. The host can itself be in a state of strain or it can be relaxed. The important dimensions in the host are plane (atomic) spacings parallel to the interface. The host can be another layer between the mismatched layer and the substrate or the host can be the substrate itself. The numerical value of mismatch in a direction, x , is given by:

$$M_x = \frac{d_{xr}^l - d_x^h}{d_x^h} \quad (58)$$

Where d_{xr}^l is a unit cell dimension in the layer in its bulk relaxed state that would be constrained to fit a parallel dimension d_x^h in the host surface during epitaxial growth (see Figure 37). Mismatch is expressed numerically, e.g. as 0.0005, or as a percentage, e.g. 0.05% or in parts per million, e.g 500 ppm.



$$M_x = \frac{d_{xr}^l - d_x^h}{d_x^h}$$

Figure 37: Schematic diagram showing mismatch as the relative difference in in-plane dimensions of the layer and substrate unit cells

The mismatch can sometimes be confused for strain, but it is not an expression of strain. For example the mismatch between a layer and a substrate with a simple cubic unit cell in an (001) orientation will be given by

$$M_{xx} = \frac{a_r^l - a_s^s}{a_s^s} \quad (59)$$

If the layer is grown on the substrate and it is fully strained then its strain value in the same direction is:

$$\varepsilon_{xx} = \frac{a_r^l - a_s^s}{a_r^l} \quad (60)$$

Note that the denominators in the two equations are different¹⁸.

To solve an expression for mismatch requires an understanding of the orientation relationship between the layer and its host.

In homogeneous strained layer epitaxy, such as growth of $\text{In}_x\text{Ga}_{(1-x)}\text{N}$ on GaN, or growth of $\text{In}_x\text{Ga}_{(1-x)}\text{N}$ on $\text{In}_x\text{Ga}_{(1-x)}\text{N}$, the crystal structures of layer and host are considered almost identical to the point that the layers and host are together considered almost as one coherent crystal. The same set of hkl *d*-spacings are used for layer and host in mismatch calculations. Perfectly coherent (fully strained) epitaxial layers generally have mismatch values <<0.02 and thicknesses below the critical thickness for introduction of misfit dislocations.

For heterogeneous epitaxy, such as GaN on sapphire, the orientation relationship is not so simple and the mismatch is larger. For example along direction ε_{yy} in the interface, the (01-10) planes in GaN align parallel to the (11-20) planes in sapphire. $d_{(01-10)}^{\text{GaN}}$ is 2.762 Å and $d_{(11-20)}^{\text{Sapphire}}$ is 2.383 Å so the mismatch is 0.15. For this large

mismatch it is not possible to grow coherent strained layers and the GaN unit cells grow with an orientation relationship to the sapphire substrate but are not strained to fit the host unit cell dimensions.

There is also a term, 'perpendicular mismatch' that is used in some analytical expressions for solving composition in epitaxial layers. Perpendicular mismatch expresses the differences in d -spacings of a layer and host material normal to the interface, and was first used for growth of coherent and yet unstrained, i.e. lattice matched InGaAs alloys grown on InP substrates. Measuring the perpendicular mismatch for deliberately lattice matched layers was easy because it involved a single diffraction experiment to measure d_z in both layer and substrate. If there was a single peak then lattice match had been achieved, if there were two peaks then there was some lattice mismatch. However, perpendicular is not a crystallographic mismatch because there is, by definition no interface across which an atomic match needs to be made. The term is not particularly useful for layers that are not intended to be lattice matched to their host.

2.2.14 Calculation of relaxation in epitaxial thin films

'Relaxation' in the context of strained epitaxial layers originates from the idea that a layer may have started to grow with a fully coherent interface, but at some stage during growth misfit dislocations have been introduced at the interface between the layer and the substrate in order to reduce the strain energy in the layer. This is known to happen in epitaxial layers when the layer thickness exceeds a certain critical value. On some occasions it is useful to define how far the strain state of an epitaxial layer is away from the extreme possibilities that it could have had. The extremes are fully strained with respect to its host, which is known also as 0% relaxed or not at all strained and exhibiting its bulk lattice parameters, which is known as 100% relaxed.

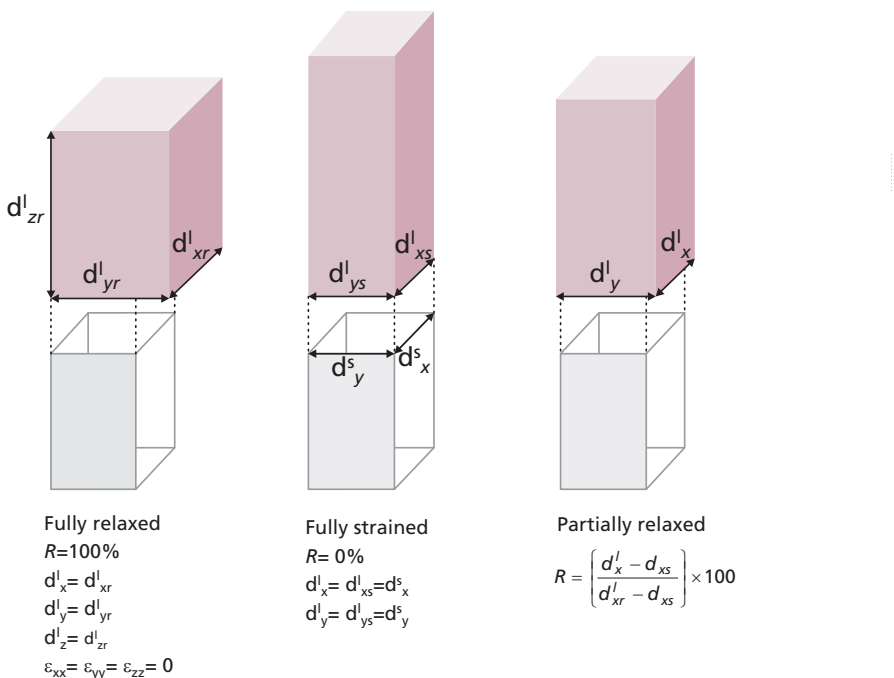


Figure 38: The state of strain of a layer can alternatively be expressed in terms of relaxation. Figure 29 is re-labelled here to illustrate layer relaxations of 100%, 0% and partial relaxation.

Relaxation, as a percentage, can be calculated according to:

$$R = \left(\frac{d_x^l - d_{xs}}{d_{xr}^l - d_{xs}} \right) \times 100 \quad (61)$$

Where, d_x^l is a measured dimension in the layer parallel to the interface; d_{xs} is the equivalent dimension that the layer would assume if it were fully strained. d_{xs} usually corresponds to some dimension in the host substrate and is therefore obtained from a database value for the substrate; d_{xr}^l is the equivalent dimension that the layer would assume in its bulk state and is therefore obtained from a database value for the lattice parameter of a layer with the same composition.

It is possible to measure relaxation >100% when the layer suffers strain beyond that required to relieve misfit. For example if there is a non-homogeneous misfit dislocation density or when differences in thermal expansion coefficients of the layers and substrate give rise to internal strains on cooling from the growth temperature.

2.3 Crystal truncation and crystallographic defects

The concepts introduced in sections 2.1 and 2.2 relate to the notion of a perfect crystal and how its behavior as an epitaxial thin film can be predicted from knowledge of its internal and perfectly ordered crystal structure. The requirement for analyses based on the calculations previously shown is that useful d -spacings and plane orientations in the crystal can be measured by XRD.

In reality, the epitaxial thin films are not entirely perfect and this can introduce some complexity into the measurement of d . The presence of crystallographic defects creates microstrains in the crystal where the d -spacing is locally changed or the crystallographic planes are locally bent (rotated). Where this kind of defect is present in small quantities or with random orientations, it has the effect of broadening the diffraction peaks and often reducing the diffracted peak intensity. Such broadening can also lead to the overlapping of peaks from different layers. Both effects can result in a reduction in the precision with which d -spacing or orientation can be measured.

The way in which defects broaden X-ray diffraction peaks can be the subject of further XRD studies of the microstructure of defective thin films. Descriptions of such studies are outside of the scope of this booklet.^{19,20} Below are presented some brief descriptions of defects along with a short explanation focusing only on how they may affect the analysis of strain, composition and thickness in thin films.

2.3.1 Thin layers: crystal truncation

The thinness of a layer is a crystal defect in the sense that it ‘truncates’ the perfect crystal that would otherwise be infinite. In the reciprocal lattice construction, the reciprocal lattice spots for an infinite crystal are delta functions. For a thin single crystal layer, that is effectively infinite parallel to the interface but finite normal to the interface, the reciprocal lattice spot is extended to a streak normal to the layer interface. The streak has a fine structure which in a high resolution diffraction pattern results in thickness fringes around a diffraction peak. The measured spacing of thickness fringes can be used in calculations to obtain an approximation of layer thickness. Some of these calculations, which are based around Bragg’s law, are presented in chapter 3.



Infinite single crystal



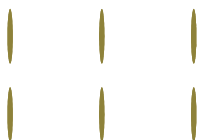
Reciprocal spots are
delta functions



PANalytical



Thin film single crystal



Reciprocal spots exhibit
truncation rods

Figure 39: Simplistic diagrams to illustrate the effect of crystal truncation on the reciprocal lattice spot shapes

2.3.2 Dislocations

Dislocations disrupt the long range order of the lattice. Close to the dislocations the lattice planes are bent and the d -spacings are varied. At the core of a dislocation the crystal planes are bent so extremely, and there are so few of them, that they do not contribute to the Bragg peak. The total Bragg peak intensity is therefore reduced in comparison with that from a perfect crystal. At some distance away from the dislocation core the crystallographic planes are only slightly distorted and so may contribute some intensity at or close to the Bragg peak. Away from isolated dislocations the crystal is perfect and characteristic d -spacings for the layer can be measured.

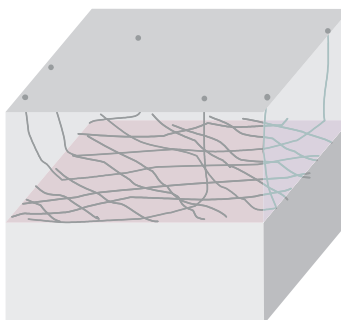
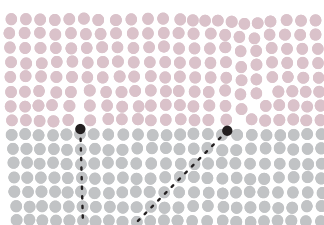


Figure 40: Diagrams illustrating dislocations. In the atomistic view looking along dislocation lines, the dislocation core is seen as the termination of a crystal plane (left). At a lower resolution, dislocations in an epitaxial layer are considered to have misfit components that form an array in the layer-substrate interface and threading components that propagate through the layer to the surface (right).

Misfit dislocations are a set of dislocations that are closely spaced and located in the interface between a substrate and a buffer layer. Their strain-fields overlap and the overall effect of the misfit dislocation array is to accommodate the difference in lattice spacing between the layer and the substrate. Crystal planes in the layer above an array of misfit dislocations take on a value close to that expected for the layer in its bulk (or relaxed) form. The misfit dislocation array is responsible for a shift in the position of a Bragg peak between the expected position for a fully strained layer and that for a relaxed layer. A misfit dislocation array is rarely perfectly ordered and so whilst there is a net shift in the d -spacings of the crystal, the corresponding measured d -spacing may be an average of a small range of statistically distributed values²¹. A peak from a relaxed layer is generally weaker and broader than that from a layer with no dislocations at the interface.

Misfit dislocations in buffer layers tend to have isolated trailing ends that thread through the layer above the interface (so called ‘threading dislocations’). These are like isolated dislocations in the sense that they don’t contribute to the Bragg peak intensity, nor to a net shift of the Bragg peak position, but rather they tend to lower the Bragg peak intensity and contribute to broadening of the peak.

2.3.3 Mosaic blocks

The regions of crystal between defects that are effectively perfect are known as mosaic blocks. A layer that contains mosaic blocks is still considered to be a single crystal, but the blocks may differ slightly in their sizes and orientations. The blocks have dimensions both normal to and parallel to the layer interfaces. Therefore the effect of truncation, which is to spread the reciprocal lattice point, applies in all dimensions. Furthermore it is unlikely that the crystal truncation and rotations are identical for each mosaic block. The combined effects of statistical variation in rotation and mosaic block crystal truncation are a general and unpredictable broadening of the peak for which a d -spacing is measured. The resulting d -spacing is a statistical average of those spacings present in the various mosaic blocks.

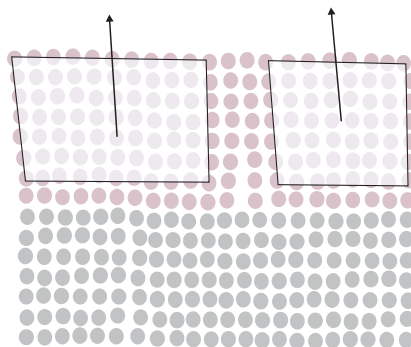


Figure 41: Mosaic blocks are considered to be the perfect regions between dislocations.

2.3.4 Point defects

Some of the host atomic positions may be occupied by impurity atoms (substitutional impurities). Impurity atoms may occupy spaces between atom sites (interstitial impurities). Some of the host atoms may become displaced and become antisite defects by occupying the wrong atomic positions, or interstitial defects by occupying spaces between lattice sites. They may leave vacancies (unoccupied sites) in the lattice. These atomic irregularities are collectively termed point defects. When the number of point defects exceeds a certain value they may create a net change in the lattice parameter of the material. The principle is the same as for substitutional alloy species that are deliberately introduced in order to expand or contract the lattice to create strained layers. However, the effects of point defects are often unknown or unpredictable. If the impurity atoms are present in significant numbers then the net strain may be measurable as a change in d -spacing. If however the number of point defects is low (as is often the case) or they are non-randomly distributed then scattering from them may simply increase the intensity tails near to Bragg peaks.

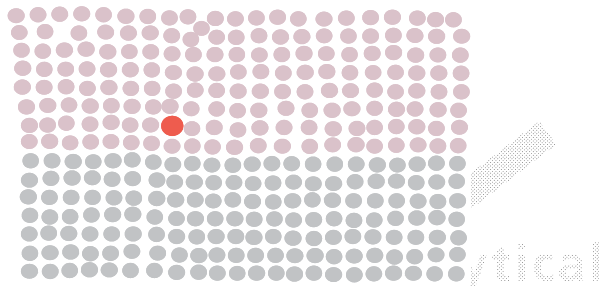


Figure 42: Point defects are isolated faults in the crystal for example, impurity atoms, anti-site defects or vacancies.

2.3.5 Stacking faults

Stacking faults occur where the normal ABABAB, or ABCABC stacking sequences are disrupted. In these polar crystals stacking faults may also cause continued layer by layer growth to have reversed polarity. Stacking faults are not as energetically favorable as misfit dislocations for relieving misfit strain and are less likely to be present in a layer for that purpose. The presence of a large number of stacking faults is most likely to lead to a broadening and weakening of the diffraction peak although some change in the net d -spacing cannot be entirely ruled out.

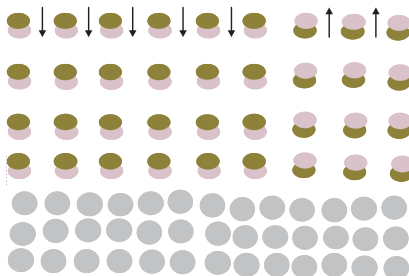


Figure 43: Stacking faults are local regions where the stacking sequence is reversed.

2.3.6 Domains

Domains are regions of the crystal that exhibit subtle structural differences. For example in GaN where polarity is an issue, regions of reverse polarity domains may exist. It would be expected that the d -spacings of reversed polarity domains will be the same and in that sense the presence of domains may not affect the measurement of d -spacings and plane orientations except in the same sense as for mosaic blocks, namely weakening and broadening of the diffraction peaks, although the effects of this type of microstructure on strain and composition measurements are not well known for epitaxial layers.

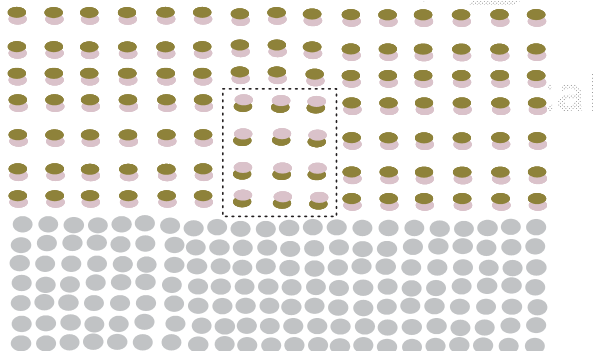
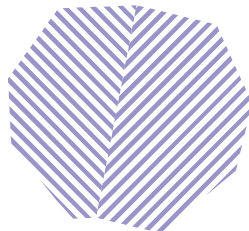


Figure 44: Extensive reversed polarity regions are called domains.

2.3.7 Twins

Twins are regions of material with identical crystal structure that exhibit a crystallographic relationship with respect to each other. Their reciprocal lattices exhibit the same orientation relationship as the real space twins. In terms of d -spacing measurements it is likely that only one of the twinned crystals will be measured at any time. If sets of d -spacings are to be measured it would be necessary to make sure that all of the d -spacings in any set originate from the same crystal.



PANalytical

Figure 45: Twins are differently oriented regions of crystal usually connected by an internal interface with a characteristic orientation relationship.

2.3.8 Phases

Phases are regions of different crystals that coexist within the same material. Each phase has its own reciprocal lattice.



Figure 46: Regions of the same crystal type constitute a phase.

In epitaxial multi-layers a phase is a layer with a unique composition. The reciprocal lattices for each phase are often similar and similarly oriented resulting in their Bragg reflections clustering together. If the Bragg reflections are sufficiently close they may well form an interference pattern within which it is not possible to identify peaks originating uniquely from diffraction from a set of planes within one layer. If this occurs the diffraction pattern must be simulated in order to ascertain strain, composition and thickness (see chapter 4). If the Bragg reflections are sufficiently distinct then each layer can be analysed independently provided the peaks can be correctly attributed.

In GaN epitaxial layers it is possible to grow cubic GaN phases within a predominantly hexagonal layer or hexagonal inclusions within a predominantly cubic layer. The reciprocal lattices for each phase are distinct, but the two phases share several common d -spacings at similar orientations. In order to investigate the d -spacings for each phase it will be necessary to find d -spacing values or orientations that are unique to each phase. For example the (0001) hexagonal and (111) cubic d -spacings are identical and the planes are usually parallel in a layer of mixed phases. The d -spacing of the hexagonal {10-14} planes has no equivalent in the cubic system. The hexagonal {11-22} planes have similar d -spacing to the cubic {311} planes but are usually oriented at different angles.

PANalytical

PANalytical

2.3.9 Precipitates

Precipitates are small phases of a different crystal existing within a host or 'matrix' crystal. The precipitate and the host crystal each have their own reciprocal lattices. The precipitates can form with an orientation relationship with the host or they can form with random orientations. Peaks from precipitate phases may be identifiable because they tend to be broader and weaker than those from the host phase. If there are strains associated with the precipitate-host interface they may weaken and broaden the peaks in the host material in the same way that isolated dislocations do.

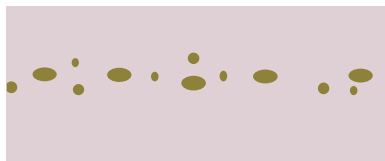


Figure 47: Precipitates are particles of one phase forming within a host matrix of a different phase.

2.3.10 Quantum dots

Quantum dots are similar to precipitates in that they usually have a different lattice unit cell dimension to the host crystal. They are similar to epitaxial layers in the sense that they often have the same orientation as the host crystal and may be strained epitaxially. Sometimes they are distributed in a regular array throughout the host layer and this periodicity gives rise to additional measurable diffraction effects²². Because quantum dots have a finite lateral dimension, the analysis of strains and compositions cannot always be simplified in the way it is for continuous epitaxial layers. The scattering from quantum dots can be very weak. Information about the strain and composition of the dots may be inferred from simulation of deviations in the shape of scattering peaks from the host layer. This type of analysis is still very much a research topic and no solutions for quantum dots are presented here.



Figure 48: Quantum dots are identical nano-sized regions of a phase. Typically they are the same sizes and shapes. Often they are formed in regular arrays and arranged in layers.

2.3.11 Pores and voids

Pores and voids may have repeatable and uniform shapes and sizes. They may be random or exhibit a long range order. In a comparable manner to quantum dots, lateral information about the sizes of pores and voids is inferred from the modified shapes of peaks from the host layer. Pores and voids are not expected to introduce strains in the host layer therefore peaks from the host material should

still be available for analysis of d -spacings. It is possible, however, that for densely packed pores the stiffness constants for the bulk material may not be applicable to the host layer. As for quantum dots this type of analysis is still very much a research topic for GaN compounds.

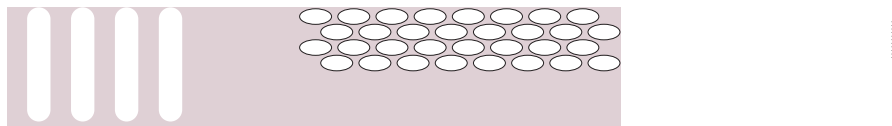


Figure 49: Pores and voids can be deliberately introduced into nano- and meso-porous materials in order to change the material's properties. In layered structures pores may be horizontally or vertically aligned.



PANalytical



PANalytical



PANalytical

3. Principles of measurement

Some methods for the determination of the alloy composition in conventional semiconductor materials are already well established. However, as the versatility and scope of X-ray diffractometers increase, and our understanding of thin films improves, new possibilities open up to improve the current methods and calculations. It is important to note that the equipment can deliver extremely precise measurements for even the simplest experiment. But the analyses of data from the simplest and quickest methods can make assumptions and approximations that reduce the precision of the final result. Some materials are not sufficiently well behaved to lend themselves to the simplest methods. At all times it is important not to expect the data to provide answers that are outside the scope of the method in use.

Section 3.1 describes Bragg's law and the measurement of Bragg diffraction peaks in both real space angular coordinates and reciprocal space coordinates with specific reference to how it will be applied in the reflection geometry for epitaxial layers.

Section 3.2 describes methods for obtaining d -spacings and thicknesses from measured data either in the form of high resolution rocking curves or high resolution reciprocal space maps.

3.1 Bragg's law and measurement of Bragg peaks

3.1.1 Measurement in a diffractometer

All XRD measurements consist of the same essential components:

- Illumination of the sample by a conditioned X-ray beam
- Diffraction of the beam by the sample that is mounted on a sample stage and may be aligned prior to the measurement or scanned during the measurement
- Detection of some of the diffracted beams by a detector in a known orientation with respect to the incident beam

The sample stage may offer various alignment axes:

- Orthogonal X, Y and Z motors that drive the sample stage so that the wafer as a whole is positioned as required with respect to the incident beam
- Phi, φ , or psi, ψ^{23} scans can be performed in order to find peaks. In an MRD, phi rotates the sample around the stage normal and psi rotates the sample within an arc containing the goniometer axis and the sample stage normal. With reference to an epitaxial wafer phi is rotated to find the correct azimuth for measurement, psi is usually used for a fine adjustment to optimise a peak alignment.

The goniometer mechanisms in the instrument are the largest and the most precise. They regulate and control the incident beam angle, omega, ω , with respect to the sample stage and the detector position, 2theta, 2θ , with respect to the incident beam direction. The incident beam angle, ω , and detected beam angle, 2θ , can be calibrated to zero positions and scanned to perform measurements (e.g. omega rocking curves, omega/2theta scans and omega/2theta vs omega reciprocal space maps).

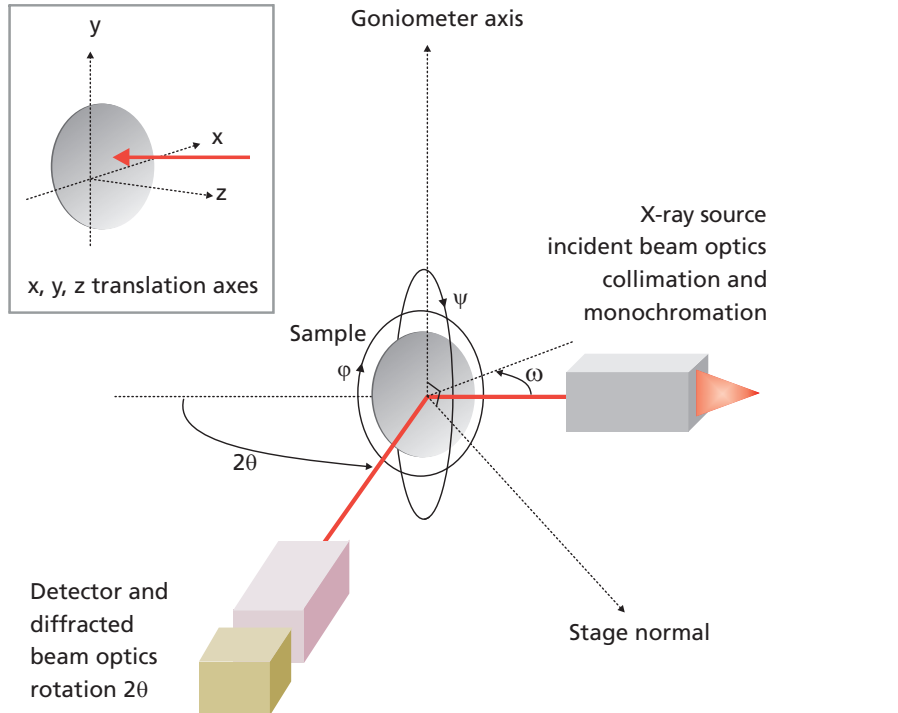


Figure 50: Illustration of the key components in a diffractometer

3.1.2 Bragg's law depicted in real space

The real space interpretation of Bragg's law is based on the concept of path difference between X-rays scattered from neighboring crystal planes with spacing, d . If the path difference is an integer number of wavelengths, $n\lambda$, then there will be constructive interference and the diffracted intensity will be a maximum. It is found that this condition is true for incident and diffracted beams both inclined at an angle θ with respect to the planes where:

$$n\lambda = 2d \sin \theta \quad (62)$$

Because the angle of incidence of the beam with respect to the planes is equal to the angle between the diffracted beam and the planes this type of scattering is often called Bragg reflection.

Note that the apparent change in direction of the beam from the incident direction to the scattered direction is called the scattering angle and is equal to 2θ .

The number of wavelengths, n , in the path difference is termed the 'order' of the reflection. For diffraction from crystallographic planes n is most conveniently only considered to be 1. This is because the higher order conditions e.g. $n=2$, are equivalent to first order diffraction from planes with integer spacing $d/2$, and so the 'order' of the reflection is accounted in the plane spacing e.g. d_{001} , d_{002} , etc., rather than in the n value. Hence the more common expression for X-ray crystallography:

$$\lambda = 2d \sin \theta \quad (63)$$

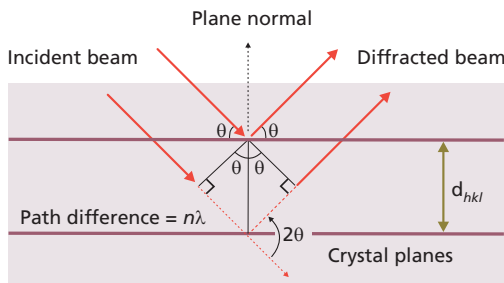


Figure 51: Real space illustration of the condition for Bragg reflection. Note that the incident beam is inclined by θ with respect to crystal planes; the scattered beam is at 2θ with respect to the incident beam, plane normal and diffracted beam are all coplanar.

3.1.3 Bragg's law depicted in reciprocal space

In the reciprocal space interpretation of Bragg's law the incident beam is represented by a wave vector \underline{K}_0 which has length $|\underline{K}_0| = 1/\lambda^{24}$. The detected beam is represented by the vector \underline{K}_H which also has the same length $|\underline{K}_H| = 1/\lambda$. Together these vectors define the scattering vector \underline{Q} , in which $\underline{Q} = \underline{K}_H - \underline{K}_0^{25}$. The angle between \underline{K}_0 and \underline{K}_H is 2θ and so the length of the scattering vector $|\underline{Q}| = 2\sin\theta|\underline{K}_0|$. This construction defines the experimental conditions.

Bragg scattering from a set of planes hkl occurs when a crystal is introduced into the experiment such that the scattering vector \underline{Q} is exactly equivalent to the reciprocal lattice vector \underline{d}_{hkl}^* . Remembering from section 2.1.1.7 that the reciprocal lattice vector is normal to the planes hkl and has length $|\underline{d}_{hkl}^*| = 1/d_{hkl}$. The Bragg condition is therefore also expressed by:

$$1/d = |\underline{Q}| \quad (64)$$

That, on substitution, rearranges to give:

$$\lambda = 2d \sin \theta \quad (65)$$

In the diagram, the origin of the experiment and the origin of the reciprocal lattice coincide. In practice this means that the center of the goniometer coincides with the crystal (or region of the crystal) that is to be investigated. Bragg condition is met when the endpoint of the scattering vector overlaps with the reciprocal lattice spot. The endpoint of the scattering vector (the instrument probe) has size and shape due to the wavelength spread in the incident beam and the angular divergences of the optical configuration used for the experiment. The reciprocal lattice spot has size and shape due to crystal truncation effects and lattice defects, so the overlap of the instrument probe and the reciprocal lattice spot may not be total at any point. However, all that is required for analyses of d -spacings are coordinate positions of the center of the reciprocal lattice spot. The shape of the diffraction peak namely the overlap function, is the subject of advanced microstructural analyses and is outside of the scope of this booklet²⁶.

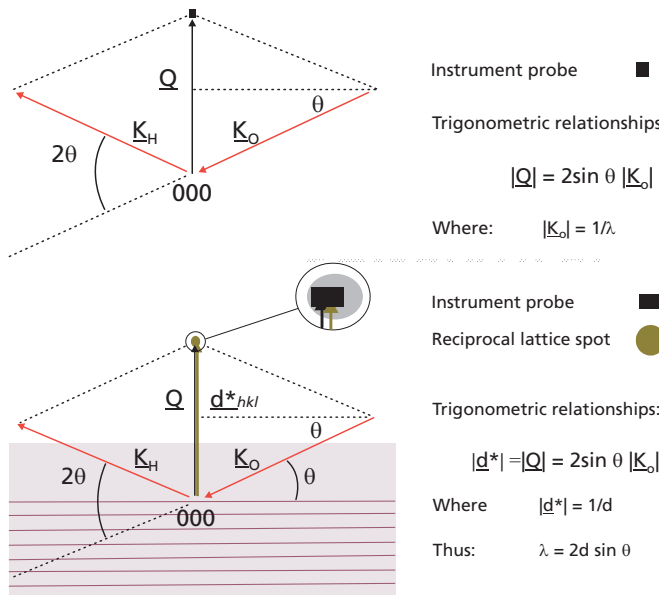


Figure 52: Top: Reciprocal space illustration of the instrument probe position in terms of the incident and scattered wave vectors. Bottom: Combination of the instrument probe position and the reciprocal lattice point in the condition for Bragg scattering.

3.1.4 Alignment of azimuth into the diffraction plane

The scattering vector is controlled by the 2theta detector position and the angle of incidence, omega, ω , which on a MRD is controlled by rotation of the sample stage. The orientation of the crystal and hence the orientation of the reciprocal lattice is determined by the starting positions of the sample stage, namely phi, psi and omega. Psi and phi are used to bring the azimuth of interest into the diffraction plane, omega is adjusted to provide a suitable start position, then 2theta and omega are used to scan the scattering vector across the reciprocal lattice spot.

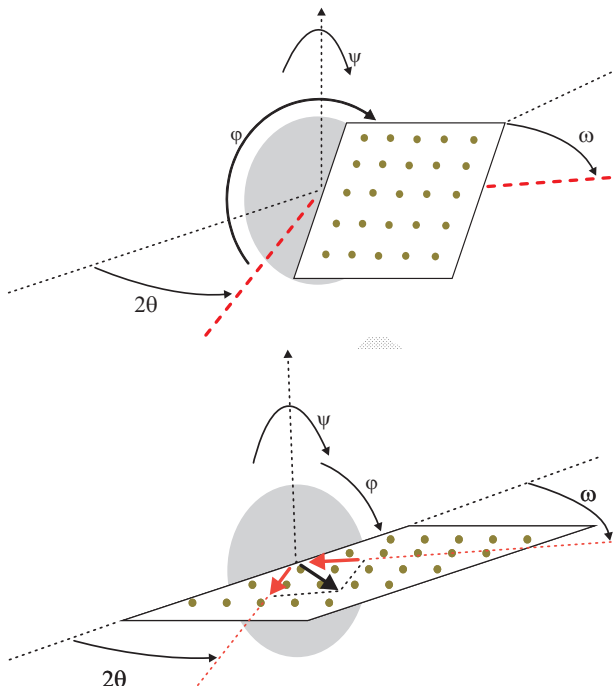


Figure 53: Before a scattering measurement is performed the azimuth containing the reciprocal lattice points of interest must be located in the same plane as the incident and scattered beams. This is the coplanar arrangement.

3.1.4.1 Major azimuths in (0001) oriented GaN layers

There are two major sets of azimuths in hexagonal GaN that contain the majority of the reciprocal lattice points. One set contains the $<0001>$ and $<11-20>$ directions and the other set contain the $<0001>$ and $<10-10>$ directions. Figure 54 shows schematic cross sections through the 3-D reciprocal lattice illustrating the sets of planes in these azimuths. Note that on an (0001) oriented sapphire wafer the GaN $<10-10>$ direction coincides with the sapphire $<11-20>$ direction which is usually perpendicular to the major flat.

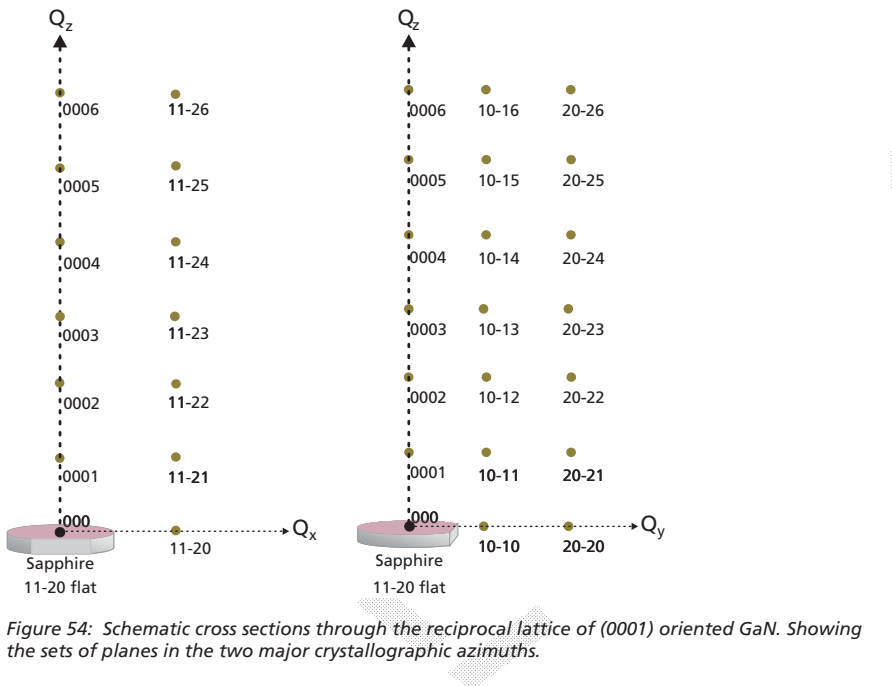


Figure 54: Schematic cross sections through the reciprocal lattice of (0001) oriented GaN. Showing the sets of planes in the two major crystallographic azimuths.

3.1.5 Accessible reflections

Whilst the reciprocal lattice construction is used to calculate the orientations of planes and their d -spacings it does not indicate the intensity of a Bragg reflection from those planes. The intensities are predicted from kinematic or dynamical calculations²⁷. Some reflections are absent (or ‘forbidden’) because the lattice structure gives rise to destructive interference. Some reflections are of negligible intensity because of the atomic arrangements of a particular material within the unit cell lead to nearly complete destructive interference.

In the reflection geometry some reflections are not accessible because to create the appropriate diffraction vector \mathbf{Q} would require that either the incident or the diffracted beam is below the sample surface. For typical wafer samples it is not possible to obtain a measurement because the incident or scattered beam would be totally absorbed by the sample. Such reflections are termed inaccessible.

Figures 55 and 56 illustrate some measured reflections for GaN (0001) oriented layers on (0001) sapphire substrates for the two major types of GaN azimuth. The table below provides approximate angles for where these reflections may be found.

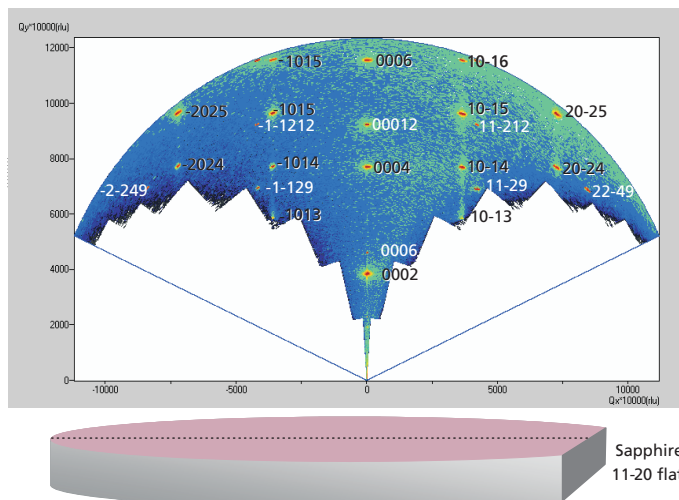


Figure 55: Top: Data collected in a large area reciprocal space map showing the accessible GaN (black) and sapphire (white) reflections found in the sapphire 11-20 and GaN 10-10 azimuth. Bottom: Schematic diagram illustrating the trace of the diffraction plane across the GaN on (0001) sapphire wafer from which the data were collected.

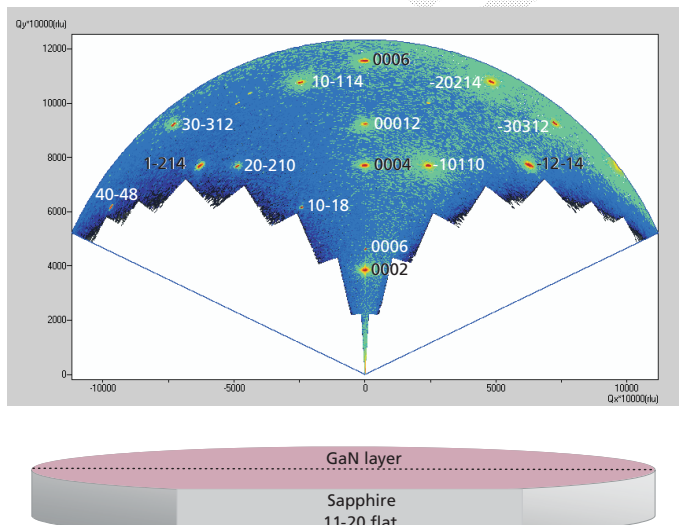


Figure 56: Top: Data collected in a large area reciprocal space map showing the accessible GaN (black) and sapphire (white) reflections found in the sapphire 10-10 and GaN 12-10 azimuth. Bottom: Schematic diagram illustrating the trace of the diffraction plane across the GaN on (0001) sapphire wafer from which the data were collected.

[10-10] GaN azimuth perpendicular to sapphire [11-20] flat			[-12-10] GaN azimuth parallel to sapphire [11-20] flat		
Reflection	2Theta(°)	Omega(°)	Reflection	2Theta(°)	Omega(°)
0002 GaN	34.567	17.283	0002 GaN	34.567	17.283
0004 GaN	72.910	36.455	0004 GaN	72.910	36.455
0006 GaN	126.072	63.036	0006 GaN	126.072	63.036
10-13 GaN -1013 GaN	63.434 "	(-0.323) ²⁸ (63.757)	-12-14 GaN 1-214 GaN	142.673 "	20.178 122.494
10-14 GaN -1014 GaN	82.051 "	15.881 66.170	000 6 sapphire	41.688	20.844
10-15 GaN -1015 GaN	105.006 "	31.921 73.0845	000 12 sapphire	90.738	45.369
10-16 GaN -1016 GaN	138.106 "	51.677 86.429	-110 8 sapphire ²⁹ 1-10 8 sapphire	61.322 "	9.148 52.1735
20-24 GaN -2024 GaN	109.175 "	11.396 97.779	-110 10 sapphire 1-10 10 sapphire	76.899 "	20.948 55.951
20-25 GaN -2025 GaN	136.523 "	31.354 105.169	-110 14 sapphire 1-10 14 sapphire	116.653 "	45.633 71.020
000 6 sapphire	41.688	20.844	-220 10 sapphire 2-20 10 sapphire	89.0348 "	12.279 76.755
000 12 sapphire	90.738	45.369	-220 14 sapphire 2-20 14 sapphire	131.18 "	41.339 89.840
11-2 9 sapphire -1-12 9 sapphire	77.2657 "	7.382 69.884	-330 12 sapphire 3-30 12 sapphire	129.967	26.734 103.233
11-2 12 sapphire -1-12 12 sapphire	102.868 "	26.962 75.906	-440 8 sapphire 4-40 8 sapphire	124.696 "	4.733 119.963
22-4 9 sapphire -2-24 9 sapphire	114.144 "	6.558 31.913			

3.1.6 Scanning

There are many different possibilities for exploring diffraction space by scanning either or both the instrument and sample. Both a change in θ , namely $\delta\theta$, or a change in ω , namely $\delta\omega$, result in a change in the diffraction vector \underline{Q} , namely $\delta\underline{Q}$.

A scan is simply a series of steps in $\delta\underline{Q}$, where an intensity value is measured for each step. The results for a scan are usually stored in a file and can be graphically presented as plots of diffraction vector against intensity (in 'diffraction space'), or angle (e.g. the 2theta angle) against intensity (in 'angular space').

The shape and size of the recorded profile is dependent both on the size and shape of the reciprocal lattice spot, the size and shape of the instrument probe and the direction in which they scan across one another. In the case of *d*-spacing measurements it is the position or centroid of the scanned peak that is of primary importance.

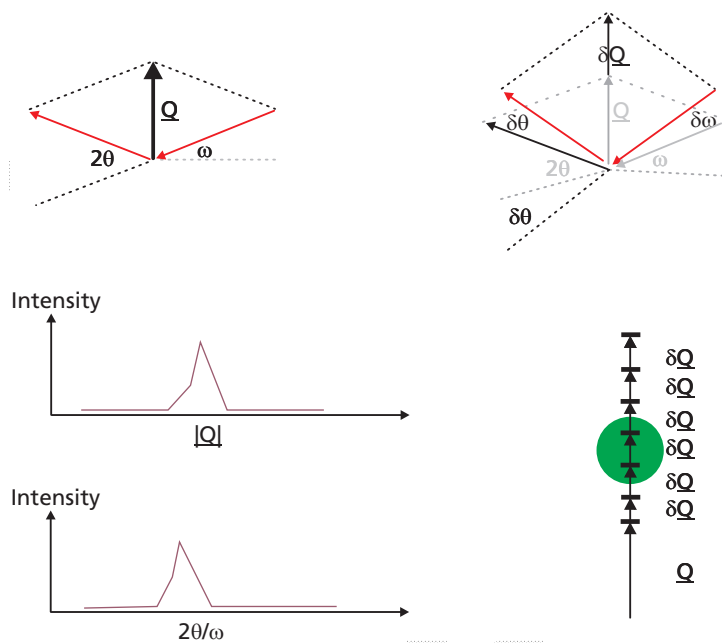


Figure 57: Clockwise from top left: The diffraction vector \underline{Q} is defined in terms of the wave vectors and the incident beam angle ω and detected beam angle 2θ ; a small change in either or both of the angles results in a small change in the diffraction vector $\delta \underline{Q}$; a scan is a succession of steps in $\delta \underline{Q}$ where the intensity is synchronously measured; scans are displayed as plots of intensity against either \underline{Q} or angle.

3.1.6.1 Scan units

Scans can be performed or displayed in angular units or diffraction space units. The diffraction space coordinates, (Q_x, Q_z) , are expressed with reference to the angular positions as follows:

$$Q_x = R (\cos \omega - \cos (2\theta - \omega)) \quad (66)$$

$$Q_z = R (\sin \omega + \sin (2\theta - \omega)) \quad (67)$$

Where $R = |\underline{K}_H| = |\underline{K}_0|$

In principle R can take on many values, for example commonly used values are:

- $2\pi/\lambda$
- $1/\lambda$
- 1
- $\frac{1}{2}$
- The length of the diffraction vector $|Q|$ is given by:

$$|\mathbf{Q}| = \sqrt{(Q_x^2 + Q_z^2)} = 2R \sin(\theta) \quad (68)$$

If there is Bragg diffraction and $R = 1/\lambda$

Then $d_{hkl} = 1/|\mathbf{Q}|$.

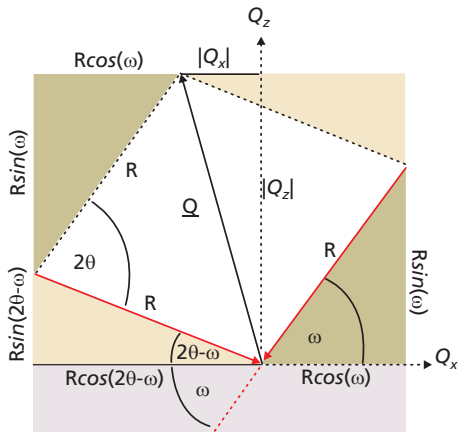


Figure 58: Schematic diagram to illustrate the relationship between the diffraction vector and the angles of incidence and detection

3.1.6.2 2Theta/omega scan

The 2theta/omega scan, $2\theta/\omega$, is one of the more common measurements in X-ray diffraction. In diffraction space this is known as a 'radial scan'. In this scan, the step size for the 2θ scan, $\delta 2\theta$, has twice the value of the change in incident beam angle ω , i.e. $\delta 2\theta = 2\delta\omega$. In diffraction space this results in the diffraction vector scanning radially outwards from the origin.

A special case of radial scan in thin films is the 'symmetric scan' in which $\omega = \theta$ and the scan is then perpendicular to the sample surface. Bragg diffraction will occur if there are crystal planes parallel to the surface and when $\theta = \theta_{\text{Bragg}}$.

For other scans also known as 'offset scans', $\omega \neq \theta$ and the difference between the two values, $\omega - \theta$, is called the 'offset' (α in Figure 59).

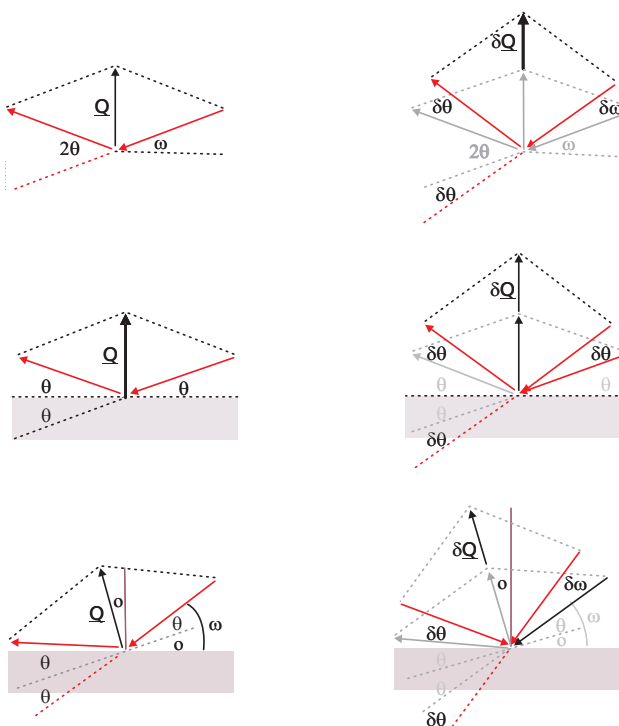


Figure 59: Top: illustration of a general $2\theta/\omega$ scan; middle: Illustration of a $2\theta/\theta$ symmetrical scan; bottom: illustration of a $2\theta/\omega$ offset scan.

3.1.6.3 $2\theta/\omega$ vs ω map

A 2-axis reciprocal space map can be obtained when $2\theta/\omega$ scans are repeated for a sequence of offset values. The difference from one offset value to the next $\delta\omega$, is called the omega step size. The total difference between the largest and smallest offset values is called the omega range.

When plotted in reciprocal space units the 2-axis maps obtained can represent the reciprocal lattice spots that they are measuring. A good representation requires that the instrument probe size is a lot smaller than the reciprocal lattice feature being measured. This is why for single crystal layers that have very small reciprocal lattice spots very high resolution methods need to be used.

The figures show an example of a 2-axis scan combining a radial scan and omega offset in high resolution. In this case the scan is performed over a small angular range with a very small probe.

The results for a map are usually stored in a file and can be graphically presented as 2-D plots. In 'reciprocal lattice units' or 'diffraction space units', the diffraction vector coordinate (Q_x, Q_z) is plotted against intensity where the intensity is indicated for example by a color bitmap or contour scale, or quasi 3-D plot.

In angular units the scan axis positions are plotted as coordinates with, for example, the $2\theta/\omega$ position plotted along the x axis and the ω offset position along the y axis.

An individual scan extracted from the map can be plotted as a single scan.

d -spacing analysis from reciprocal space maps is presented in section 3.2.1.

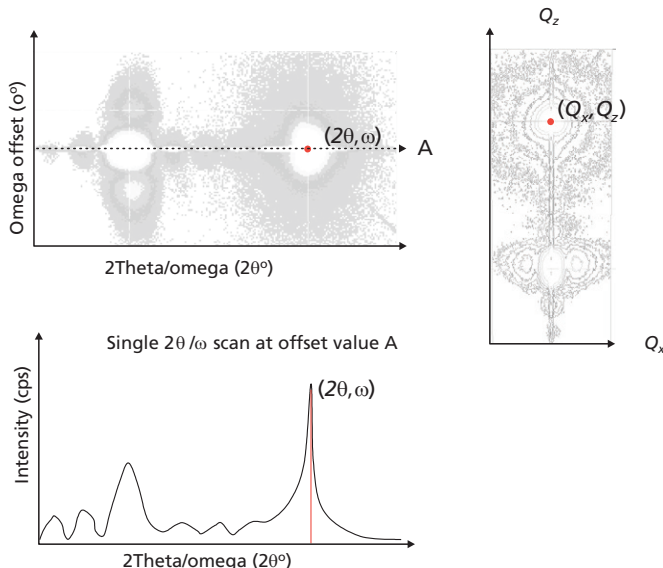


Figure 60: Clockwise from top left: A $2\theta/\omega$ versus ω map presented in angular units; A $2\theta/\omega$ versus ω map presented in reciprocal space units; Data are extracted at offset position A in the angular map to provide a single $2\theta/\omega$ scan.

3.1.6.4 Omega rocking curve

An omega rocking curve is a special quick method for scanning through a reciprocal lattice spot or a group of reciprocal lattice features. It tends to work only for reciprocal spots shapes that are quite narrow in one dimension. In the experimental configuration for collecting rocking curves, an open detector is used meaning that the 2θ angular acceptance is large. For example the detector accepts scattered beams with an angular divergence of about 3° compared to a typical high-resolution setup with a triple-bounce analyser which accepts an angular range of about 0.003° . In the reciprocal space view this means that the

instrument probe is very large. As it is scanned across the reciprocal lattice spot the detail in the spot is reproduced in the scan because only one part of it is intercepted at each omega position.

d-spacing analysis from omega rocking curves is presented in section 3.2.2

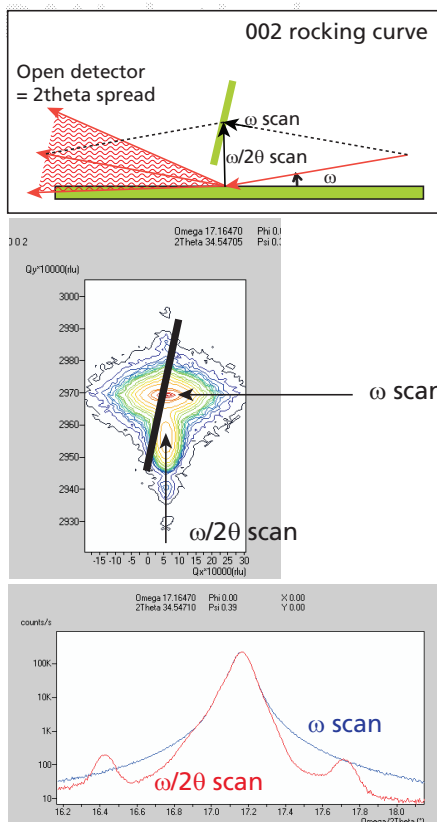


Figure 61: Top: illustration of the large instrument probe for an open detector; middle: illustration showing the directions of an ω scan and an $\omega/2\theta$ scan with the trace of the instrument probe over the reciprocal lattice spots; bottom: the resulting ω and $\omega/2\theta$ scans

3.1.7 Experimental procedure

The experimental procedure consists of combining the most suitable optical components, calibrating the goniometer zero positions, bringing the sample into alignment and performing a scan or series of scans.

3.1.7.1 Equipment

High resolution reciprocal space maps can be obtained, for example using the X'Pert PRO MRD with an incident beam monochromator (220 Ge symmetric 2-crystal 4-reflections) and an X-ray mirror or an incident beam hybrid mirror + monochromator combination together with a diffracted beam analyser crystal (220 Ge symmetric 3-reflections). The sample stage is a high precision goniometer. The X-ray mirror is not always necessary but can increase the speed of the measurement by providing greater intensity.

Many other experimental configurations are possible and new methods may evolve to suit specific requirements, for example, to reduce the measurement time or increase the collection intensity.

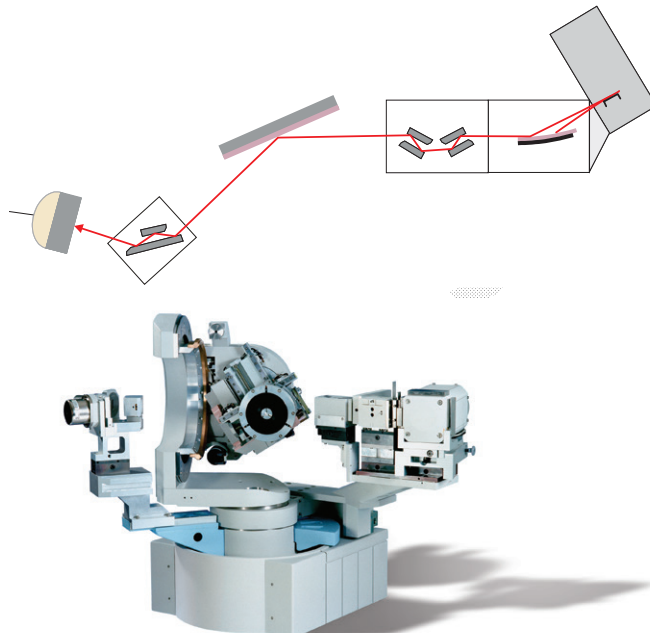


Figure 62: Illustration and photograph of a typical experimental arrangement showing, from right to left, X-Ray tube, mirror, monochromator, sample, analyser and detector

3.1.7.2 Placing the 2θ axis on an absolute scale

The scattering angle can be placed on an absolute scale, in high resolution, by scanning the analyser crystal and detector assembly through the $2\theta = 0$ position with the sample out of the incident beam. The 2θ peak position is then calibrated as zero. The high intensity of the direct beam may mean that an attenuator will be required, e.g. a 0.1 mm Cu filter should be inserted before the detector.

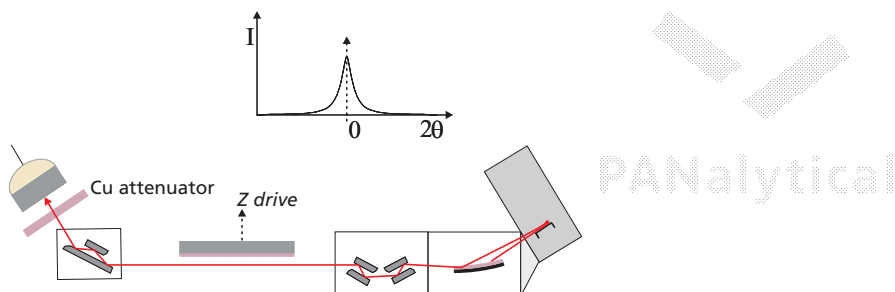


Figure 63: Illustration of the experimental positions used to measure and calibrate the $2\theta = 0$ position

3.1.7.3 Placing ω on an absolute scale

The sample to be measured should then be placed on the sample stage and the z-movement adjusted until the intensity at $2\theta = 0$ is reduced to approximately 5% of the direct beam. At this point the sample should be scanned in omega and the omega axis zero position set to the position of maximum intensity (see Figure 64). This ω peak position is then set as the zero position and this zero position then corresponds to the condition in which the sample surface is parallel to $\omega = 0$. For measurements the z axis should then be readjusted until the intensity is half the direct beam intensity.

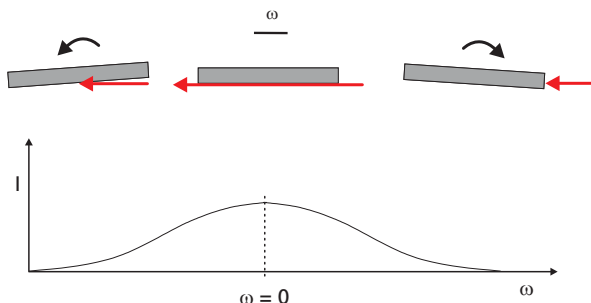


Figure 64: Illustration of the experimental positions and resulting scan used to measure and calibrate the $\omega = 0$ position

3.1.7.4 Setting the φ and ψ positions for a reflection

The practical details of alignment depend on the nature of the sample and how well the orientation of the sample is known. Here are presented only the broad principles of alignment. For a more detailed practical description the reader should refer to other texts, e.g training and application notes.

A reflection must be chosen for measurement and ω and 2θ are set to the appropriate values. Typically these are obtained from databases such as the table shown in section 3.1.5. Alternatively ω and 2θ can be calculated, where θ is obtained from Bragg's law (see sections 3.1.2 and 2.1.1.3) and $\omega = (\theta - \phi)$, where ϕ is the angle between the reflecting planes and the surface sample surface (see section 2.1.1.5 for an equation for ϕ).

If the orientation of the wafer is known, for example with reference to a flat, then the azimuth angle ϕ can be obtained from a stereographic projection or from a database. For a symmetric reflection, ϕ can in principle take any value, but for many of the calculations it is necessary to use the same value of ϕ that is required for one of the asymmetric reflections. In which case the asymmetric reflection is aligned first and the same azimuth position ϕ is maintained during alignment and measurement of the corresponding symmetric reflection.

If the orientation of the wafer is unknown then the Bragg peak must be found empirically, for example by setting 2θ , with an open detector, to the expected value for a required reflection and then scanning ϕ and ω in a large 2-axis map (e.g. ranges 360° and 10° respectively) until a peak can be found.

When a peak has been found a finer ϕ vs ω map (e.g. ranges 5° and 2° respectively) can be performed to optimise the alignment.

This is followed by a similar finer ω vs ψ alignment (e.g. ranges 2° and 5° respectively).

In both ϕ and ψ alignments it is possible that a double peak or U-shaped peak is observed. In which case the optimised ϕ and ψ positions are at the mid-cord or the line of mirror symmetry of the U shape and the optimised ω value is at the highest intensity position along this line.

3.1.7.5 Performing a rocking curve

A rocking curve is an omega scan or an omega/2theta scan in both cases with an open detector. A 2θ value is not measured precisely. In a rocking curve at least two peaks are collected, for example a substrate peak and a layer peak. The angular difference, $\Delta\omega$, between the substrate peak and a layer peak is the measurement that is required for analysis. Note that for a rocking curve when the intensities are large an attenuator may be required.

3.1.7.6 Performing a TA scan

With the ω axis aligned on a peak position, the secondary optics can now be changed to include the analyzer, and the 2θ axis is scanned and the peak re-located. We now have ω and 2θ values for the peak and in some determinations this can be adequate for the measurement, but if the relaxation has lead to large smeared scattering peaks then a reciprocal space map should be collected around

this position. The substrate and layer peaks can be measured in a similar way or both the layer and substrate can be collected in one reciprocal space map.

3.2 Calculating d -spacings, layer thicknesses and multi-layer repeat periods

Section 3.2.1 describes methods for obtaining d -spacings from reciprocal space maps.

Section 3.2.2 describes methods for obtaining d -spacings from rocking curves by comparison of the angular coordinates of the layer reflection position with that of the substrate reflection.

Section 3.2.3 describes methods for obtaining layer thicknesses and multi-layer repeat periods from fringe spacings.

Section 3.2.4 describes the application of the refractive index correction.

3.2.1 d -spacings from reciprocal space maps

The sample rotations, ω , ϕ and ψ bring the reciprocal lattice into an orientation such that useful spots are accessible in the diffraction plane (see Figure 53). In a 2-D reciprocal space map it is important that the plane containing the reciprocal lattice spots of interest is coincident with the diffraction plane. The reciprocal space map contains Bragg spots that correlate with reciprocal lattice spots of the crystal. The Bragg spots have coordinate positions expressed either as reciprocal lattice coordinates, e.g. (Q_x, Q_z) or angular coordinates e.g. $(2\theta, \omega)$ (see Figure 60). With the help of database coordinates for known crystals the user must identify and label the layer and substrate reciprocal lattice spots in their measured diffraction pattern. The user can then attribute coordinate values to specially selected reciprocal lattice points. The coordinate values are used to calculate d -spacings. There are a number of routes for obtaining appropriate d -spacing values. Below are some basic examples.

3.2.1.1 Calculation of d -spacings with reference to 000

This method assumes that 2θ and ω zero positions are precisely calibrated as described in sections 3.1.7.2 and 3.1.7.3. Reciprocal space maps are measured to collect Bragg scattering from a number of reciprocal lattice spots. 2θ and ω coordinates for these spots can then be obtained.

If the system has been set up such that all the rotations are placed on an absolute scale then this is equivalent to calibrating the position coordinates for the 000 lattice points to (0, 0). In this case the d -spacings can be obtained from one reflection alone. The equations for d_x and d_z are simply:

$$d_x = \frac{1}{Q_x} = \frac{\lambda}{\cos \omega_1 - \cos(2\theta_1 - \omega_1)}$$

PANalytical (69)

and

$$d_z = \frac{1}{Q_z} = \frac{\lambda}{\sin \omega_1 + \sin(2\theta_1 - \omega_1)} \quad (70)$$

For example, with reference to Figure 65 it can be seen that the d -spacings for (11-20) and (0004) in GaN can be obtained from the position coordinates of a single 11-24 reflection. This method will only provide correct results if the sample and goniometer are precisely aligned and if there is no tilt of the GaN unit cell with respect to the surface. i.e. $\omega = 0$ is parallel to (0001) plane in GaN.

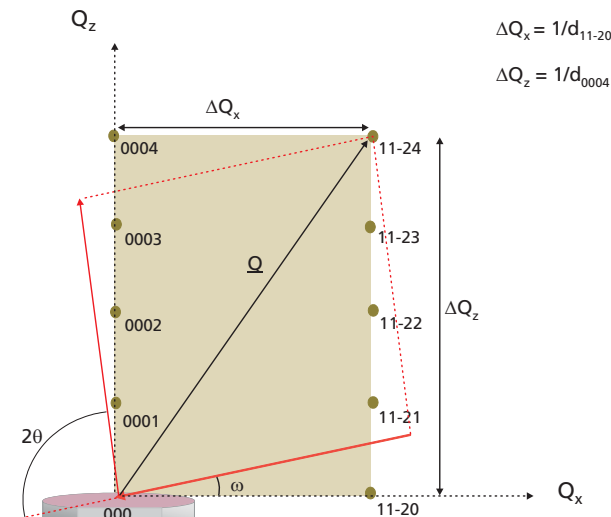


Figure 65: Illustration of how d_x and d_z can be obtained from measurement of a single reciprocal lattice spot when there is no layer tilt

3.2.1.2 Calculation of d -spacings from two measurements to account for offcut

Crystallographic tilt is common in semiconductor epitaxial layers and so most measurements of d -spacing incorporate a tilt correction. For small tilts it is common to combine measurements from two reflections. For example with reference to Figure 66:

$$\frac{1}{d_{11-20}} = \Delta Q_x = \sqrt{(\Delta Q_x^{11-24} - \Delta Q_x^{0004})^2 + (\Delta Q_z^{0004} - \Delta Q_z^{11-24})^2} \quad (71)$$

and

$$\frac{1}{d_{0004}} = |Q^{0004}| \quad (72)$$

Measurements correspond to either the Q_x - Q_z plane or the Q_y - Q_z plane. The x , y and z orientations are chosen to correspond conveniently to the ε_{xx} , ε_{yy} and ε_{zz} axes respectively. Measurements from the x - z and y - z planes are treated separately. If any averaging is required, this is done at the end of the calculation.

The values d_z and d_x are sometimes otherwise known as d_{\perp} and d_{\parallel} . In the case where they correspond to unit cell dimensions, they are also sometimes termed a_{\perp} and a_{\parallel} or a and c .

Tilts in the layer lattice with respect to the surface can arise if the substrate is offcut and if there are dislocations at the layer/substrate interface. If the tilt is small then the strain calculations will be unaffected. These simplified calculations rely on the coincidence or near coincidence of the principal crystallographic axes and the biaxial strain axes so that the assumptions of no shear stresses can be used.

If a more complete description of the strain is required because the tilt angle is large, then an alternative analysis, employing the full strain tensor and accounting for axial rotations, may be more appropriate.

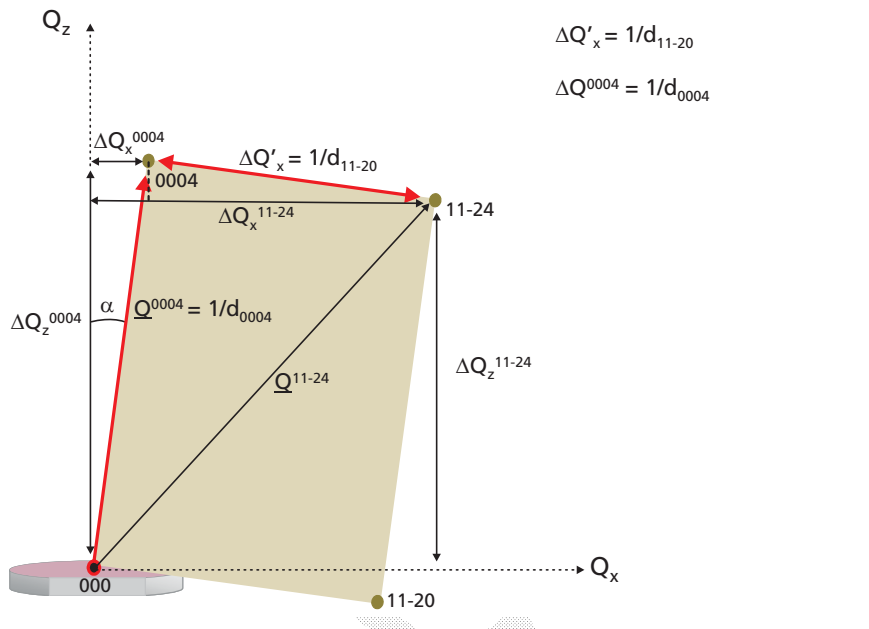


Figure 66: Illustration of how ΔQ_x and ΔQ_z can be obtained from measurement of two reciprocal lattice spots where there is layer tilt

3.2.2 *d*-spacings from rocking curves

Single rocking curves can often provide data very rapidly for analysis of epitaxial layers. The principal requirement for rocking curve analysis is that the layer and substrate (or layer and buffer layer) share the same crystal structure, they have the same orientation and that the unit cell dimensions of the crystals are sufficiently similar that their Bragg peaks are very close (peak separation is up to only a few degrees). The analysis does make a lot of assumptions for example that the peak on the rocking curve corresponds to the centroid of the Bragg peak in reciprocal space. To achieve this it is necessary for the crystal layers to have almost no defects so that their peaks are not too broad. For well-behaved materials, such as single crystal semiconductor device structures which do not exhibit large loss of symmetry and whose crystal orientations have a simple relationship with the surface, rocking curves are extremely useful. When the layers contain many defects, the peaks can appear asymmetric and it may happen that the whole peak is not being captured in the rocking curve in which case it would be necessary to collect a reciprocal space map.

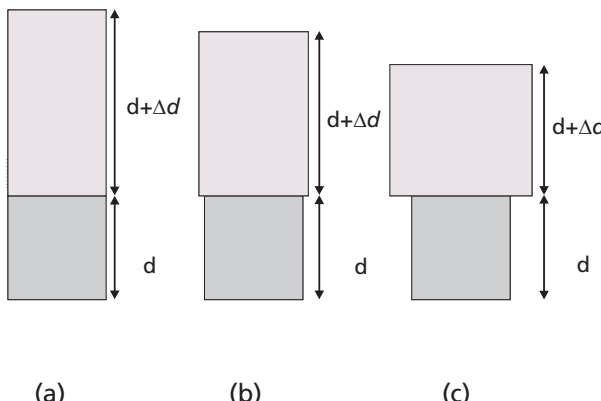


Figure 67: Illustration of how a layer d -spacing can be represented as an incremental addition to a comparable substrate d -spacing. (a) Fully strained, (b) partially relaxed, (c) fully relaxed.

Figure 67a shows a schematic illustration of a unit cell from an epitaxial layer which is fully strained in order to have perfect in-plane registry with the underlying substrate. Figure 67c illustrates the unit cells of the layer and the substrate in their fully relaxed state. Here, the lack of registry between the two in-plane lattice parameters is accommodated by interfacial misfit dislocations. Figure 67b illustrates an intermediate case where there is still some strain in the layer and there are interfacial dislocations. The layer in this case is said to be partially relaxed. In all three cases the plane spacing in the layer normal to the interface is different from the plane spacing in the substrate and it is this difference, Δd , that is measured.

The basic principle of the analysis is that small differences in d -spacing, Δd , result in changes in the Bragg scattering angle $\Delta\theta$, and also that rotations in the plane orientation due to strain, $\Delta\varphi$, and rigid body tilts of the layer with respect to the interface, $\Delta\alpha$, rotate the Bragg peak position. All three of these effects require rotation of the sample orientation, $\Delta\omega$, in order to collect the peak. The rocking curve method plots intensity versus ω , and employs an open detector to catch all possible 2θ values, so both the effects of Bragg scattering and plane rotation are combined in the ω measurement. From a rocking curve that provides a substrate and a layer peak, the peak separation, $\Delta\omega$, is the key value, since $\Delta\omega = \Delta\theta + \Delta\varphi + \Delta\alpha$. Most of the subsequent analysis then involves identification of these separate contributions. One of the advantages of this approach is that the open detector maximizes the chances of capturing the peak, making the experiment more rapid to set up. Sometimes the detector is scanned to increase the angular range of detection, but because of the open detector, the angle 2θ is not actually measured.

3.2.2.1 Obtaining a d -spacing from a symmetrical rocking curve where there is no layer tilt

If the unit cells of the layer and the substrate are parallel, i.e. there is no layer tilt, a symmetric rocking curve which includes the Bragg peaks from the planes parallel to the interface in both the layer and the substrate is easily obtained. As the sample is rotated over a small range in ω , the Bragg conditions for the layer and substrate are satisfied at different ω values (labeled 1 and 2 in Figure 68).

Because the detector is relatively large and captures a range of diffraction angles it can capture each of the different Bragg intensity peaks without being moved. The peak splitting between the layer reflection and the substrate reflection, $\Delta\omega$, in the rocking curve in this simple case is entirely due to the difference in plane spacing Δd and therefore $\Delta\omega = \Delta\theta$. From Bragg's law for the substrate:

$$\lambda = 2d_s \sin\theta_s \quad (73)$$

and for the layer:

$$\lambda = 2(d_l) \sin(\theta_s + \Delta\theta) \quad (74)$$

that can be solved to give, for example:

$$d_l = \frac{d_s \sin\theta_s}{\sin(\theta_s + \Delta\theta)} \quad (75)$$

Values for d_s and θ_s are obtained from databases.

It should be noted that values for $\Delta\omega$ and $\Delta\theta$ can be negative as well as positive.

The sign of Δd is always the opposite to that of $\Delta\theta$.

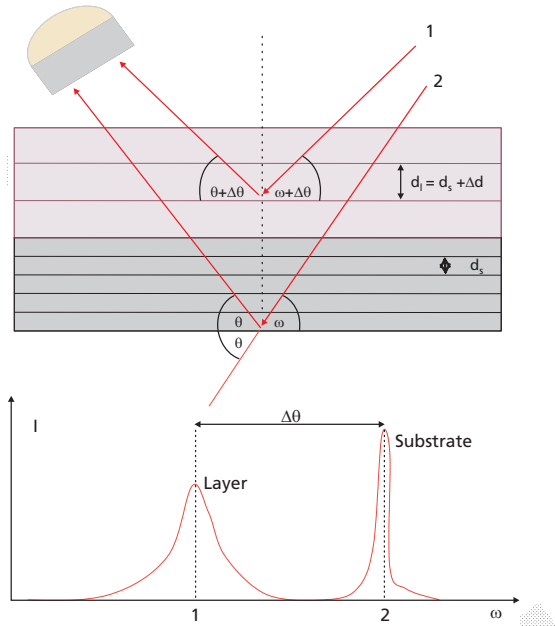


Figure 68: Illustration of how a small difference in layer and substrate d-spacing is measured as a peak splitting in a rocking curve

3.2.2.2 Obtaining a d-spacing from two symmetrical rocking curves where there is layer tilt

If there is any tilt (rigid body rotation) of the layer unit cell with respect to the substrate unit cell then the measured $\Delta\omega$ value at azimuth $\phi=0$ ($\Delta\omega_0$) will contain a component of tilt, $\Delta\alpha$, i.e.

$$\Delta\omega_0 = \Delta\theta + \Delta\alpha \quad (76)$$

If the rocking curve measurement is repeated for the azimuth, $\phi+180^\circ$, then the sense of α is reversed whilst $\Delta\theta$ remains the same:

$$\Delta\omega_{180} = \Delta\theta - \Delta\alpha \quad (77)$$

and so

$$\Delta\theta = \frac{(\Delta\omega_0 + \Delta\omega_{180})}{2} \quad (78)$$

The analysis can then proceed as in section 1.

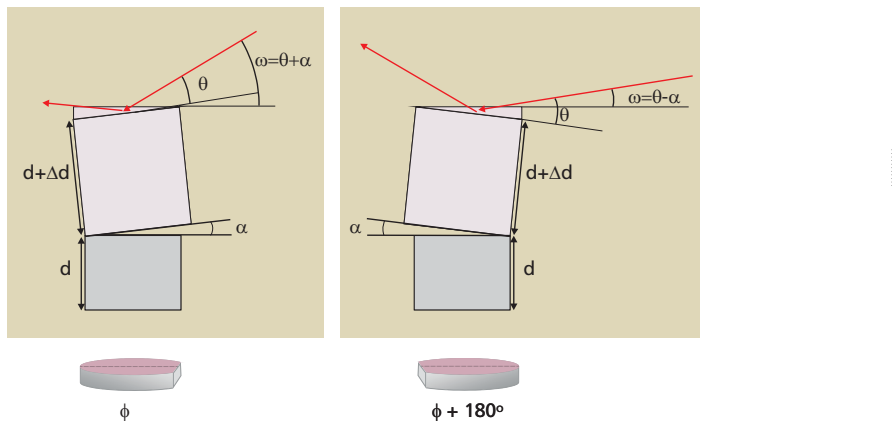


Figure 69: Illustration of how measurement of the same reflection from opposite directions is used to measure tilt between layer and substrate

3.2.2.3 Obtaining a d -spacing from two asymmetrical rocking curves where there is layer tilt

Measurements of symmetric rocking curves provide values for plane spacing perpendicular to the sample surface, d_z . Calculations of composition and strain require that plane spacings parallel to the interface d_x are also measured. A measure of d_x can be obtained using planes that are inclined. Figure 70 illustrates the inclined planes in a layer unit cell and the inclined planes in the substrate that are used as a reference. The substrate planes are inclined at an angle ϕ_s with respect to the interface plane. The layer planes are inclined at an angle $\phi_s + \Delta\phi$ with respect to the interface planes. The plane spacing for the layer will also be different to that of the substrate, $d_L = d + \Delta d$. Thus there are potentially three contributions to the rocking curve peak splitting $\Delta\omega$:

$$\Delta\omega_0 = \Delta\theta + (\Delta\alpha + \Delta\phi) \quad (79)$$

If a rocking curve is obtained for the same set of planes for the azimuth, $\phi + 180^\circ$ then as before,

$$\Delta\omega_{180} = \Delta\theta - (\Delta\alpha + \Delta\phi) \quad (80)$$

and so

$$\Delta\theta = \frac{(\Delta\omega_0 + \Delta\omega_{180})}{2} \quad (81)$$

Furthermore, if $\Delta\alpha$ has been obtained from a pair of symmetric rocking curves, then $\Delta\phi$ can be obtained from:

$$\Delta\phi = \frac{(\Delta\omega_0 - \Delta\omega_{180})}{2} - \Delta\alpha \quad (82)$$

PANalytical

To obtain the layer in-plane spacing d_x the following procedure is used:
From Braggs law:

$$d_l = \frac{d_s \sin\theta_s}{\sin(\theta_s + \Delta\theta)} \quad (83)$$

also from geometry:

$$d_x = \frac{d_l}{\sin(\phi_s + \Delta\phi)} \quad (84)$$

therefore

$$d_x = \frac{d_s \sin\theta_s}{\sin(\theta_s + \Delta\theta) \sin(\phi_s + \Delta\phi)} \quad (85)$$

To solve this equation d_s , θ_s and ϕ_s are obtained from databases and crystallographic tables.

The layer plane spacing perpendicular to the interface, can also be obtained from the asymmetric measurements where:

$$d_z = \frac{d_s \sin\theta_s}{\sin(\theta_s + \Delta\theta) \cos(\phi_s + \Delta\phi)} \quad (86)$$

The above analysis can be repeated for an azimuth at 90° to obtain d_y .

PANalytical

PANalytical

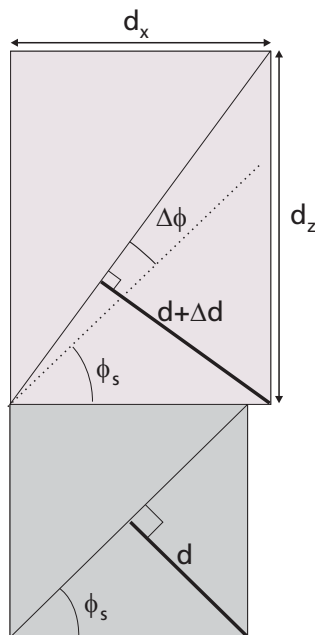


Figure 70: Illustration of the components of d-spacing strain and tilt for an inclined plane in a strained layer

3.2.3 Using fringes to calculate superlattice periods and layer thicknesses

In principle, all periodic length scales in a structure contribute to the scattering pattern in some form. However in many materials, because of inhomogeneities in length scales, scattering from them tends to be weak and is either lost as background scatter or contributes to a general peak broadening. This kind of broadening is considered for example in polycrystalline materials using the Scherrer equation³¹. In epitaxial thin films with very flat surfaces and interfaces and in which the film thicknesses are not subject to random fluctuations, the contributions of scattering from interfaces and multi-layers is strongly reinforced and can often be observed as fringes in the diffraction pattern.

The fine details in the diffraction patterns from highly perfect layers arise from dynamical effects in which there are multiple interferences and reflections throughout the crystal. Generally, for high quality epitaxial layers, details in the diffraction patterns are best analyzed by simulation and fitting (see chapter 4) however some simple calculations can be performed using the angular separation of fringes to obtain approximate values for layer thickness and superlattice³⁰ periodicity.

Figures 71-73 show some examples of simulated diffraction patterns from layered structures. Figure 71 shows the pattern around the 004 Bragg reflection from a single 100 nm thick InGaN layer on a GaN substrate. The peaks corresponding to the substrate and the layer can be easily identified. Around the layer peak are fringes that are identifiable because they are equally spaced in angle, ω . Figure 72 shows the pattern around the 004 Bragg reflection from a multi-layer superlattice with alternating 5 nm thick InGaN and 5 nm thick GaN layers repeated 50 times. The diffraction pattern also shows thickness fringes associated with the total thickness of the multi-layer which is 500 nm. Figure 73 shows the pattern around the 004 Bragg reflection from a multi-layer structure containing a single layer, multi-layer and capping layer. Features in the diffraction pattern from a more complicated structure like this cannot be easily attributed to individual length scales and it is more likely that the details of a measured structure like this would be obtained through direct pattern simulation and fitting (see chapter 4).

It has been shown that for two fringes, numbered n_1 and n_2 , that arise in the vicinity of Bragg peaks from planes parallel to the surface³²:

$$2t \sin \omega_1 = n_1 \lambda \quad (87)$$

$$2t \sin \omega_2 = n_2 \lambda \quad (88)$$

Hence

$$t = \frac{(n_1 - n_2) \lambda}{2(\sin \omega_1 - \sin \omega_2)} \approx \frac{(n_1 - n_2) \lambda}{2\Delta\omega \cos \omega_1} \quad (89)$$

Where ω_1 , ω_2 correspond to the angular positions of the peaks n_1 and n_2 and $\Delta\omega = (\omega_1 - \omega_2)$. Note that if n_1 and n_2 are neighboring fringes then

$$|(n_1 - n_2)| = 1 \quad (90)$$

And therefore

$$t = \left| \frac{\lambda}{2\Delta\omega \cos \omega_1} \right| \quad (91)$$

For reflections from planes that are not parallel to the interface the following equation can be used:

$$L = \frac{\lambda \sin(\theta + \phi)}{2\Delta\omega \sin\theta \cos\theta} \quad (92)$$

Where $\Delta\omega$ is the angular separation of neighboring fringes, θ is the Bragg angle of associated Bragg peak, ϕ is the angle between the Bragg planes and the sample surface.

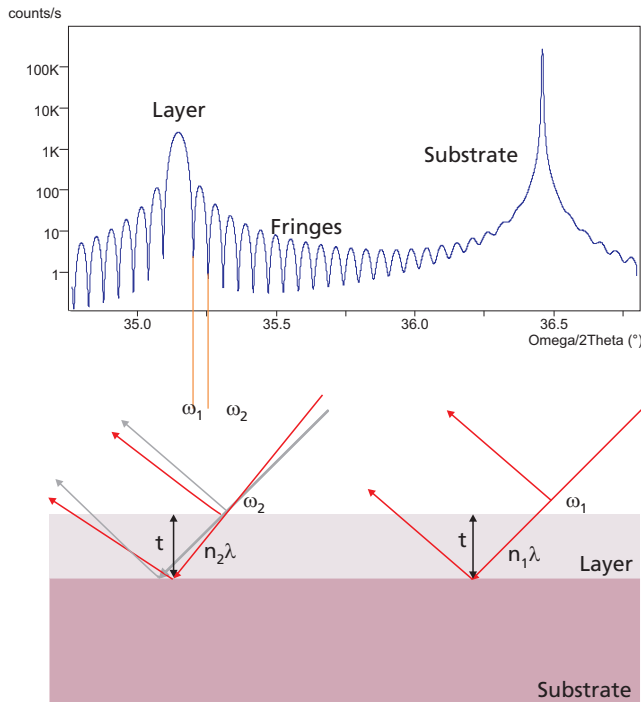


Figure 71: Top: Illustration of layer thickness fringes in a diffraction pattern from a single 100 nm thick InGaN layer on a GaN substrate. Bottom: The path difference between waves diffracting at the top surface of the film and those diffracting at the lower surface is a function of the angle of incidence and the film thickness, constructive and destructive interference effects are seen as a fringe modulation close to the main Bragg peak.

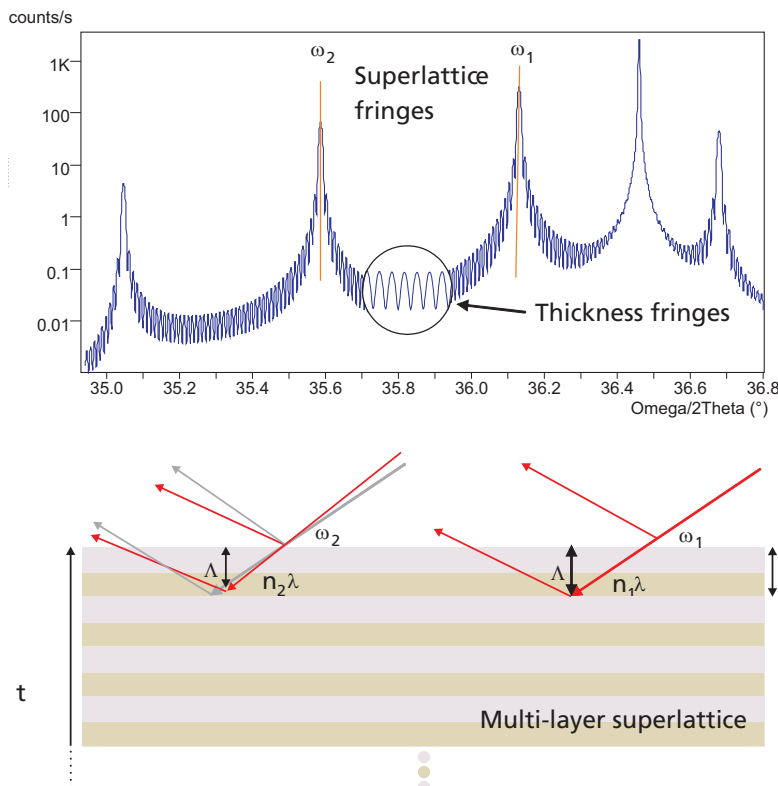


Figure 72: Top: Illustration of layer thickness fringes and superlattice fringes in a diffraction pattern from a multi-layer on a GaN substrate. Bottom: The changing path differences between waves diffracting at the top and lower surface of a repeat period gives rise to fringing.

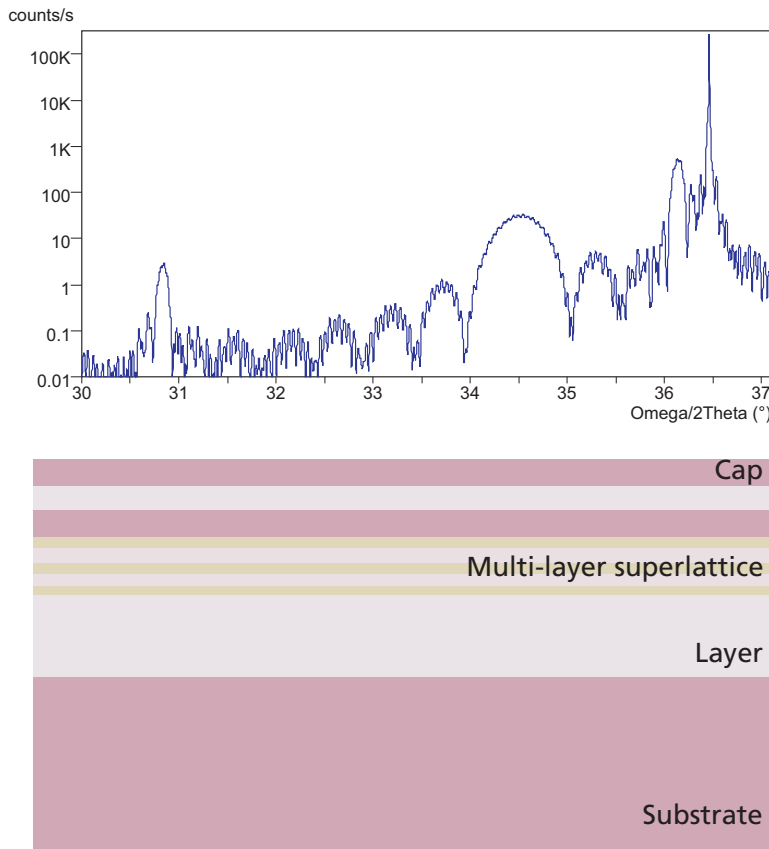


Figure 73: Top: Simulated diffraction pattern from complex multi-layer on a GaN substrate. Bottom: The complexity of the structure makes it difficult to attribute features in the diffraction pattern to individual length scales in the structure.

3.2.4 Refractive index correction

The angles that are measured in a diffraction experiment are those that are occurring between the incident and scattered beams and the sample surface outside of the sample, usually in air. Bragg's law actually relates the diffraction angle to the wavelength of the irradiating beam inside the sample. Due to the dielectric susceptibility of the material the irradiating beam is modified on entering the material. This modification is complex but can in certain circumstances be expressed in its most simple form by the refractive index, n , of the material. The

angle of incidence in air is modified to the angle of refraction within the material and according to Snell's law:

$$\sin r = \frac{\sin i}{n} \quad (93)$$

Where, with reference to Figure 74, r is the angle of refraction and i is the angle of incidence. Both of these angles are measured with respect to the surface normal. For a surface symmetric Bragg reflection, this relationship can be reworked in respect of the real Bragg angle in the material, θ_m , and the observed Bragg angle in air, θ_a , as:

$$\cos \theta_m = \frac{\cos \theta_a}{n} \quad (94)$$

This relation can also be expressed more usefully as:

$$\sin \theta_m = \frac{\sqrt{n^2 - \cos^2 \theta_a}}{n} \quad (95)$$

Bragg's law with reference to the parameters in the material is expressed as:

$$\lambda_m = 2d \sin \theta_m \quad (96)$$

Replacing $\sin \theta_m$ with an expression containing the measurable values θ_a gives the equation:

$$\lambda_m = \frac{2d}{n} \sqrt{n^2 - \cos^2 \theta_a} \quad (97)$$

This is the simplest possible correction for refractive index, more rigorous analyses are possible. The refractive index of materials such as GaN for X-rays is typically of the order 0.99999. The refractive index correction therefore has little impact on the results for Bragg angles in excess of around 30° and for this reason it is often ignored. At 30° without the correction for refractive index the d -spacing measurements are underestimated by about 0.004%. Above this angle the error reduces to less than 0.001% at 90°. Below 30° the error increases more rapidly and at Bragg angle of 1° the error can be of the order 3%. The effects of refractive index are therefore much more pronounced at glancing incidence and glancing exit geometries and for small scattering angles.

The refractive index itself is a complex number. A simplification of it is given by:

$$n = \left(1 + \chi_0\right)^{\frac{1}{2}} \quad (98)$$

The isotropic dielectric susceptibility, χ_0 , for a material can be calculated from:




$$\chi_0 = -\frac{r_e \lambda^2 N_A Z}{\pi A} \rho \quad (99)$$

Where r_e is the electron radius, N_A is Avogadro's constant, Z is the number of electrons in a unit volume, A is the mass of atoms in a unit volume, ρ is the macroscopic density of the material³³.

However, this is still an approximation for single crystals because the dielectric susceptibility χ_{ij} is a tensor property³⁴ and is related to the crystal symmetry in a manner comparable to the stiffness tensors described in chapter 2. The true refractive index actually changes with the relative incident and scattered beam directions and is also a complex expression affecting polarization and absorption of the beam. Often where refractive index effects need to be incorporated in more rigorous terms they are included in numerical simulations of entire scattering patterns rather than individual analytical calculations.

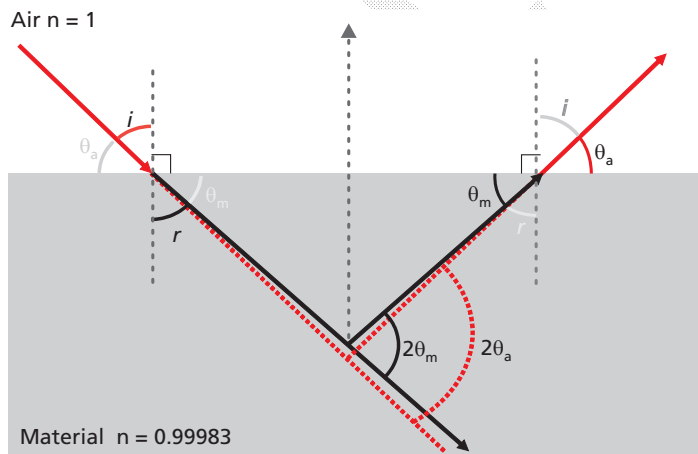


Figure 74: Illustration of the incident and refracted angles required for the refractive index correction




4. Solutions for strain composition and thickness via simulation and fitting

4.1 Introduction

As illustrated in Figure 73, for many multi-layer device structures it may not be possible to attribute peaks in the diffraction pattern to individual layers in the multi-layer structure. This is because the peaks in the pattern arise as a result of coherent simultaneous scattering by layers rather than isolated scattering events from individual layers. In this case the details of the layer structure, strain composition and thickness can be obtained by simulating the diffraction patterns from a number of sample structures and finding the sample structure that gives the best fit of the simulated pattern to the measured diffraction pattern³⁵.

4.2 Theoretical simulation of diffraction

The major theoretical approaches used as the basis for simulating the fine structure around Bragg peaks incorporate ideas based on dynamical diffraction or kinematical diffraction. Both of these theories are detailed elsewhere in the literature and are not described in any detail here³⁶.

The kinematic theory considers scattering from an atom or molecule in terms of its form factor and considers how this is modified by the assembly of these units into a crystal structure, described by the structure factor. The theory considers that the scattering intensity from crystal units is simply added to give a Bragg peak positions and intensities. Modifications to this are made to incorporate broadening of the Bragg peaks from instrumental effects and crystal size effects. It is also possible to include interference patterns from multiple layers and thin layers and methods have been devised to model the satellite peaks from superlattices.

For highly perfect semiconductor single crystal thin films, the kinematical models are not always adequate and more rigorous dynamical diffraction models are more appropriate. In the dynamical models the aim is to solve the wave equation for the entire illuminated area of the sample. The X-ray wave front is considered to be coherent throughout the entire sample volume that is irradiated. Rather than consider the addition of isolated scattering events the material is considered as a medium with a varying periodic dielectric susceptibility. There is a dynamic relationship between the exciting field of the incident beam and the excited field of the material and together these create the internal wave-field. The dynamical approach includes the observed effects such as extinction (reduced intensities) and subtle peak shifts that are measurable in highly perfect single crystals.

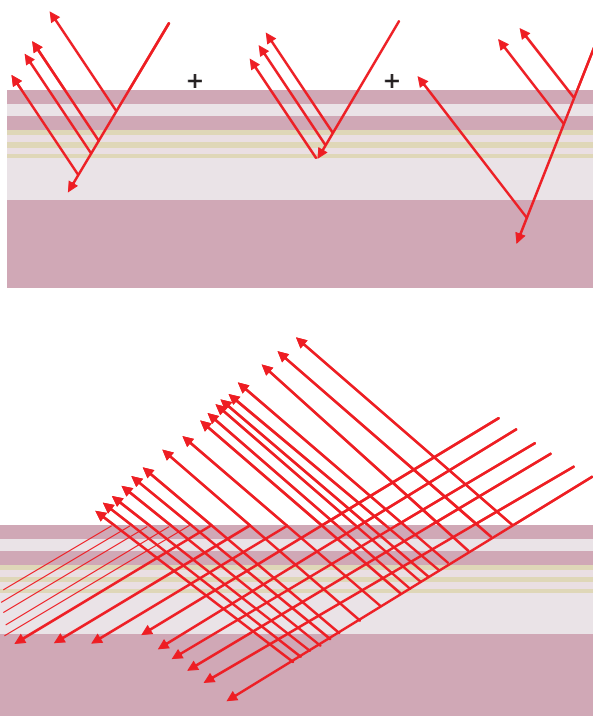


Figure 75: Top: The kinematic theory adds contributions from different scattering regions in an illuminated volume. Bottom: The dynamical theory considers all interactions of the incident beam and the material in a single scattering event.

4.3 Simulation and fitting software

All models necessarily include some simplifications and work still continues in this area to explore ideas for improvements³⁷. Commercial software packages exist that will perform simulations of high resolution diffraction patterns.

There are usually some limits on the kinds of layer structures that can be described in the models. For example the models specify epitaxial orientation relationships and a limited number of layer substrate relationships. Also the models need to include descriptions of the instrument because the optics used for the experiment, affect the resolution of the scan and the shapes and widths of the peaks. The software may also be suitable for a number of measurement types, for example, very high resolution omega/2theta scans or omega rocking curves. It may be limited to particular reflections, for example avoiding extreme glancing incident or glancing exit reflections where refraction effects become more dominant.

4.3.1 Data collection

The software to be used in simulation may determine what kind of data file is appropriate. A simulation typically assumes that all of the available diffracted intensity is collected. This means that for omega rocking curves a wide open detector is used and when high-resolution omega/2theta scans are used the material is sufficiently perfect that nearly all of the intensity is captured. For many device structures that do not incorporate buffer layers this criterion can be readily satisfied. However, gallium nitride materials pose quite a challenge for traditional omega rocking curve data collection. Because the device structures almost always include a GaN buffer layer, some of the layers are not defect free and their diffraction Bragg peaks are quite broad. For materials that exhibit broad peaks omega rocking curves are often difficult to simulate. This is because for most reflections the detector sweeps across the reciprocal lattice spots usually at an inclined angle and whilst the total intensity of the scattering may be collected, it becomes spread across the rocking curve (see Figure 76). When a higher resolution omega/2theta scan is performed, for example in a symmetric scan with a triple bounce analyser, it collects only part of the total intensity. In this case, finer features, such as fringes may be more easily observed closer to the strongest Bragg peaks but the overall intensity of the signal is much reduced and the lower intensity satellites that are further from the main Bragg peaks may not be detected. Sometimes, for a symmetric reflection, it is necessary to measure a reciprocal space map and then to add all of the individual scans to obtain a 'projected scan' in which all of the intensity is collected, but it is not spread across the scan in the manner of a rocking curve. Collection with the highest resolution methods can take a long time for GaN, because the signal strength is diluted as a result of peak broadening. Methods are constantly researched to find the optimum combination of resolution and intensity to capture the diffraction pattern from GaN most efficiently and rapidly³⁸.

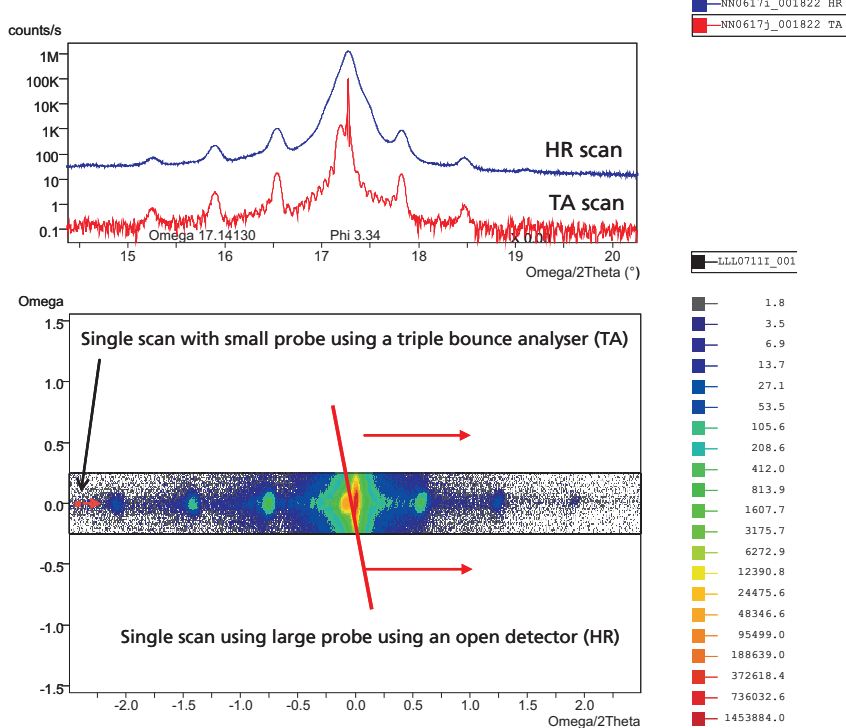


Figure 76: Top: Comparison of an HR scan with a TA scan for the same sample and reflection.
Bottom: Illustration of the different instrument probe sizes for the HR scan (large red line) and the TA scan (small red spot).

4.3.2 Sample file

A sample file is a list of all of the layers in the multi-layer structure. The layers must be presented in the correct order, usually starting with the substrate and ending at the surface. Information about the layers is required, such as their thicknesses, alloy compositions, state of relaxation, whether there is any alloy composition grading and what form the grading takes. The crystallographic orientations of the substrate and the layers must be considered along with the Bragg reflection that is used for the measurement. Figure 77 shows an example of a sample file in X'Pert Epitaxy software.

```

Layer:0, Substrate, Sapphire, thick = 600.000000 um, AlO, 0 0 1, offcut = -0.015
Layer:1, None, Wurtzite, thick = 7.000000 um, GaN 161389ppm, 0 0 1, Steps = 1, R% = 100.0
Layer:2, Superlattice, thick = 0.071500 um, No. of Repeats = 10
Layer:2.0, None, Wurtzite, thick = 0.004950 um, GaN 161389ppm, 0 0 1, Steps = 1, R% = 0.0
Layer:2.1, None, Wurtzite, thick = 0.0022um, In0.10Ga0.90N 174722ppm, 001, Steps = 1, R% = 0.0
Layer:3, None, Wurtzite, thick = 0.076900 um, GaN 161389ppm, 0 0 1, Steps = 1, R% = 0.0

```

Figure 77: A sample file lists all of the structural parameters for each layer in order.

4.3.3 Fitting

During fitting the simulation is compared with the measured data, then some, or all, of the sample and convolution parameters used in the simulation model are changed and a new comparison is made. A measure of the comparison is called the ‘fit value’. The fit values for a number of simulations are compared and the set of parameters (sample and convolution parameters) whose simulation results in the smaller fit value is selected. The process is repeated until it reaches an end point. The selected algorithm determines the method by which the sample and convolution parameters are varied from simulation to simulation and how an end point is reached. The set of sample and convolution parameters that give the smallest fit value are called the ‘best fit’ for that particular fitting run, and can be used to update the sample and settings files.

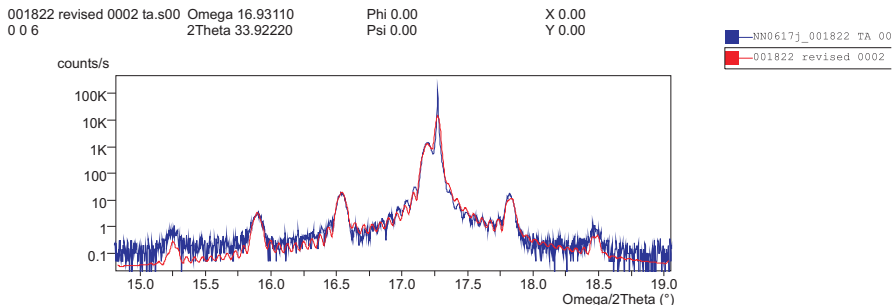


Figure 78: Trial simulated diffraction patterns obtained with different parameter sets are compared with the data until a best fit is obtained (measured data are shown in blue, simulation is shown in red).

For example, in X'Pert Epitaxy, during fitting the following processes can be identified:

- Smoothing the measured and simulated data and treating background intensity
- Comparing the simulation with the measured data to obtain a fit value
- Changing some or all of the simulation and convolution parameters
- Identifying a better parameter set
- Deciding when to end the fitting process and providing the best parameter set

There are many methods and algorithms available for each of these fitting steps. Software programs offer choices from specifically adapted procedures to span a range of fitting requirements. Some of the possible fitting algorithms used are, for example, Smoothfit, Levenberg-Marquardt, Principal Axis, Genetic Algorithms and Simulated Annealing.

4.4 Imperfections

Obtaining a good fit of a simulated diffraction pattern to a measured pattern can be difficult with GaN-based device structures. The reason for this is that GaN-based device structures tend to contain many more defects than other compound semiconductors that are grown on more suitable substrates.

4.4.1 Peak broadening from defects

Simulations of defective crystals are difficult to generalize, because there are so many possibilities for the kinds of defects that can lead to peak broadening. For dynamical theories defects are introduced by 'perturbation' of regions in which coherence is partially lost. In kinematic theories the peaks tend to be broadened after the simulations, by mathematical functions such as Gaussian or Lorenzian functions, to simulate the effects, for example, of mosaic block size. A broadening function can be convoluted with a simulated scan to model in the simplest possible way a general 'diffuse scattering' effect without reference to any particular crystallographic defect. The simple additions that are made to models tend to be general approximations that may allow a cosmetic adjustment so that a simulated scan may look more like a measured scan.

4.4.2 Anomalous peak intensities

Some GaN measurements, in particular the 0002 Bragg reflection from (0001) surface oriented GaN thin films, show what appear to be anomalously high GaN peak intensities. The GaN buffer layer peak is more intense with respect to the overlying GaN and InGaN and AlGaN alloy layers than would be predicted by either the kinematic or dynamical theories. It is likely that the reason for this is due to defects, but the exact cause of this is currently unknown and certainly not well modeled by current software.

4.4.3 Summary

Diffraction pattern simulation and fitting is used routinely for device structures fabricated from GaN and related compounds. Because of the spreading of the peaks and the relatively low intensities of the highest resolution scans, methods have been developed to enhance the intensities that can be obtained from these structures and to increase the speeds with which the data can be collected. Despite the challenges that face simulation and fitting of diffraction patterns from GaN and related compounds, much valuable information can be obtained from a good, if not perfect, fit of a simulated profile to a measured profile. Certainly, by matching the peak positions and fringe periodicities, most of the useful information about a multi-layer structure can be obtained from the diffraction pattern, even if the whole pattern including peak broadening is not perfectly matched.



PANalytical



PANalytical



PANalytical

5. Studies of defects

5.1 Introduction

Most GaN thin films are deposited heterogeneously on various substrates e.g. sapphire, SiC, or silicon wafers. On these substrates the lattice misfit between the GaN and substrates is accommodated by dislocation arrays. Much of development effort in GaN buffer layer technology is aimed at controlling the dislocation densities and improving the crystalline quality of GaN buffer layers as virtual substrates for subsequent device overgrowth. Strategies for improving buffer layer crystalline quality may include patterned overgrowth, the incorporation of strained interlayers, growing on exotic or offcut crystal orientations and composition grading, all of which require optimization of growth conditions. There is a requirement for measurement of crystalline quality in order to appraise the success of any design strategy or growth condition. XRD has an important part to play as a rapid and non-destructive method of quality assessment. This chapter briefly describes how XRD can be employed to investigate quality issues.

5.2 Characterization of dislocations and mosaic blocks

The notion of misfit dislocations and their associated threading arms has been introduced in section 2.3.2. Dislocations are characterized by their line direction and their Burgers vector³⁹. When the line direction is parallel to the Burgers vector the dislocation is called a screw dislocation. When the line direction is perpendicular to the Burgers vector the dislocation is an edge dislocation and when the line direction is neither of those it is called a mixed dislocation⁴⁰. Dislocation types can be characterized using electron microscopy⁴¹. The efficiency with which an interfacial dislocation can relieve mismatch stresses depends upon its character. The effect of a threading dislocation on the buffer layer can also be dependent upon its character. For example, a threading dislocation with a screw component may give rise to tilt between mosaic blocks whereas a threading dislocation with an edge component may give rise to twist between mosaic blocks. Individual dislocations are characterized using electron microscopy, whereas XRD measures the net effect of a population of dislocations. How the dislocations are arranged, for example randomly or in low angle grain boundaries will also affect how the total volume of illuminated crystal will diffract.

The concept of mosaic blocks has been introduced in section 2.3.3. Mosaic blocks are envisaged as regions of dislocation-free crystal. Figure 79 illustrates two mosaic blocks in an epitaxial layer. Considering the same sets of planes in neighboring blocks, the factors that affect the size and shape of the reciprocal lattice spots that represent them are their dimensions and relative orientations. Crystallite size effects are measurable, together with d -spacing variations (micro-strains) in the direction parallel to the diffracting planes normal. Sizes parallel to the interface are known as lateral correlation lengths and dimensions normal to the interface

are depth-wise correlation lengths. If the mosaic blocks are rotated around an axis normal to the interfacial plane they are said to be 'twisted'. If they are rotated about an axis parallel to the interfacial plane they are said to be 'tilted'. Some authors use the results of XRD measurements of tilt and twist to comment on the relative proportions of dislocation types and dislocation arrangements that are believed to be present in the GaN layers.^{42,43,44}

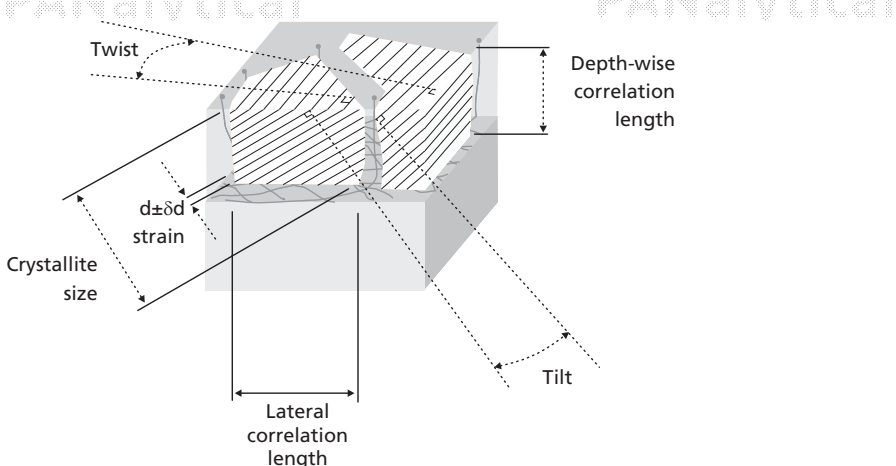


Figure 79: Illustration of two mosaic blocks in a layer showing parameters that contribute towards a statistical spread in the diffraction peak

5.3 Broadening of reciprocal lattice spots

The concept of the reciprocal lattice has been introduced in section 2.1.1.7 and the inverse effect of crystal truncation on the size of the reciprocal lattice spot has been briefly introduced in sections 2.3.1 and 2.3.3. Expanding on these concepts we can make the following simplistic inferences: A rotation, $\delta\phi$, in the angular position of diffracting planes will cause a corresponding rotation, $\delta\phi$, in the position of the reciprocal lattice spot. A limiting dimension, L , in the scattering crystal, will effectively create a spread of dimension proportional to $1/L$, in the same direction as L , in the reciprocal lattice spot. The effects of rotation and broadening of a reciprocal lattice spot occur for each individual mosaic block. The observed reciprocal lattice spot for a scattering volume of crystal is considered to be due to a statistical summation of the contributions from all of the individual mosaic blocks that are contained in the illuminated volume. (The theory for how the individual contributions should be summed is the subject of ongoing research^{45, 46, 47}). These changes in the reciprocal lattice spot are three-dimensional and when making measurements of peak broadening it is important to specify the direction of the measurement.

This concept of peak broadening is simplified in Figure 80 for broadening from mosaic blocks exhibiting tilt, twist, micro-strain and correlation lengths. Twist and tilt values correspond to rotational spread around the centroid of the spot. A dimensional spread in the reciprocal lattice spot corresponding to the inverse of a correlation length corresponds to a mean value of all of the lengths present in the crystal. The term correlation length in this context is a term that has arisen in the studies of diffuse scatter from single crystal epitaxial layers, but it is in principle a crystal truncation similar to the finite size effect described in polycrystalline scattering. However, crystal size measurements in polycrystalline samples are defined in the direction of the reciprocal lattice vector (normal to the scattering planes), whereas correlation lengths tend to be defined normal (depth-wise) and parallel (lateral) to the epitaxial layer surface.

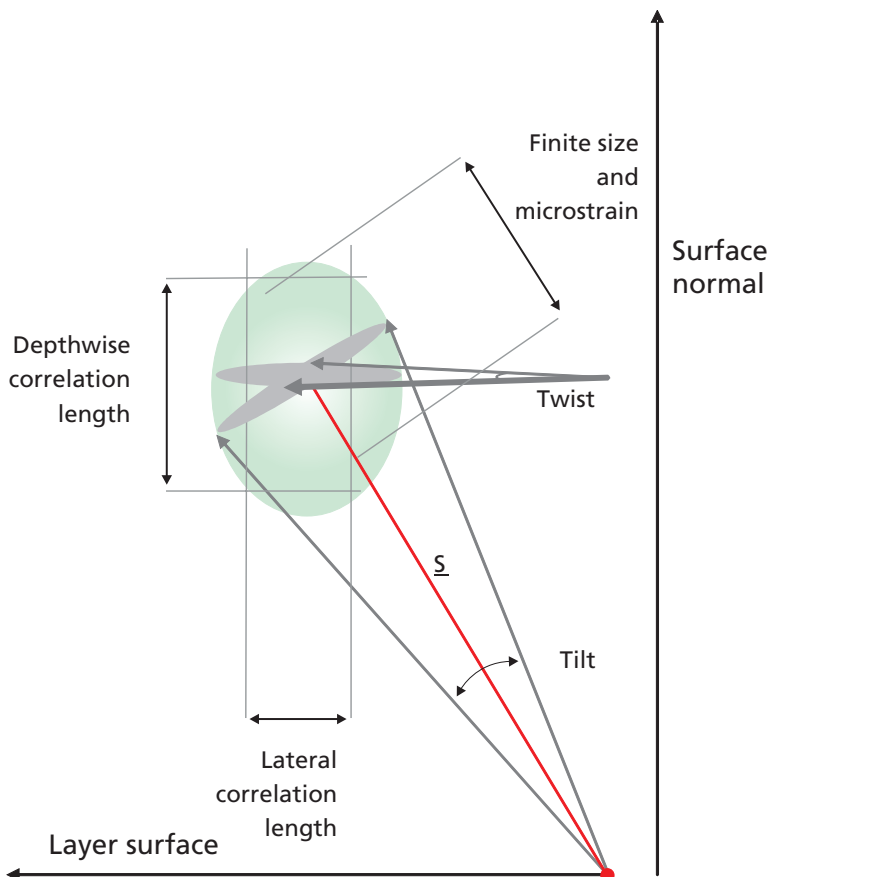


Figure 80: Illustration of the orientations of spread in a reciprocal lattice spot arising from the real space features illustrated in the previous figure

5.4 FWHM as a measure of crystalline quality

Measurements of crystal quality focus on the measured angular width of a reciprocal lattice spot, which needs to be defined, for example as the Full Width at Half Maximum (FWHM) or the integrated width of a Bragg diffraction peak⁴⁸.

Direct measurement of reciprocal spot size from the diffraction peak FWHM assumes that the instrument probe size is sufficiently small that instrumental broadening is a negligible contribution to the peak width. This is a reasonable assumption for high-resolution measurements on GaN materials that demonstrate broad peaks.

There may be other less significant effects contributing to diffuse scatter around Bragg peaks, for example scattering from point defects, but these are often ignored for buffer layers because effects from misfit and threading dislocations are considered to dominate.

5.5 Measurement strategies

Studying the shape of reciprocal lattice spots can involve scanning from numerous angles and understanding the instrument function for these various angles may not be easy. However, some simplistic approaches can be made to obtain information that can be of particular use for quality assessment. Most approaches assume that there is a dominant contribution to peak spreading i.e. it is mainly due to tilt or twist and there are some methods for assessing whether this kind of simplification is valid, for example by studying how the reciprocal lattice spot size changes for different orders or by looking for directions in which it is particularly elongated. Some of these approaches are described below.

5.5.1 Accessible reflections

Figure 81 illustrates schematically the reciprocal lattice spots that can be measured in different types of reflection geometry. (For a more detailed discussion of the limits for accessible reflections see reference⁴⁹).

The coplanar arrangement (as previously shown in Figure 53) is the most commonly used geometry for epitaxial layers. It offers the most precise measurements and the instrument probe is well defined within the omega/2theta diffraction plane. For the coplanar geometry there are the possibilities of investigating peak broadening in symmetric reflections or asymmetric reflections.

The in-plane geometry can be used to gain access to reciprocal lattice spots from planes that are perpendicular to the substrate-layer interface and is particularly useful for isolating twist rotations and, in principle, for direct measurement of lateral correlation lengths. However, due to the extended illuminated dimension of the grazing incident beam, instrumental broadening can potentially be significant.

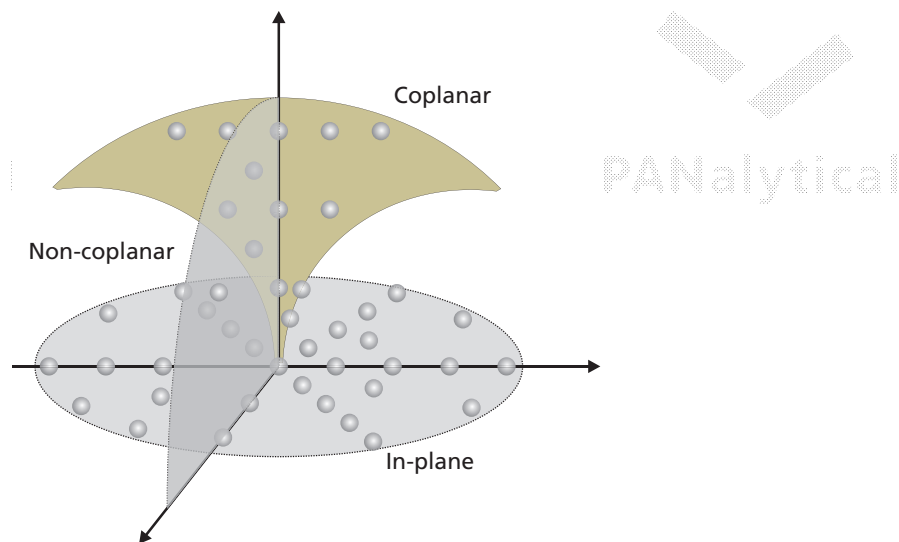


Figure 81: Illustration of the reciprocal lattice spots that can be accessed in the coplanar, non-coplanar and in-plane diffraction geometries

For the cases where in-plane scattering is not possible, or for a more rapid assessment, the non-coplanar arrangement can offer an alternative geometry for measuring the projected twist angle.

5.5.2 Coplanar symmetric reflections

Broadening in the direction parallel to d_{hkl} is considered to arise from both micro-strains (local variations in d -spacing) and a truncation length directly related to the number of scattering planes. Measurements of peak width in this direction can be achieved by radial 2theta/omega scans and are common in powder diffraction where the broadening effect is typically called the 'size/strain effect' and is treated using models such as the Scherrer equation or Williamson and Hall plots⁵⁰. It is necessary to measure at least two orders of reflection in order to separate the effects of strain broadening and size broadening.

Broadening due to the lateral size effect occurs in the direction parallel to the layer surface. For a symmetric reflection this is a direction perpendicular to the reciprocal lattice vector and hence perpendicular to the 2theta/omega scan. For small angular ranges it is coincident with the width of an omega scan. In reciprocal lattice coordinates broadening due to lateral correlation lengths will be the same for all reciprocal lattice spots (see Figure 82). Broadening due to tilt occurs tangentially around the reciprocal lattice origin. In reciprocal lattice units, the angle subtended at the origin is the same for all tilt-broadened reciprocal lattice spots. Therefore, by comparing at least two symmetric reflections, for example two of the 0002, 0004 and 0006 reflections in (0001) oriented GaN, it can be established whether the peak

broadening is primarily due to tilt or lateral correlation length, or is a combination of both.

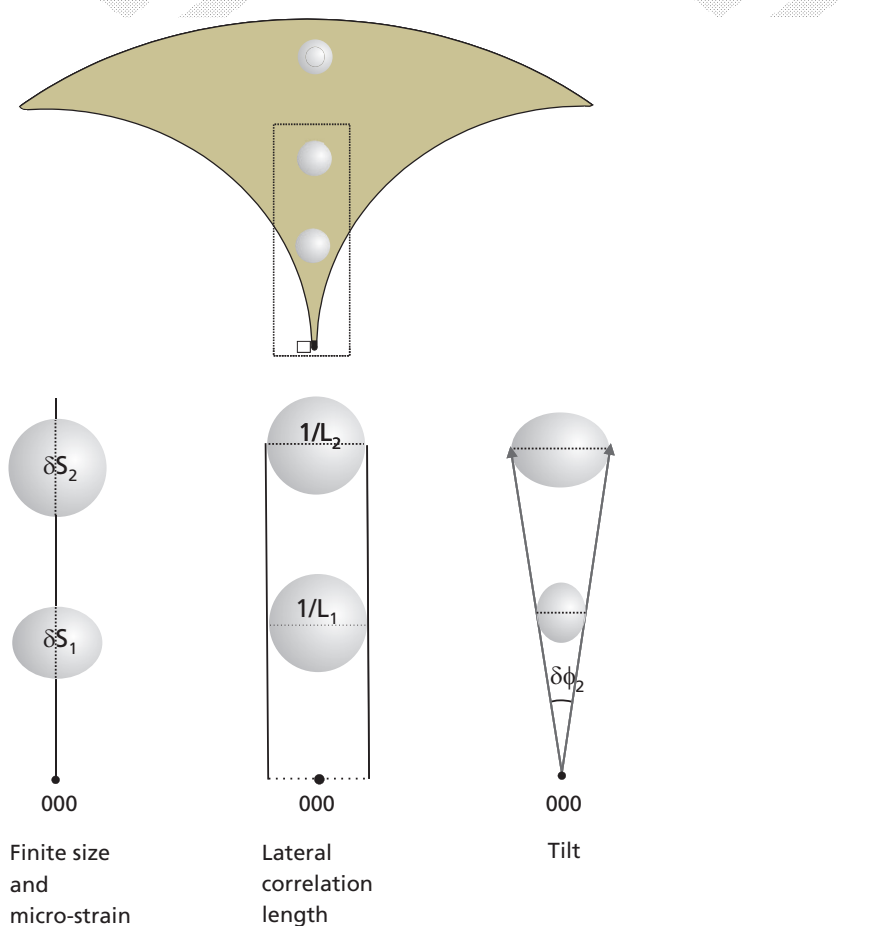


Figure 82: Illustration of how different types of spreading can be distinguished using peak width data from at least two coplanar symmetric reflections.

5.5.3 Coplanar asymmetric reflections

The concepts of broadening due to lateral correlation length and due to tilting are also considered in the analysis of the shape of a single asymmetric peak in reciprocal lattice units. Providing that the spot is elliptical in shape a measure of the width and orientation of the major axis of the ellipse can be taken. For the analysis it is assumed that this width is the vector sum of two components, the tilt that causes broadening tangentially to the reciprocal lattice vector and the lateral correlation length that causes broadening parallel to the sample surface. These

vectors are de-convoluted and for example in X'Pert Epitaxy software values for tilts and lateral correlation length can be obtained from a single measurement across the major axis of the ellipse. The details of the calculations are presented elsewhere⁵¹.

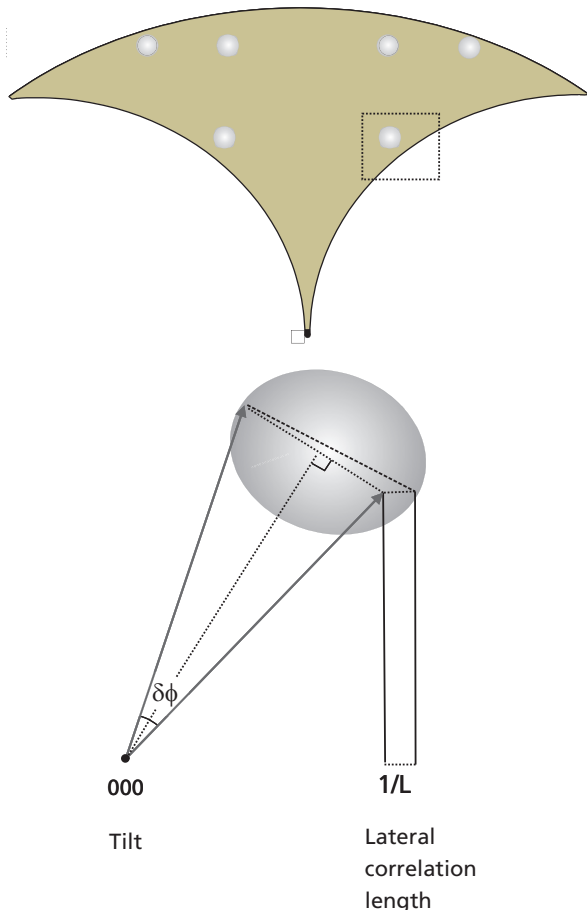


Figure 83: Illustration of how different types of spreading can be distinguished using peak width data from one coplanar asymmetric reflection

5.5.4 In-plane reflections

For in-plane reflection the same principles apply as for coplanar symmetric reflections. By considering two orders of reflection twist and lateral correlation lengths can be distinguished. In principle along the direction of the diffraction vector, finite size and micro-strain can be considered.

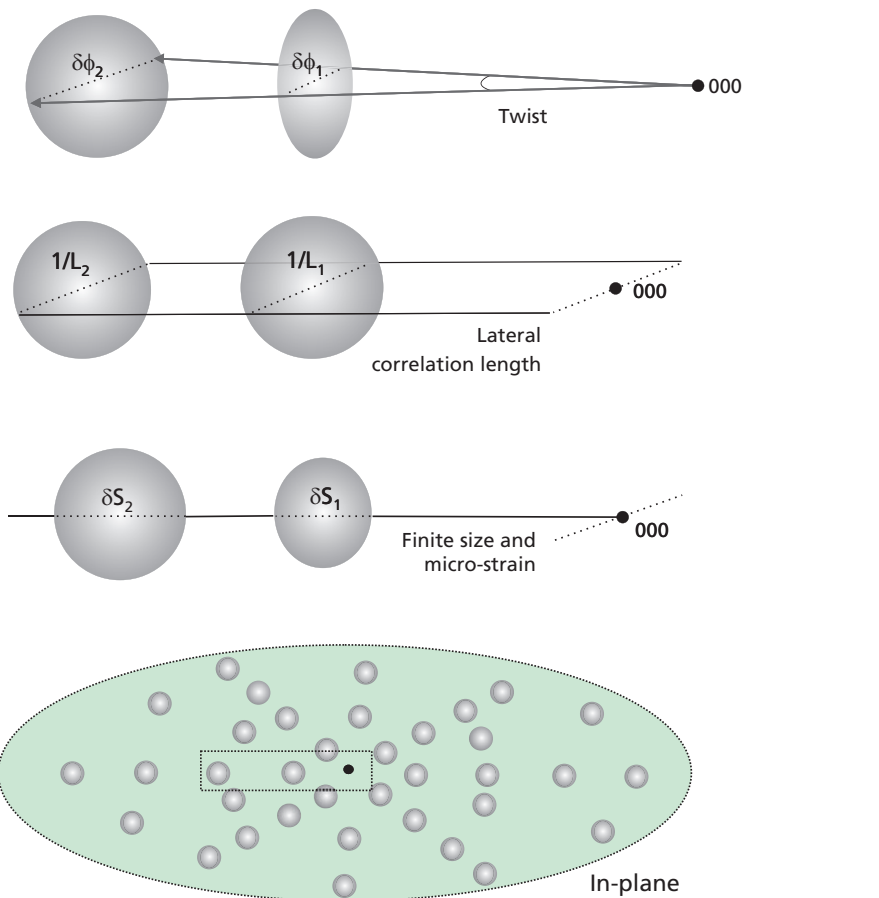


Figure 84: Illustration of how different types of spreading can be distinguished using peak width data from at least two in-plane reflections

5.5.5 Non-coplanar reflections

Non-coplanar reflections are accessed by rotating the sample normal away from the diffraction plane using a chi, χ (also called psi, ψ) axial rotation. Some resolution may be lost due to the psi offset of the sample. Single reflections have been used where it is assumed that broadening due to twist is the dominant effect. The broadening due to twist is measured using a phi scan or an omega scan. Whilst a phi rotation may be a more direct measure of twist, the instrument function is not well characterized in this orientation, whereas an omega scan may offer improved resolution.

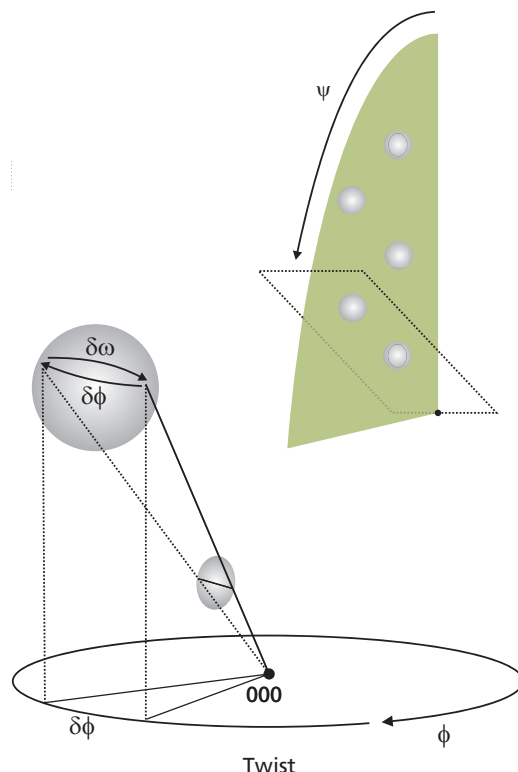


Figure 85: Illustration of how different types of spreading can be distinguished using peak width data from two non-coplanar reflections

5.5.6 Summary

At the time of writing, studies of defect structures in GaN and related compounds are the subject of active research. Models for understanding these defects are continuously being improved and their sophistication increases as more knowledge is added. This chapter provides an introduction to some of the basic principles in the analyses of defect structures. For more details on methods and calculations of results the reader should refer to current literature⁵².

References

- 1 For further reading see basic text on crystallography e.g. A. Kelly, G.W. Groves and P. Kidd, *Crystallography and Crystal Defects* (Wiley 2000) ISBN 0-471-72043-7
- 2 P.F. Fewster *Journal of Materials Science: Materials in Electronics* **10** (1999) 175-183
- 3 Source X'Pert Epitaxy Materials Database
- 4 A. Kelly, G.W. Groves and P. Kidd, *Crystallography and Crystal Defects* (Wiley 2000) ISBN 0-471-72043-7
- 5 J. Nye, *Physical Properties of Crystals* (Oxford 1995) ISBN 0-19-851165-5
- 6 The Voigt notation is followed here, although the Wooster notation is sometimes used, therefore care has to be taken when looking up numerical values.
- 7 W.A. Brantley, *J. Appl. Phys.* **44** (1973) 534-535
- 8 Standards on piezoelectric crystals (1949) as referenced in 5
- 9 J.M. Hinkley and J. Singh, *Physical Review B*, **42** (1990) 3546-3566
- 10 D.J. Dunstan, *J. Materials Science: Materials in Electronics* **8** (1997) 337-375
- 11 L.D. Landau and E.M. Lifshitz, *Theory of Elasticity* (Butterworth 1998) ISBN 0-7506-2633-X
- 12 G.E. Dieter, *Mechanical Metallurgy* (McGraw-Hill 1988) ISBN 0-07-100406-8
- 13 Poisson's ratio is also sometimes denoted by σ (note the absence of suffixes), and the strains more generally by u_{ik} , the displacement tensor components, see ref 1.
- 14 A.F. Wright, *J. Appl. Phys.* **82** (1997) 2833-2839 and references therein
- 15 Values as used in X'Pert Epitaxy
- 16 F.D. Auret and J.H. van der Merwe, *Thin Solid Films*, **23**, (1974) 257; *Ibid.*, **27**, (1975) 329, J. H. van der Merwe, *Philosophical Magazine A*, **45** (1982) 127-143
- 17 Vegard's rule is assumed for InGaN, AlGaN alloys.
- 18 For very small values of mismatch the difference between the two expressions can be negligible for a fully strained layer. In these cases, in particular for composition calculations, the value for mismatch is substituted for the true strain as an approximation to simplify the mathematics because a^s is a known value whereas a^t is unknown.
- 19 See for example: P.F. Fewster, *X-Ray Scattering from Semiconductors* (Imperial College Press 2003) ISBN 1-86094-360-8
- 20 See for example: M. Birkholz, *Thin Film Analysis by X-Ray Scattering* (WILEY-VCH 2006) ISBN 3-527-31052-5
- 21 See for example P. Kidd, P.F. Fewster and N.L. Andrew *J. Phys. D: Appl. Phys.* **28** (1995) A133-A138
- 22 See for example, P.F. Fewster, V. Holy and D Zhi, *J. Phys. D: Appl. Phys.* **36** (2003) A217-A221
- 23 In many texts and instruments this axis is also known as Chi, χ .
- 24 In physics, the wave vector $|K_0|$ is more generally expressed as $= n/\lambda$. But for the purposes of solving Bragg's law in XRD its most convenient form is where $n = 1$.
- 25 Q is also referred to in texts as \underline{S} and is also known as the 'change of momentum'.
- 26 For further discussion see for example: P.F. Fewster *X-Ray Scattering from Semiconductors* (Imperial College Press 2003) ISBN 1-86094-360-8 and references therein.
- 27 See P.F. Fewster, *X-Ray Scattering from Semiconductors* (Imperial College Press 2003) ISBN 1-86094-360-8
- 28 These reflections are in principle not accessible because the angles of incidence are either less than zero or greater than 2theta. However, if there is a spread in the incident beam angle (i.e. the instrument probe size is large) they may be partly detected.
- 29 The reflections marked in italics are not present in the figure because sapphire does not have total sixfold symmetry. These reflections will be present and their opposites absent at azimuths 60° and 180° away from the one shown.

- 30 In the context of thin film epitaxy, a superlattice is a multi-layer structure in which a group of layers are repeated many times. The superlattice exhibits a one dimensional periodicity in the same manner as a crystallographic *d*-spacing but with a much larger repeat dimension, called the superlattice period, Λ , which has values typically in the range 1 – 10 nm.
- 31 See for example: M. Birkholz *Thin Film Analysis by X-Ray Scattering* (WILEY-VCH 2006) ISBN 3-527-31052-5
- 32 See for example: P.F. Fewster, *X-Ray Scattering from Semiconductors* (Imperial College Press 2003) ISBN 1-86094-360-8; section 4.4.2.1
- 33 See for example: P.F. Fewster, *X-Ray Scattering from Semiconductors* (Imperial College Press 2003) ISBN 1-86094-360-8 ; section 2.8
- 34 See for example J.F. Nye *Physical Properties of Crystals* (OUP) 1985 ISBN:0198511655
- 35 See for example P.F. Fewster, N.L. Andrew, O.H. Hughes, C. Staddon, C.T. Foxon, A. Bell, T.S. Cheng, T. Wang, S. Sakai, K. Jacobs and I. Moerman, *J. Vac. Sci. Technol. B*. **18** (2000) 2300-2303.
- 36 See for example: P.F. Fewster, *X-Ray Scattering from Semiconductors* (Imperial College Press 2003) ISBN 1-86094-360-8, Takagi, *Acta Cryst* **15**, 1311 (1962), Taupin, *Bull Soc Franc Miner Cryst* **87**, 469 (1964), Halliwell, Lyons and Hill, *J. Cryst Growth* **68** 523 (1984), Lyons, *J. Cryst Growth* **96**, 339 (1989), Fewster & Curling -*J Appl Phys* **62**, 4154 (1987).
- 37 V. Holy and P.F. Fewster. *J. Phys. D: Appl. Phys.* **36** (2003) A5-A8
- 38 J.F. Woitok and A. Kharchenko, *Powder Diffraction*, **20** (2005) 125-127, P.F. Fewster, *J. Appl. Cryst.* **37** (2004) 565-574, P.F. Fewster, *J. Appl. Cryst.* **38** (2005) 62-68.
- 39 See basic text on dislocations e.g. A. Kelly, G.W. Groves and P. Kidd, *Crystallography and Crystal Defects* (Wiley 2000) ISBN 0-471-72043-7
- 40 For a review of dislocations in GaN see e.g. S. C. Jain, M. Willander, J. Narayan, R. V. overs- traeten, *J. Appl. Phys.*, **87** (2000) 965
- 41 H. Zhou, A. Ruhm, N-Y Jin-Phillipp, F. Phillip, M. Gross, H. Schroder, *J. Mater. Res.*, **16** (2001) 261-267
- 42 V. Srikant, J.S. Speck, D.R. Clarke, *J. Appl. Phys.* **82** (1997) 4286
- 43 T. Metzger, R. Höpler, E. Born, O. Ambacher, M. Stutzmann, R. Stömmer, M. Schuster, H. Göbel, S. Christiansen, M. Albrecht, H.P. Strunk. *Philosophical Magazine A*, **77** (1998) 1013-1025
- 44 V.V. Ratnikov, R.N. Kyutt, T.V. Shubina, T. Paskova, B. Monemar, *J. Phys. D: Appl. Phys.* **34** (2001) A30-A34
- 45 S. Danis, V. Holy, *Z. Kristallogr. Suppl.* **23** (2006) 141-146
- 46 V.M. Kaganer, A. Shalimov, J. Bak-Misiuk, K.H. Ploog, *Phys. Status Solidi*, **A204** (2007) 2561-2566
- 47 J. Gronkowski, J. Borowski, *Cryst. Res. Technol.*, **36** (2001) 8-10
- 48 See for example: M.E. Vickers, M.J. Kappers, R. Datta, C. McAleese, T.M. Smeeton, F.D.G. Rayment, C.J. Humphreys, *J. Phys. D: Appl. Phys.*, **38**, (2005) A99-A104
- 49 O. Yefanov, *J. Appl. Cryst.* **41** (2008) 110-114
- 50 B. Poust, B. Heying, S. Hayashi, R. Ho, K. Matney, R. Sandhu, M. Wojtowicz, M. Goorsky, *J. Phys. D: Appl. Phys.*, **38** (2005) A93-A98
- 51 See chapter 4.7 in P.F. Fewster, *X-Ray Scattering from Semiconductors* (Imperial College Press 2003) ISBN 1-86094-360-8
- 52 See for example M.A. Moram and M.E. Vickers, *Rep. Prog. Phys.* **72** (2009) 036502 (40pp), and references therein.